Fluorescence-based Multi Responsive Micro-sensor for Local Single Cell Analysis

Hengjun LIU

Fluorescence-based Multi Responsive Micro-sensor For Local Single Cell Analysis

Hengjun LIU

Abstract

Measurements of cellular temperature and pH can provide critical information on cell activities. The development of micro- and bio-compatible sensors that can reveal temperature and pH changes in cells has become an urgent demand. But very few fluorescent micro-sensors that can simultaneously detect pH and temperature changes in their surroundings have been reported. The interference between different indicators is also another difficulty in sensor fabrication. On the other hand, an effective method of injecting a certain amount of sensors (as small as a single sensor) into a target cell is also necessary for intracellular measurements. Unfortunately, the conventional methods for intracellular measurements are either damaging the cell easily or requiring long injection time. Consequently, in this study, we propose a synthesis method of a novel multi-fluorescent micro-sensor for simultaneous measurements of temperature and pH and also a rapid injection method of a single sensor into a target cell by applying local vibration stimulus on the sensor using optical tweezers.

Firstly, we proposed a synthesis method of a novel multi-fluorescent micro-sensor based on polymeric microbeads which can respond to both pH and temperature change of the surroundings. Two different kinds of fluorescent dyes (Rhodamine B and FITC) are introduced to a single microbead simultaneously, but the positions of FITC and Rhodamine B are different. So any interference from each fluorescent dye is expected to be negligible by this method. Fluorescence microscopy is used to monitor fluorescent probes. Fluorescence responses of Rhodamine B and FITC to both temperature and pH were studied. The results showed that Rhodamine B demonstrated an excellent linear relationship between relative fluorescence intensity and temperature, while it was found to be independent on pH. The calibrated sensitivity of Rhodamine B is −3.4%/◦C, with a temperature accuracy of 0.1 ◦C. On the other hand, FITC is found to be sensitive to both

pH and temperature. We propose a temperature compensation method for pH calibration. After temperature compensation, the pH accuracy calibrated based on the pH sensitivity of FITC improves from 1.5 to 0.2.

Then we proposed to use the multi fluorescent micro sensor which can respond to pH and temperature changes to measure the temperature and pH changes of influenza virus-infected and uninfected cells on the surface. After the virus solution was added into the cell dish, the fluorescent sensor was attached to virus-bound and virus- unbound cell surfaces using optical tweezers. The temperatures and pH in virus-bound cell and virus-unbound cell were determined using a fluorescence microscope by monitoring the changes in the fluorescence intensity of the sensor. We found that influenza virus multiplication increased the temperature of cells by approximately 4–5 ℃ and decreased the pH of cells by approximately 0.5-0.6.

In order to realize selective adhesion and quantitative injection of a single sensor on cell surface, we introduced liposome layers containing photochromic material (spiropyran) on the surface of the micro-sensor. Zeta potential of the liposome layers can be switched between negative and positive by photoisomerization of spiropyran. A single sensor can be manipulated by opticaltweezers and transferred to a cell surface, thereafter adhering selectively to the cell surface under UV illumination without excess sensor adhesion. Then we proposed rapid injection of fluorescence sensors into a target cell by applying local vibration stimulus circularly near the sensor using optical tweezers. The results showed that the vibration applied on the sensor could push down the sensor, inducing a downward displacement. This displacement caused a corresponding deformation of the cell membrane, which increased the contact area between the sensor and the cell membrane. Without vibration, the sensor was injected into the cytoplasm in 5 hours by lipofection at an injection rate of 40%. By applying the vibration stimulus, we succeeded in the rapid injection of the sensor in 30 min at an injection rate of 80%.

At last, we proposed the design of octacalcium phosphate (OCP) analysis chip and also the fabrication of multi fluorescence micro sensor pillars with different sizes for calcium, pH and temperature sensing respectively in microfluidic chip. The chip allows the co-culture of OCP and osteocyte and the sensors in the middle channel can respond

to the changes of surroundings in the chip. PEG-DA mixed with different fluorescent dyes (Fluo-3, FITC, Lumidot 480 for calcium, pH and temperature sensing, respectively) was used as the material of sensor pillar. All of the sensor pillars can be excited by same laser wavelength and recognized with each other by their different size (calcium sensor: Φ20μm, pH sensor: Φ15μm, temperature sensor: Φ10μm). Their fluorescence responses to calcium, pH and temperature changes were detected. Then after delivery of OCP and injection of fluoride solution in the chip, the fluorescence changes of different sensor pillars were observed for 1h by fluorescence microscopy. Calcium, pH and temperature changes of surroundings in the chip during OCP-HA conversion can be calculated based on the fluorescence changes of the sensor pillars. The results showed that calcium ion concentration in the surroundings decreased for 50 nM while pH value in the surroundings decreased for 0.4 in the chip during OCP-HA conversion.

Acknowledgements

It is my great pleasure to acknowledge all people who concern this work.

First I would like to express gratitude to Professor Fumihito Arai, Department of Micro-Nano Systems Engineering, Nagoya University, Japan for his constant support, guidance, encouragement, patience, and giving me a chance to be a researcher.

I would like to extend my sincere to Professor Yasuhisa Hasegawa in Department of Micro-Nano Systems Engineering, Professor Kenji Fukuzawa in Department of Micro-Nano Systems Engineering, Professor Noritada Kaji in Department of Applied Chemistry, Professor Hisataka Maruyama in Department of Micro-Nano Systems Engineering, Professor Tomohisa Tanaka in Department of Micro-Nano Systems Engineering, for kind agreement with being my doctoral committee member. I would also like to thank to Professor Osamu Suzuki in Division of Craniofacial Function Engineering, Tohoku University, and Professor Ayae Honda in Department of Frontier Bioscience, Hosei University for their kind help on my research.

I would like to personally thank to Dr. Taisuke Masuda, Dr. Takeshi Hayakawa, Dr. Lin Feng, Dr. Shinya Sakuma, Dr. Kousuke Nogawa, Mr. Hirotaka Sugiura, Mr. Takayuki Hasegawa, Mr. Shuichiro Kakiyama, Ms. Miyako Niimi, Ms. Yuka Yamagishi, Ms. Ningga, Ms. Yiling Sun for their kindness, friendship and support. I would like to extend my thanks to the entire lab members to share the precious time in my doctoral course.

Thank the Ministry of Education, Culture, Sports, Science and Technology (MEXT) of Japanese government and China Scholarship Council (CSC), for financial support under MEXT scholarship, without it my study at Nagoya University, Japan, would have not been possible.

I would like to express my deepest gratitude to my parents, my husband, my son, and my whole family for their encouragement and support in all of my daily life.

Finally I thank my God, for letting me pass through all the difficulties. I have experienced your guidance day by day. I would also like to thank the brothers and sisters in Motoyama Church for their encouragement and pray. Thank you, Lord.

2015

Hengjun LIU

Contents

List of Figures

List of Tables

Chapter 1

Introduction

1.1 Single-cell analysis

The cell is the basic structural, functional, and biological unit of all known living organisms. The study of cells is a natural step in the reductionist approach to studying organisms. It was once assumed that cell populations were homogeneous, but the latest evidence shows that heterogeneity does in fact exist even within small cell populations [1][2]. Individual cells can differ dramatically in size, protein levels, and expressed RNA transcripts. Cellular heterogeneity is well known in bacteria and cancer cells even within the same tumor [3]. These differences in individual cells may come from the genetic changes and micro-environmental differences [4]. And these variations are keys to answering previously irresolvable questions in cancer research, stem cell biology, immunology, developmental biology, and neurology. Single cell analyses are needed in the fields of describing the given “state” of a cell, defining normal cell-to-cell variation, understanding cellular responses in the tissues and complex environments, and overcoming limitations in measurement approaches. Single cell analysis would give an accurate assessment of the behavior of the cell since one cell is studied at a time.

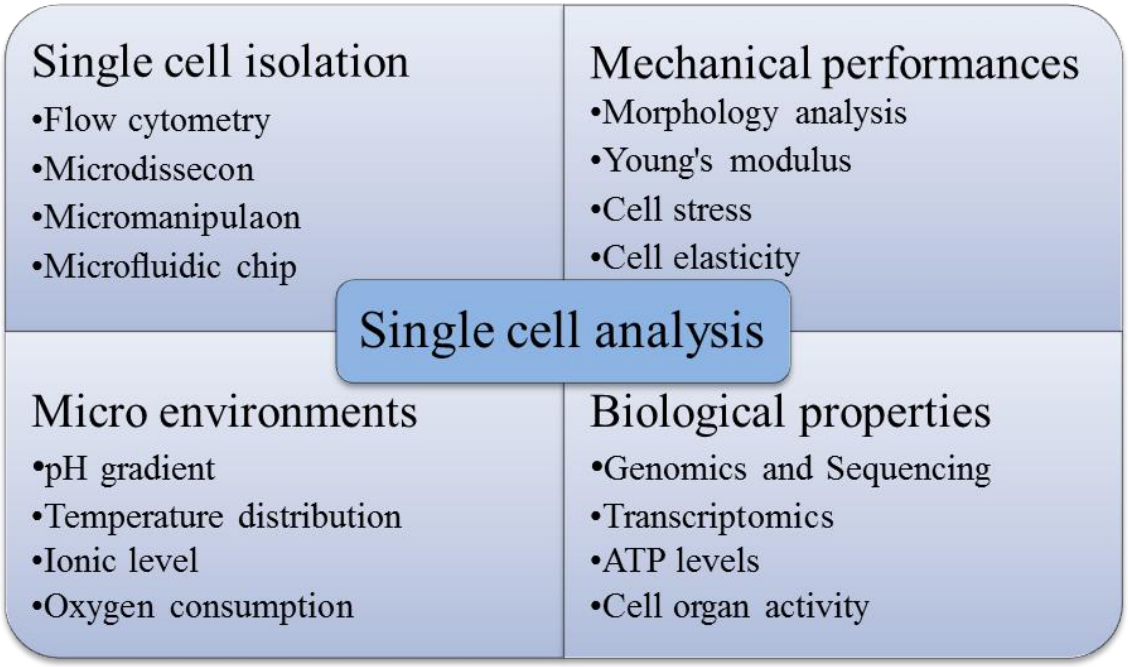

Figure 1.1: Single-Cell Analysis technologies in various fields.

Single-cell technologies are used in various application fields as shown in Fig.1.1 [5]–[9]. The single cell technologies are including microfluidics, microfabrication, cell sorting, cellular manipulations, cellular measurements which has contributed to biology and medical applications a lot. For example, direct and quantitative single-cell analysis of human immunodeficiency virus type 1 reactivation from latency has been studied and they demonstrated that cellular activation and virus reactivation following stimulation with proinflammatory cytokines can be uncoupled [10]. Moreover, the smart-seq method was used for profiling full-length mRNA from single cells by analyzing CTCs from melanomas, and distinct gene expression signatures as well as alternative splicing events specific to the disease were identified [11]. Recently, single cell analysis based on the microfluidic chip equipped with high-throughput and high-accuracy automation systems is being studied widely [12], [13]. Currently there are many single cell analysis programs support individual research studies that focus on the discovery and early development of exceptionally innovative tools for high-risk/high-impact projects and

the studies that accelerate the integration and translation of technologies to characterize single cells.

1.2 The importance of pH and temperature on single cell analysis

Cellular events, including cell division, gene expression, enzyme reaction, and metabolism, are fundamentally regulated by the intracellular chemical environment (temperature, pH, and dissolved oxygen)[14]–[16]. Research has proven that temperature plays an important role in many cellular events, and has close relationships with cell state and cellular functions [16]. On the other hand, the intracellular pH modulates the function of many organelles and plays a pivotal role in many physiological and pathological processes [17], [18]. Even a very small change in temperature or pH can lead to different reactions within a cell. The cellular pathogenesis of diseases is always characterized by extraordinary heat production or pH change within a cell. It has been reported that the heat production is also greater in tumor cells than that of normal cells [19], and the intracellular pH of MDCK cells dropped by some 0.3-0.4 between 3 and 5 hours after influenza virus infection [20]. Therefore, measurements of temperature and intracellular and extracellular pH can provide critical information on cell activities. The approaches for pH and temperature measurements of cells are shown in Fig.1.2. The different approaches possess different characteristic and suitable for different cells which will be discussed later.

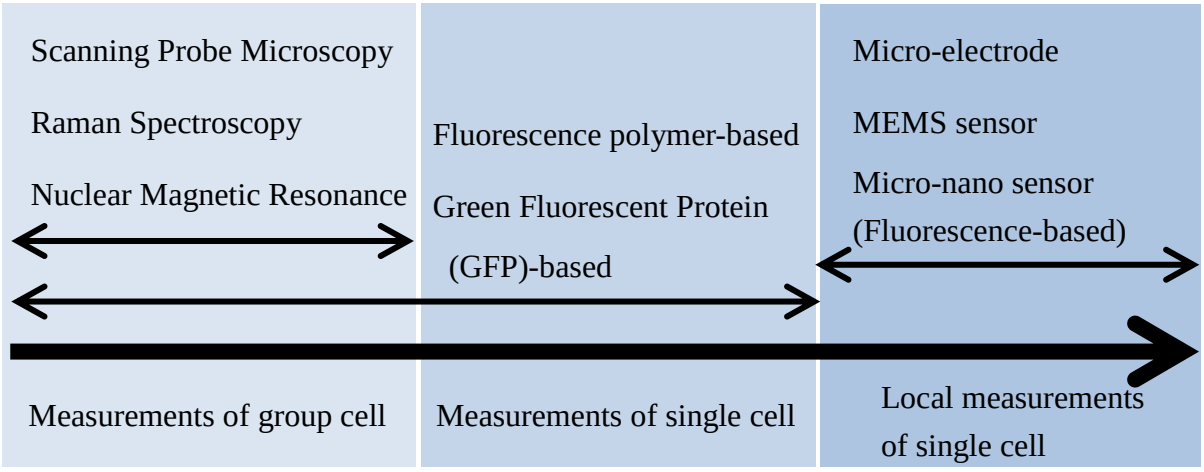

Figure 1.2 The approaches for pH and temperature measurements of cells.

1.3 Non-luminescent approaches for single-cell measurements on pH and temperature

Non-luminescent approaches, just like its name, are the approaches that their sensing properties are not directly related to luminescence [21]. Conventionally, microelectrode and electrochemical sensors equipped with micromanipulators have been used for cellular measurements [22]–[24]. Recently, with the development micro-electro-mechanical systems (MEMS) [25]–[27], many micro sensors have been fabricated using MEMS technology for application on cell measurements [28], [29]. These methods were widely and successfully to measure intracellular pH and temperature by inserting the probe directly in cells. Figure 1.3 shows the diagrammatic image of the probe sensor for cellular measurements. The directness of the microelectrode method makes it in some ways the ideal technique.

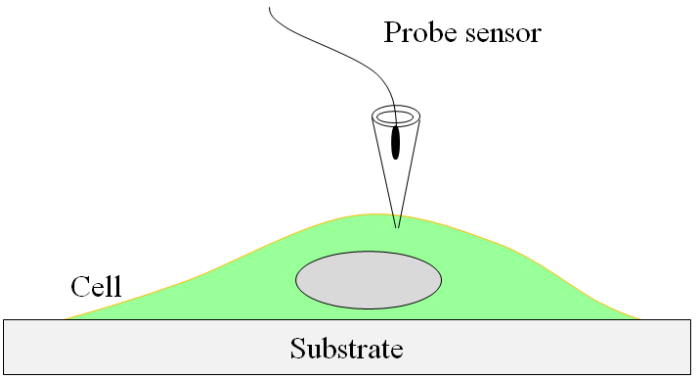

Figure 1.3: The diagrammatic image of micro probe on cellular measurements.

1.3.1 Thermometry

Non-luminescent thermometry differs in the sensing mechanism from one method to another. They offer a wide range of application possibilities with high thermal sensitivity.

1.3.1.1 Microelectrode

A microelectrode is an electrode of very small size, used in electrophysiology for either recording of neural signals or electrical stimulation of nervous tissue. Microelectrodes are used for the measurements of pH, oxygen, carbon dioxide and ions. Many thermal probes have been designed and fabricated by some industrial companies. Figure 1.4 (a) shows a kind of sheath type thermocouples for temperature measurement designed by Shinnetsu Corporation, Japan. It has the advantages of the small size of external diameter of the sheath, high sensitivities and easy for operation. Figure 1.4 (b) shows the construction and operating principal of a thermocouple. When fused together the junction of the two dissimilar metals such as copper and constantan produces a “thermo-electric” effect which gives a constant potential difference of only a few millivolts (mV) between them. The voltage difference as a temperature gradient is generated along the conducting wires. Then the output voltage from a thermocouple is a function of the temperature changes. The voltage output is the temperature difference

between the two dissimilar junctions, $V_{out}=V_1 - V_2$.

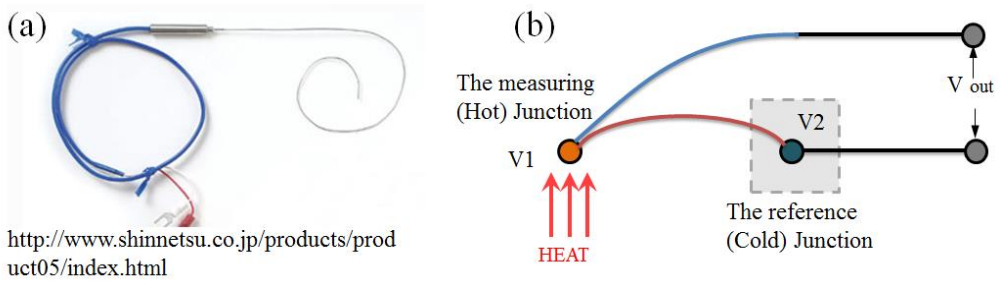

Figure 1.4: (a) The product of sheath type thermocouples for temperature measurement (b) The construction and operating principal of a thermocouple.

1.3.1.2 Thermocouple

For temperature measurement, sheath type thermocouples and micro thermometers are designed and fabricated with very small in size, providing excellent sensitivity [30]. Thermocouple (TC) is widely used in settings that require detection of temperature changes. TC device for detecting intracellular temperature has been reported by Changling Wang [29]. The probe is made of a sandwich structure consisting of the tungsten (W) substrate, an insulating layer made of polyurethane, and a platinum (Pt) film. As shown in Fig. 1.5 (a) and (b), they produced two types of TC probes, with different thickness of Pt film (50nm and 100nm). The TC probe was inserted into one U251 cell (Fig. 1.5 (c)) by the micromanipulation system and the thermoelectricity readings were recorded. This method showed a precise detection of temperature with temperature resolution of 0.1 ℃ or less in a very short time (400 ns) (Fig. 1.5 (d)). It was verified by observing temperature fluctuation in a single U251 cell after the addition of camptothecin, a DNA topoisomerase I inhibitor that can promote tumor cell death. This novel method has a great future in clinical applications as it allows real time monitoring of intracellular temperature change, however, it requires a lot of operating

time and skilled users to undertake the experiment.

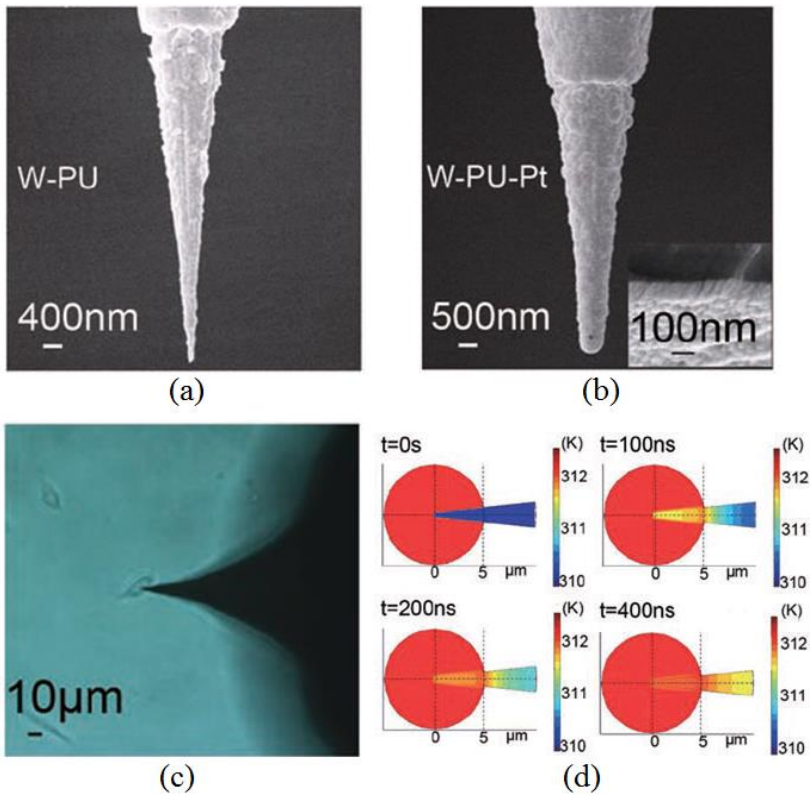

Figure 1.5: (a) SEM image of tungsten probe coated by polyurethane. (b) SEM image of the thin platinum film as an outermost layer. (c) Optical microscopic image of a living U251 cell inserted by the TC probe. (d) The simulated results of the TC probe response to a cell 2 ℃ higher than the environment. [29]

1.3.1.3 Other MEMS sensor

The micromachining technology that emerged in the late 1980s can provide micron-sized sensors and actuators. These micro transducers are able to be integrated with signal conditioning and processing circuitry to form micro-electro-mechanical-systems (MEMS) that can perform real-time distributed control. MEMS technology is being used widely in sensor fabrication, cell manipulations and cell measurements. J. El-Ali et al. presented a SU-8 based polymerase chain reaction (PCR) chip with integrated platinum thin film heaters and

temperature sensor as shown in Fig. 1.6 [31]. The device is fabricated in SU-8 on a glass substrate. The experiments showed that the temperature distribution in the PCR chamber is homogeneous and that the chip is capable of fast thermal cycling. With heating and cooling rates of up to 50 and 30 ℃/s, respectively, the performance of the chip is comparable with the best silicon micro machined PCR chips presented in the literature. The SU-8 chamber surface was found to be PCR compatible by amplification of yeast gene ribosomal protein S3 and Campylobacter gene cadF. So it shows a potential application in cell temperature measurement.

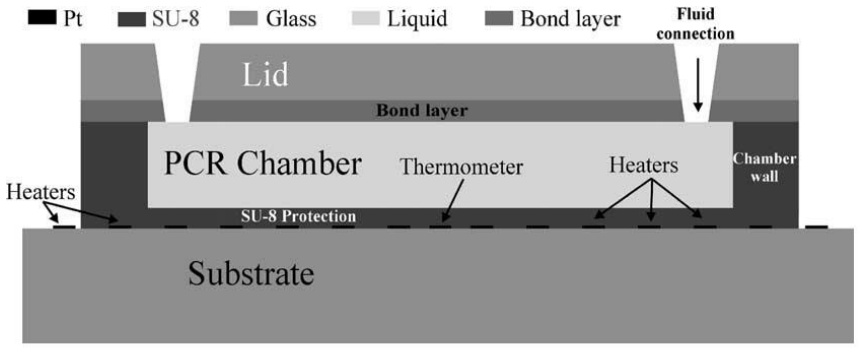

(a)

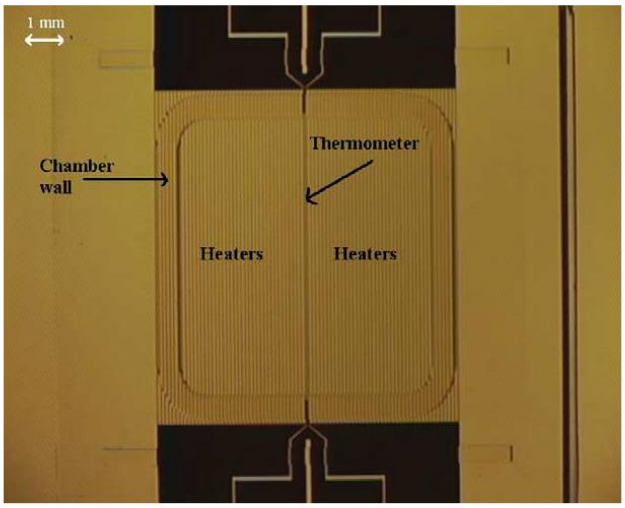

(b)

Figure 1.6: (a) Schematic of PCR chip design with a SU-8 based PCR chamber on a glass substrate. (b) Optical image of realized chip prior to bonding of lid. [31]

1.3.2 pH probe

For pH measurements, glass electrodes were first used to measure intracellular pH by Caldwell [32], [33], but his electrodes were too large to be used in cells smaller than crustacean muscle fibers or cephalopod giant axons. R. C. Thomas reported a new design of pH-sensitive microelectrode which had an extreme tip needs to be inserted into cell [34]. The design and fabrication of the microelectrode is shown in Fig. 1.7. A selected borosilicate glass micropipette was mounted vertically in the microforge, held by the second micromanipulator. A sealed pH micropipette was chosen with external dimensions near the tip similar to the corresponding internal dimensions of the borosilicate micropipette. The third micromanipulator was then used to lower the pH micropipette into positon inside the borosilicate micropipette as shown in Fig. 1.7 A. The other end of the fine polyethylene tube was already connected to a 2.5 ml syringe full of air. The cold microforge wire loop was placed close to the micropipettes about 150 μm from their tips, as shown in Fig. 1.7 B. The softening point of the pH glass is over 150˚C lower than that of the borosilicate glass, so that as the heat was increased the pH glass was softened and blown outwards to seal to the inside of the borosilicate glass, as illustrated in Fig. 1.7 C. Figure 1.7 A and B show the microelectrode just before, and C after, the formation of the final glass-to-glass seal. The length of electrode shown in A is about 1.5cm, in B and C is about 300 μm. The tip can be as small as 1 μm in external diameter. The application of the microelectrode on intracellular pH measurement is shown in Fig. 1.7 D. The microelectrode can respond to the internal pH changes induced by the ammonium solution. The pH-sensitive micro-electrode gives an accurate and direct reading of intracellular pH. The electrodes are once prepared can be used for many weeks and can difficult to continuous measurements of intracellular pH from one

cell for many hours.

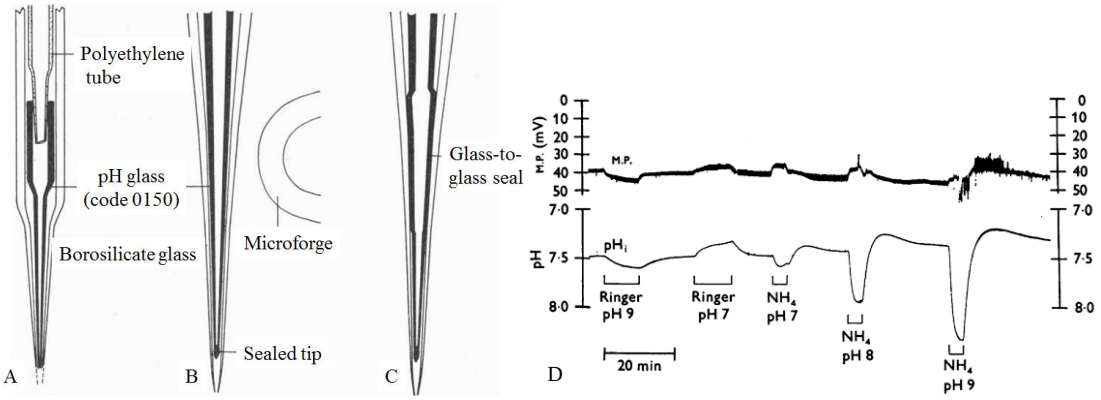

Figure 1.7: A-C: Diagrams showing construction of recessed-tip pH-sensitive micro-electrod, D: pen recording intracellular pH of external (NH4)2SO4, 5mM applied at pH7 and 9. [34]

1.4 **Fluorescence-based sensor using micro-nano particles for single cell analysis**

Luminescence micro sensors are using the fluorescence emitted from materials to measure the temperature. The detection of temperature happens when the temperature of the luminescent material changes which result in the changes of the intensity of the fluorescence, the excitation spectra, the lifetime, or the wavelength of the fluorescence [35]–[37]. So, small molecular fluorescent probes have been widely used for cell detection, and fluorescence measurements such as fluorescence intensity and lifetimes are two of the most promising methods for on-chip cell analysis[38]–[41]. However, the widely used small-molecule indicators typically possess problems such as fast leakage, lack of membrane permeability, poor photostability, or sensitivity to ionic strength [42], and these problems have limited their practical applications. To overcome this, fluorescence-based microbeads have potential as sensors in medicine and biotechnology, especially since multiple indicators can be attached to a single particle. By using

different kinds of micro-nano particles, different micro-nano sensors can be fabricated for cell sensing.

1.4.1 Micro/nano sensors based on different particles

Nanoparticles (NPs) are particles that are very small in size and large surface-to-volume ratios, generally range from 2 nm to several μm. Nanoparticles are good candidates for single cell intracellular temperature measurement. First, multiple indicators can be attached to single particles; second, nanoparticles may be less vulnerable to leakage through cell membranes; third, the nanoparticles can be manipulated and transferred controllably for cell measurement [42]. Many kinds of particles can be used as the carrier of the micro/nano sensors.

1.4.1.1 Polymeric microspheres

Polymeric microspheres are being used widely as the carrier of the particle sensor considering of its simple processing, low price and stable performance. Fluorescent nanoparticles, termed "nanothermometers", has been fabricated by K. Oyama et al. by embedding temperature sensitive dye in a poly(methylmethacrylate) (PMMA) network [43]. It is demonstrated that the walking nanothermometers can monitor temperature changes without sensitivity to pH (4-10) and ionic strength (0-500 mM). Fluorescein loaded amino functionalized polystyrene microspheres are used for real-time pH sensing in living cells [44]. The sensor-loaded microsphere 1 was prepared by coupling 5(6)-carboxyfluorescein onto 2 μm aminomethyl microspheres derivatized with an aminohexanoic acid spacer as shown in Fig. 1.8. Intracellular pH in living cells is measured in real time at the single cell level using the fluorescent sensor. The results showed that the fluorescence ratio increased as a function of intracellular pH (in equilibrium with extracellular pH) from 6.0 to 8.0.

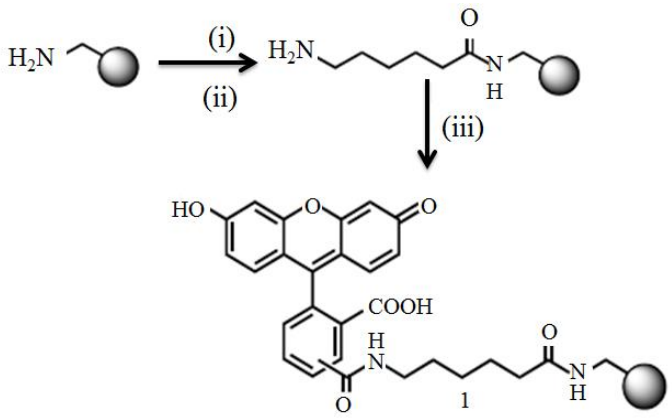

Figure 1.8: Preparation of fluorescein-labelled amino functionalized polystyrene microspheres. [44]

1.4.1.2 Silica nanoparticles

Fluorescent dyes encapsulated in silica nanoparticles have been produced for quantitative chemical sensing in live cells. The fluorescein encapsulated in these particles tend to be brighter and more photo stable than the corresponding free dyes in solution [45], [46]. The encapsulation of fluorophores into silica nanoparticles and their application as optical sensors for intracellular sensing has been reported by Anja Schulz and Colette McDonagh [47]. The discussed studies showed that these silica NPs possess great potential for real clinical and biomedical applications. They discussed that surface functionalization can also be used to create one or more shells around a NP core, allowing the encapsulation of spatially separated fluorophores as showed in Fig. 1.9.

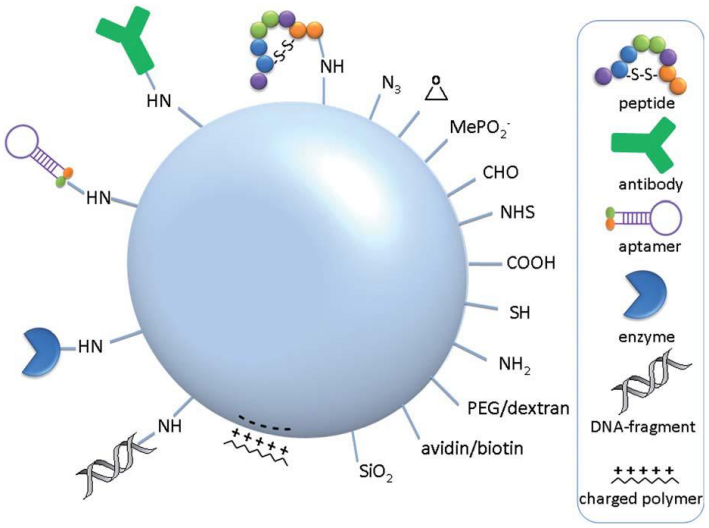

Figure 1.9: Schematic illustration of the surface functionalisation of silica NPs with, for example, peptides, antibodies, aptamers, enzymes, DNAfragments and different functional moieties. [47]

1.4.1.3 Gel-microbeads

pH-sensing gel-microbead impregnated with a pH indicator has been developed by Maruyama et al [48], [49]. Gel-microbead is made by salting-out of hydrophilic photo-crosslinkable resin and is manipulated by optical tweezers. Moreover, gel-microbead is polymerized by UV illumination and connected to other gel-microbead under an electrolyte solution. The pH value was measured by observing the color of the pH indicator inside the gel-microbead. W. Wu et al. also reviewed recent advances and challenges in the developments of hybrid micro-/nano gels toward applications for optical sensing of pH, temperature, glucose, ions, and other species as well as for intracellular imaging [50]. Three types of hybrid micro-/nano gel probes had been described in Fig. 1.10. In a Type 1 probe the specific antibodies, aptamers, or other selective analyte-recognition ligands are covalently linked to the hybrid micro-/nano gels. In a Type 2 probe the optical moiety acts directly as the chemical/biochemical signal receiver. In a Type 3 probe the stimuli-responsive polymer gel network chains act

as the chemical/biochemical signal receiver. The stimulus-responsive polymer microgels become ideal candidates for biomaterial applications since they can respond to various environmental stimuli such as change in pH, temperature, ionic strength or magnetic fields [51].

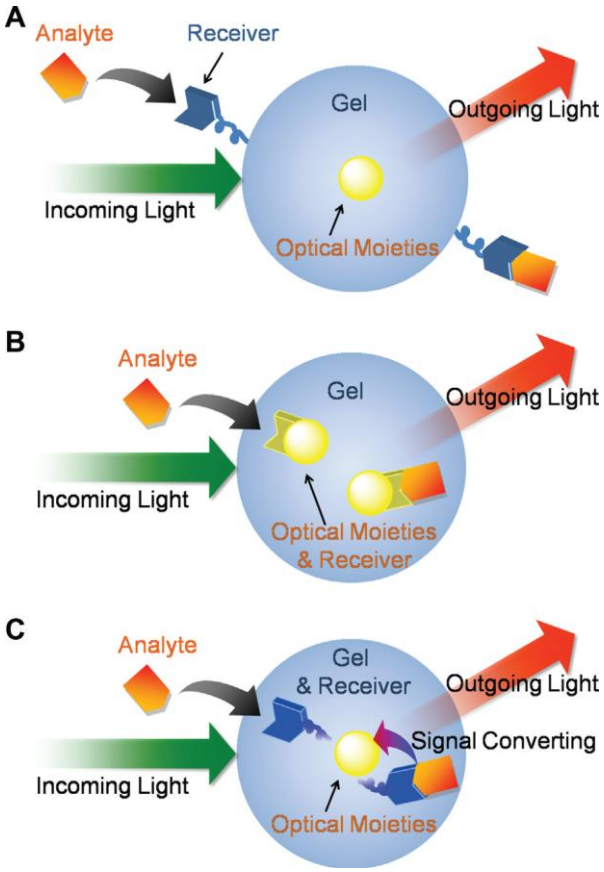

Figure 1.10: Schematic diagrams showing three types of hybrid micro-/nanogel-based optical probes: (A) Type 1 where the antibody or specific targeting ligand acts as a chemical/ biochemical signal receiver. (B) Type 2 where an optical moiety acts directly as the chemical/biochemical signal receiver. (C) Type 3 where a responsive polymer gel network chain acts as the chemical/biochemical signal receive. [50]

1.4.1.4 Lipobeads

Lipobeads is the beads that coated by liposomes as shown in Fig. 1.11. Liposomes have a long history of development as carriers of agents for triggered release, and

continue to be actively investigated [52]. The metastable character of liposomes together with fluorescein allows for applications on including pH and temperature. Figure 1.11 shows the schematic image of liposome and also the applications on encapsulating small molecular and polystyrene beads. Dr. S. Timothy et al. introduced a new type of composite material, gold-coated liposomes [52]. Fluorescein was encapsulated at self-quenching concentrations within the temperature-sensitive liposomes. K. P. McNamara et al. describes the synthesis and characterization of micrometric phospholipid-coated polystyrene particles, named lipobeads, with pH-sensing capability and their application for intracellular pH measurements in murine macrophages [53]. The fluorescent lipobeads are used to measure the pH in single macrophages. The absorbed particles remain stable for over 6 h in the cells when they are stored in a phosphate-buffered saline solution at pH 7.4.

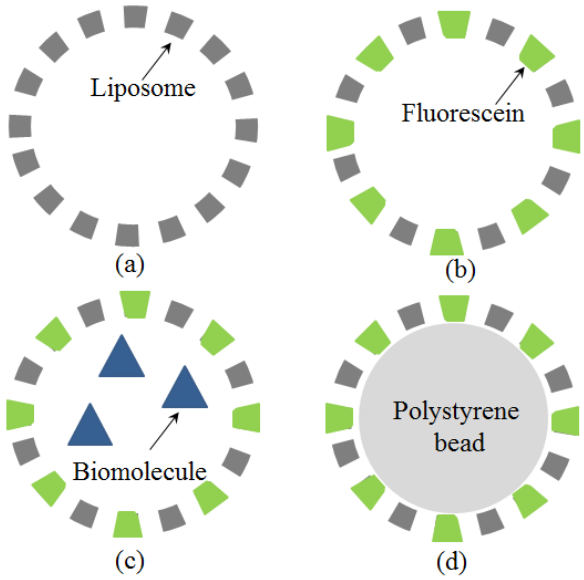

Figure 1.11: The schematic image of liposome and its applications on encapsulating small molecular and polystyrene beads. (a) unmodified liposome, (b) Liposome containing fluorescein, (c) biomolecule loaded fluorescent liposome, (d) lipobead (liposome coated polystyrene bead).

1.4.2 Delivery of particle sensor into cytoplasm for intracellular measurements

An accurate method of measuring intracellular temperature and pH could thus help clarify intricate cellular processes and develop new applications in biology and medicine. Thus, the development of micro-nano sensors with high sensitivities to temperature and pH, high spatial resolution, and effective injection technologies into single cells has become an urgent demand. And in order to pass through the cell membrane, a number of advanced biological, chemical, and physical methodologies have been developed in the last three decades, including micro-nano pipette injection [54], endocytosis and lipofection [55], optoporation [56], and optical injection [57].

1.4.2.1 Micro-nano pipette injection

Microinjection is an effective technique to introduce foreign materials into a biological cell. This technology has been widely applied in gene injection [58], intracytoplasmic sperm injection [59], drug development [60] and other biomedical areas. Single cell nanosurgery system based on micro/nano manipulators is shown as Fig. 1.12. Many researchers have contributed to the development of microinjection technology, and most of the developments mainly focus on the microinjection system, such as automatic injection, injection force control and sensing, and batch microinjection and so on [61]. Bending spring rate investigation of nanopipette for cell injection was proposed by Yajing Shen et al. [62]. Nanopipettes with a tip size of 300 nm are fabricated from various glass tubes by laser pulling followed by focused ion beam (FIB) milling as shown in Fig.1.13 (a). A yeast cell penetration test is performed on these nanopipettes, which have different bending spring rates as shown in Fig.1.13 (b) and (c). This method provides many possibilities for cell injection.

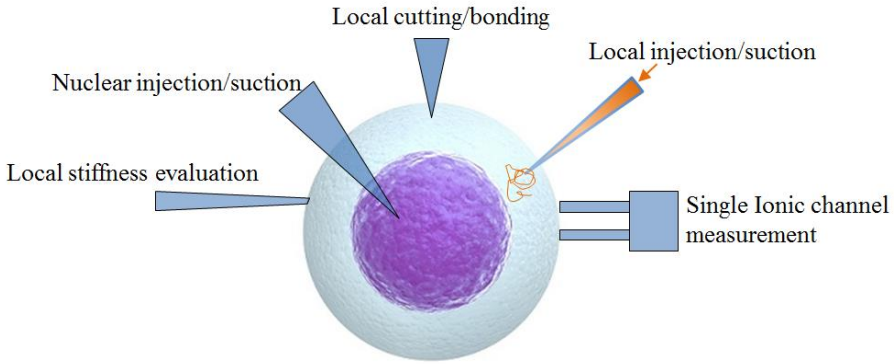

Figure 1.12: Single cell nanosurgery system based on micro/nano manipulators.

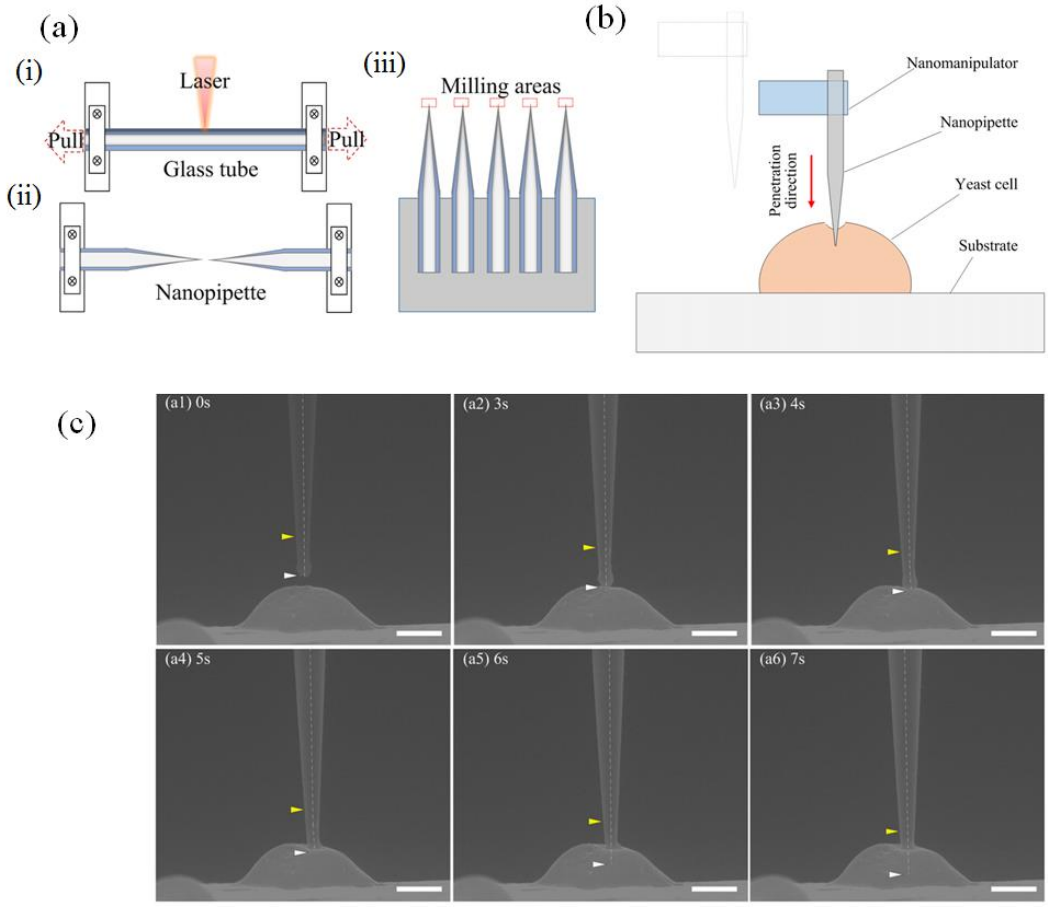

Figure 1.13: (a) Preparation of a nanopipette. (i) The middle section of the glass is scanned by laser. (ii) The nanopipette is manufactured by laser pulling. (iii) The tip of the nanopipette is milled to a given size by FIB. (b) Experimental setup for yeast cell penetration test by nanopipette based on nanomanipulation. (c) SEM images at different time points of yeast cell penetration testing of a quartz nanopipette. [62]

1.4.2.2 Nanorobotics injection

Nanorobotics is currently under research and development which can be manipulated with nanoscale resolution. The applications of nanorobotics can be in nanomedicine, detection of small environmental conditions, and can also be a new tool for small particle delivery.

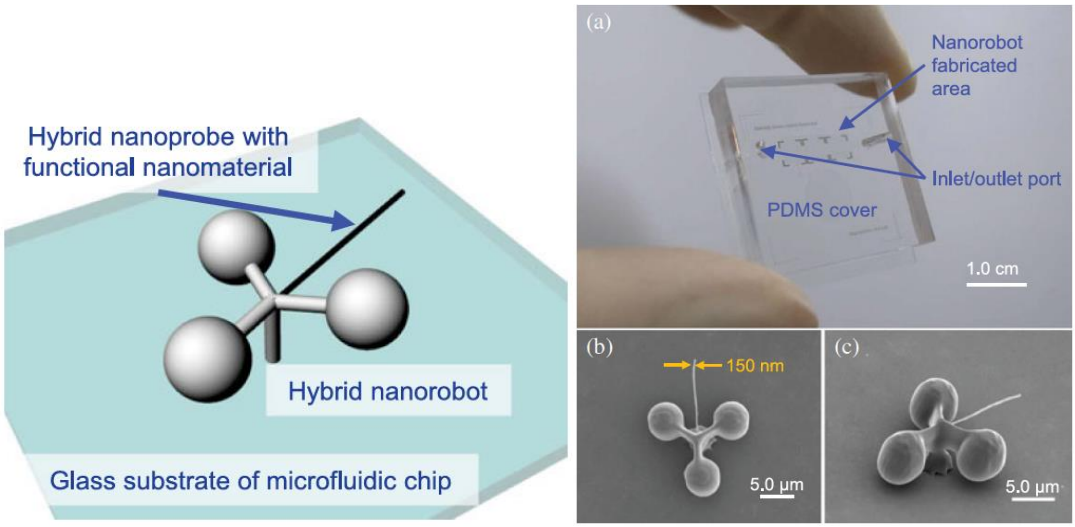

(a) (b)

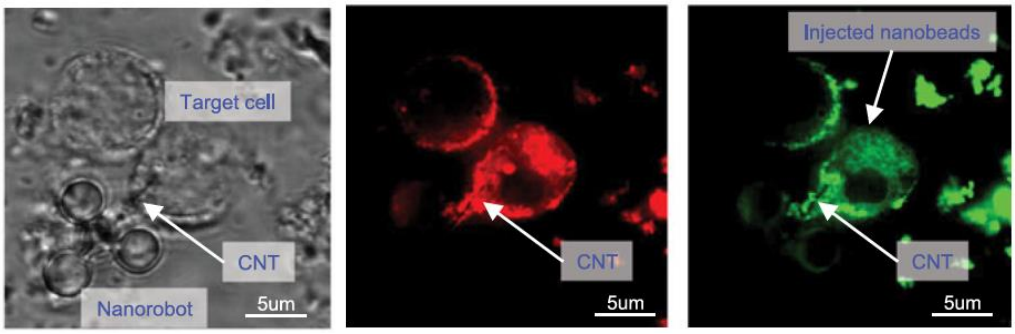

(i) Bright field (ii) Cell membrane (561 nm) (iii) Nanobeads (488 nm)

(c)

Figure 1.14: (a) Concept of the hybrid nanorobot with a functional nanomaterial. (b) Image of fabricated hybrid nanorobot. (c) Result of cell puncture by the hybrid nanorobot. [63]

On-chip nanorobot integrating functional nanomaterials for single-cell punctures has been fabricated by T. Hayakawa and coworkers [63]. On-chip robots of nanometer size were fabricated by femtosecond laser exposure (nanorobots) as shown in Fig. 1.14 (a)

and (b). They also integrated carbon nanotubes (CNTs) with the nanorobot and created a new function for the nanorobot, such as injection of nanoparticles in single cell. A single-cell puncture with this nanorobot has been done by irradiating the CNTs with an infrared laser and generating heat at that point. As shown in Fig. 1.14 (c), an optical manipulation of the nanorobot and injection of nanobeads have been realized with high spatial flexibility and high positioning accuracy. This method provides a new approach for cell injection.

1.4.2.3 Endocytosis and lipofection

Endocytosis is a type of active transport that moves particles into a cell. Figure 1.15 shows the characteristic of endocytosis. The plasma membrane of the cell invaginates, forming a pocket around the target particle. The pocket pinches off, resulting in the particle being contained in a newly-created intracellular vesicle formed from the plasma membrane. Honghao Sun et al. design receptor-targeted nano sensors aimed at drug release after endocytosis [64]. Figure 1.16 (a) shows the principle of the nanosensor cellular internalization by endocytosis. Cell uptake studies showed significant uptake of HA-coated nanosensors in HeLa cells as shown in Fig. 1.16. (b).

Lipid layers have been used for encapsulation and controlled delivery of soluble drugs [65] and polymer particles [66] into cells for lipofection. Lipofection, as shown in Fig. 1.17, is a technique used to inject biological particles into a cell by means of liposomes, which can easily merge with the cell membrane since they are both made of a phospholipid bilayer. CH.X. Bao et al. had proved the lipid fusion of two membrane-coated beads and they also cited that the whole lipid fusion process involved the docking, hemifusion, and full fusion of the bilayer [67]. So the sensor encapsulated in liposome could be delivered into cytoplasm by lipofection.

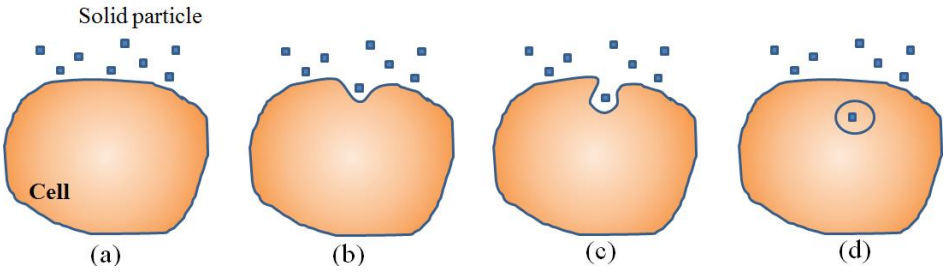

Figure 1.15: The characteristic of endocytosis. (a) Cell and small particles in extracellular fluid. (b) The membrane starts to bend. (c) The cell membrane forms a pocket around the target particle. (d) The pocket pinches off resulting in the formation of a vesicle.

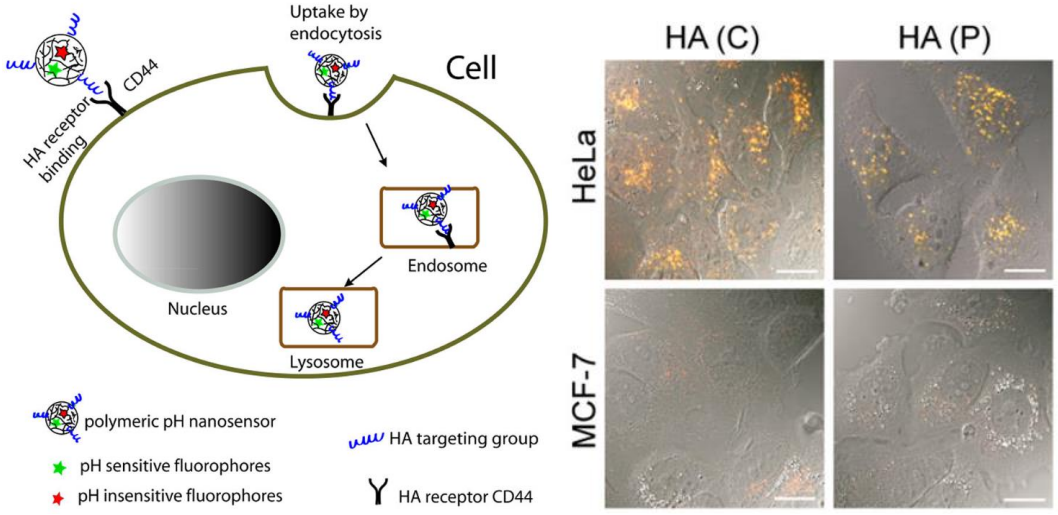

Figure 1.16: (a) Illustration of the nanosensor cellular internalization. (b) Uptake of HA-conjugated nanosensors by CD44-positive HeLa cells and CD44-negative MCF-7 cells. [64]

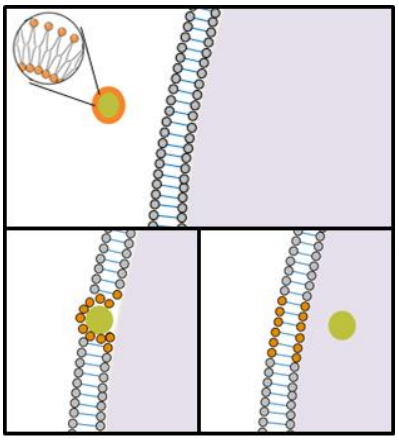

Figure 1.17: Diagrammatic sketch for lipofection mechanism

1.4.2.4 Optoporation

The laser microbeam has enabled highly precise noncontact delivery of exogenous materials into targeted cells without compromising cell viability, which has been a highly challenging task for traditional methods [68]. Its principle is the the generation of a transient hole or holes on the plasma membrane of a cell usually for the purpose of optical injection. Kamal Dhakal et al. used a focused femtosecond laser beam to create a small transient hole in the cellular membrane (optoporation) in order to inject an impermeable dye molecule into targeted living mammalian cells [69]. The transient hole on cell membrane was produced by optoporation and the fluorescence dye was also injected in cell successfully as shown in Fig. 1.18. The dye bound to the intracellular actin network and rise in fluorescence intensity was also observed by them.

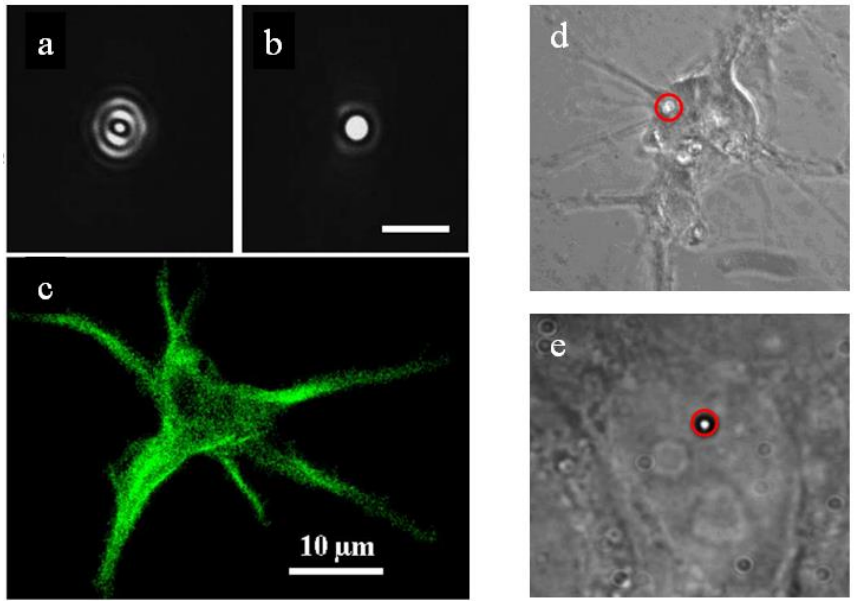

Figure 1.18: (a-b) Symmetric laser spot focused above and at the sample's surface plane. (c) Rat cortical neuron approximately 30 minutes following fs laser optoporation and injection with rhodamine phalloidin. (d-e) A transient hole (marked by red circle) observed during optoporation. [69]

1.4.2.5 Optical tweezers

For quantifiable delivery of a broad range of bioactive molecules to a single cell, laser-assisted intracellular delivery techniques are being explored. Optical tweezers, which are arguably the most versatile single-molecule manipulation technique, are widely used in single-molecule measurements [70], optical injection of small particle [71], [72], and cell palpation [73], [74].

Principle of optical tweezers

It was known that light generate optical pressure before the invention of a laser. Optical tweezers is a technique to hold and to manipulate a micron-sized object by radiation pressure force exerted by a focused laser beam under a microscope [75]. Arthur Ashkin first reported the acceleration and trapping of small particles based on this phenomenon in 1970 [76]. The trapping was observed by using dual laser setting with opposite direction and it is realized at balancing point of the lasers as shown in Fig. 1.19. In 1986, Ashkin reported the optical trapping using a focused laser beam [75]. This method can trap with only one beam as shown in Fig. 1.20.

For the large particles that are larger than the light wavelength (particle size >> λ), the optical force can be described with Mie scattering scheme as shown in Fig. 1.21. The Figure 1.21 (a) shows focusing of a laser beam. a and b shows the light ray, and they are refracted when passing through a spherical inside. It is suitable for the object of which refractive index is high enough compared with a surrounding medium. F_a and F_b are the optical pressure which are generated by the ray light a and b. Fig. 1.21 (b), (c) is the schematic diagram of forces which are generated by the displacement of focal point of laser beam. The resulting force is always pointing in the direction of the beam focus. So the objects can always be trapped in the center of the laser beam.

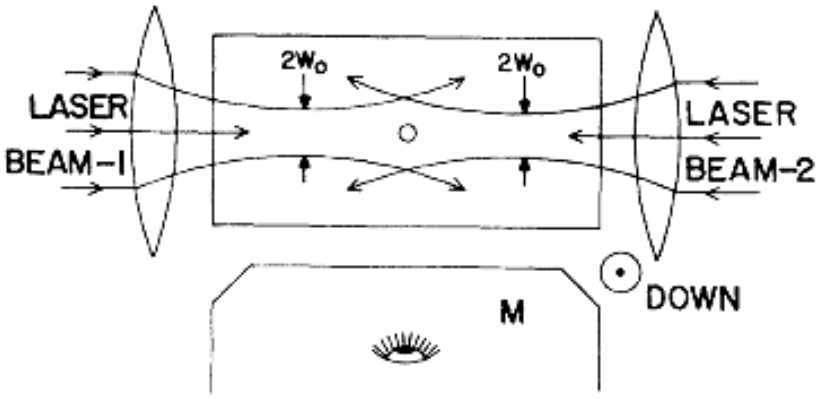

Figure 1.19: Ashkin's first optical trapping using opposed beams. [76]

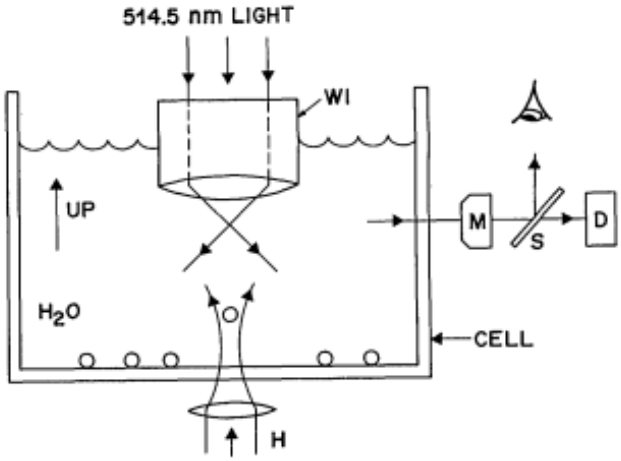

Figure 1.20: Practical optical trapping using a focused laser beam. [75]

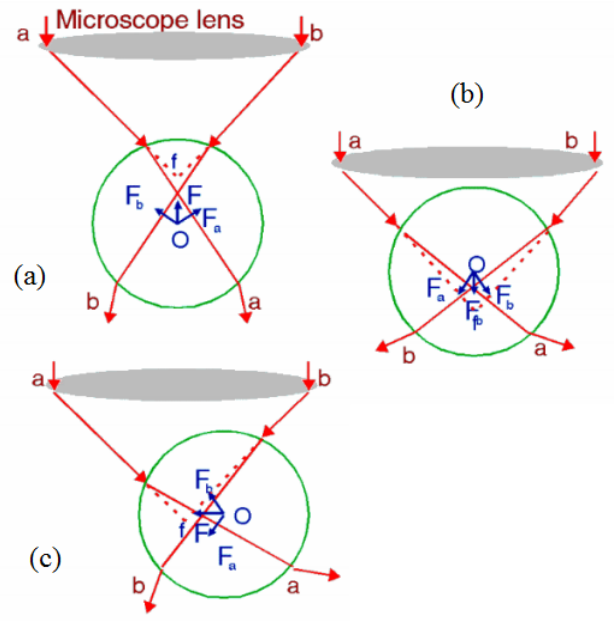

Figure 1.21: Schematic diagram of applied optical pressure with focused laser beam.

Optical trapping and manipulation of small objects

There are many applications of the optical tweezers as I reviewed before, I will discuss its application on trapping and manipulation of small objects. It is applicable to objects from nanometer to micrometer size. A. Ashkin used the optical tweezers to trap and manipulate the viruses and bacteria [77]. Tobacco mosaic virus which is a rugged rod-like protein was trapped at this experiment. But the 514nm wavelength laser damaged to bacteria cells. Then, they proposed to use infrared (IR) laser beams to trap and manipulate single cells, and optical damage was avoided by this method [78]. The optical tweezers can provide optical pressure and trapping force pointing at the beam center. Some measurements also have been performed by using optical tweezers. J. P. Mills et al. proposed to use the optical tweezers to trap and move microbeads which are bonded with a red blood cell (Fig. 1.22) [79]. The stiffness measurement of a red blood cell was conducted by using the ability of force sensing.

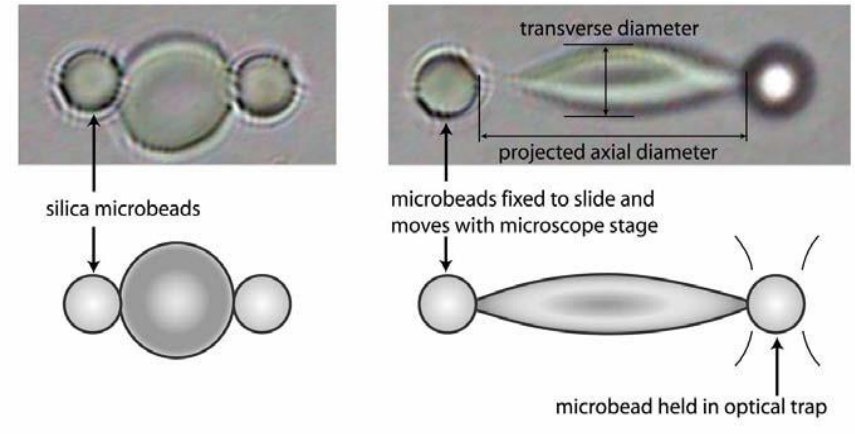

Figure 1.22: Illustration of an optical trap method for cell stretching. Two silicamicrobeads, each 4.12 μm in diameter, are non-specifically attached to the red cell. Right bead was optically trapped. [79]

Optically driven injection of small particles

The optical driven injection has increasingly attracted attention as it is a contactless and aseptic technique. It relies on the transient increase of a cell membrane's permeability induced by a laser beam, allowing micro-nano scale objects to diffuse across the membrane. In the photoporation mechanism, usually extremely high peak laser powers [80] and therefore possesses a danger of damaging the cell [81]. In this regard, less harmful approaches to the optical driven injection of objects through membranes are in strong demand.

Alexander S. Urban introduced a novel strategy for active optical injection which relies on the combination of optical forces of optical tweezers and plasmonic heating of gold-coated liposomes exposed to laser light [82]. They applied the optical tweezers on the cell and the freely diffusing gold-coated liposomes are propelled toward the cell under the optical forces of optical tweezers (Fig. 1.23 (a)). Combined with plasmonic heating effect of gold-coated liposomes, the liposomes can be injected into cytoplasm with a fast average injection time of 5.7s for one liposome. Optical injection results of RhB fluorescently tagged gold-coated liposomes are shown in Fig. 1.23 (b). They demonstrated quantitative focal activation of individual cells by the use of optical manipulation to gold-coated liposomes.

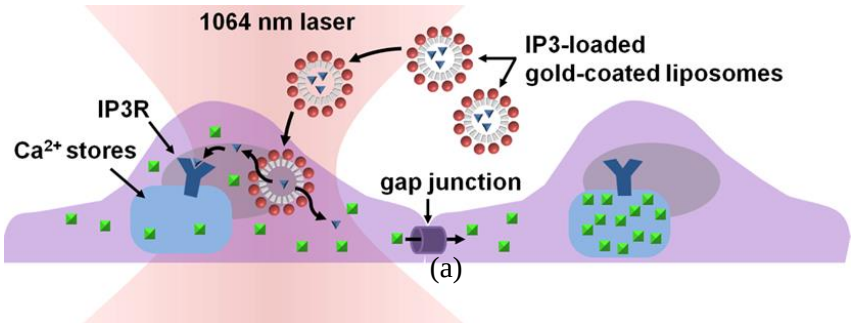

(a)

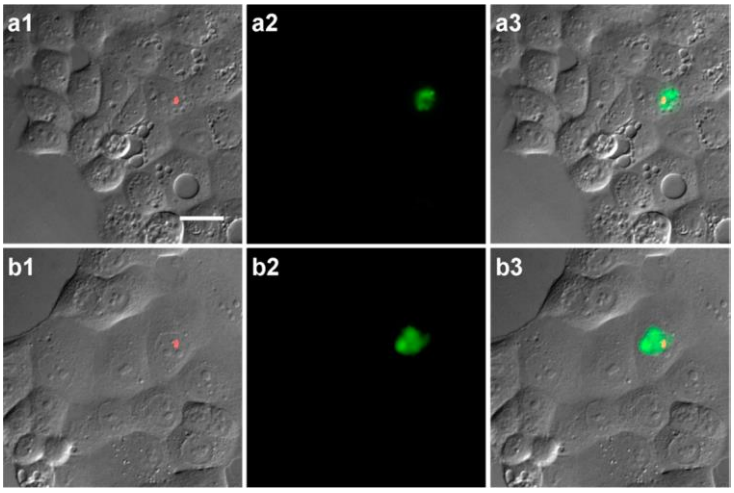

(b)

Figure 1.23: (a) Freely diffusing gold-coated liposomes encapsulating inositol trisphosphate (IP3) encounter the 1064 nm laser beam and are propelled toward the cell. (b) Optical injection results of RhB fluorescently tagged gold-coated liposomes. Column 1 is the experimental field with the location of the optical injecting laser overlaid in red. Column 2 shows the resulting RhB fluorescence signal after 60 or 120 s of optical injection. Column 3 is merged image. [82]

1.5 Fluorescence-based pillar sensor

Except for the particle sensors, with the development of MEMS technology, micro-fabricated pillar arrays are being used widely in the measurement of mechanical interactions between cells and their underlying substrates [83], cells forces onto their environment during motility [84], and also in the field of cellular temperature measurement [85]. Pillar arrays has been fabricated in different hard and soft materials, such as Si/SiO_2 material system [86], [87], micropatterned flexible substrates (PDMS)

[88], poly(ethylene glycol) diacrylate (PEGDA) [89].

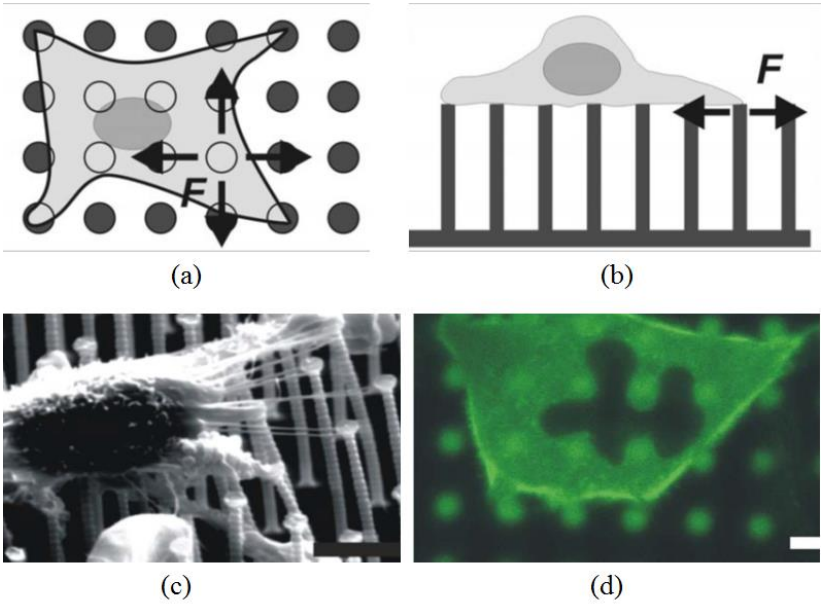

Figure 1.24: (a) Top view of cell lying on a pillar substrate to analyse cellular traction forces. (b) Side view of a cell adhering onto a pillar array. (c) Electron micrograph (viewing angle 45 °) of fibroblast on top of silicon pillars. (d) Fluorescent top view of fibroblast in between epoxy pillars. [90]

Micropillar force sensor arrays are produced by Wouter Roos [90] for biophysical studies of cellular and intracellular mechanics and for the assembly of suspended biofilament networks. Schematic images of pillar arrays used to analyze cellular traction forces are shown in Fig. 1.24 (a) and (b). Forces in two dimensions can be measured. Fibroblasts on different substrates (silicon pillars and epoxy pillars) are analyzed as shown in Fig. 1.24 (c) and (d). The force of the pillars on the right of Fig. 1.24 (c) is about 2 μN. Pillar stiffness is calculated as 1.4 ± 0.4 N/m. Fig. 1.24 (d) shows how the nucleus of a cell is deformed by the pillars.

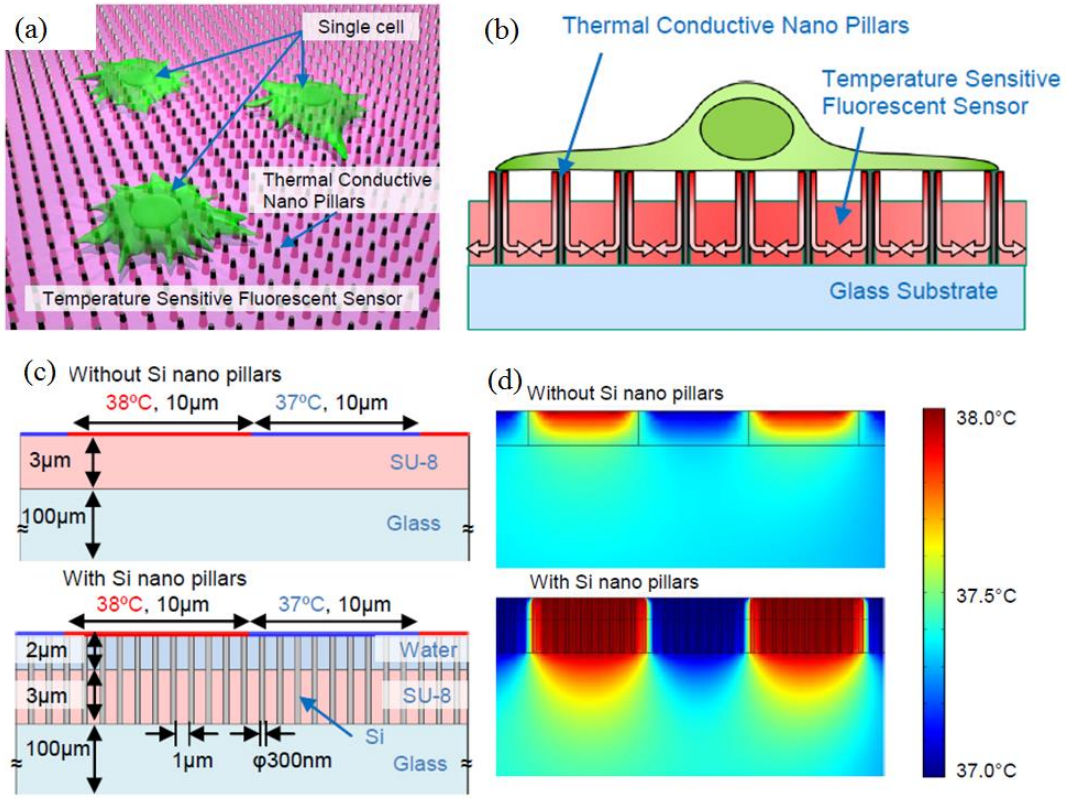

Figure 1.25: (a) The concept of temperature measurement device. (b) Consists of the device: glass substrate, high thermal conductive nanopillars and temperature sensitive fluorescent sensor. (c) Model of thermal conduction analysis. (d) Results of thermal conduction analysis. [85]

Except for the cell forces and deformations, high thermal conductive nano pillars have been designed and fabricated by Takeshi Hayakawa for temperature distribution measurement of a single cell. Figure 1.25 (a) and (b) show their concept. In this device, target cell temperature is transferred to the temperature sensitive fluorescent sensor patterned on glass substrate through Si nano pillars. Therefore, single cell temperature can be measured through detecting the fluorescence changes of sensor. Figure 1.25 (c) and (d) show the results of thermal conduction analysis. The Si nano pillars show high thermal conductive and high efficient thermal conduction which enables temperature measurement with high sensitivity.

1.6 Thesis overview

As a summary, there are many approaches for cellular measurements. However, each method has advantages and disadvantages that are summarized in Table 1.1.

Probe sensors The probe sensors are possible for intracellular measurement of individual cell measurement. But it always has a high requirement for the operation skills and the operator should be trained for a long time. Also the inserting of the probe sensor into cell for intracellular measurement can damage the cell easily.

Fluorescent probes The fluorescent probes include fluorescent polymers, green fluorescent protein, and other color indicators (e.x. Quantum dots). They are suitable for intracellular measurement because they can pass through the cell membrane and stain the whole cell. As the same time, the massive fluorescent dyes that passed through the cell membrane should be an extra stimulus to the cell. The interference between different kinds of fluorescent probes makes it hard for multi-sensing in cell.

Particle sensors The fluorescent sensors based on particles show great potential on cellular measurements, since it is possible to be injected into an individual cell. Its stimulus and damage to cell is expected to be small comparing with other injection methods. It is also worth waiting for the multi-sensing using particle sensors by introducing more than one fluorescent dye into the particle.

For the particle sensors, an effective injection method is necessary for intracellular measurements. Table 1.2 shows a summary of conventional approaches for sensor injection. Micro injection using micro probe is a directly method for intracellular measurements since the probe is inserted into cytoplasm. But it will also damage the cell easily. The nanoparticles can be injected into cell by endocytosis without damaging the cell membrane. But the quantitative injection of nanoparticles into an individual cell

is difficult. The lipofection method is based on the membrane fusion of lipid membrane between liposome-coated particle sensors and cell membrane. Similar with endocytosis, the quantitative injection of nanoparticles into an individual cell is also difficult to be realized. Therefore, a selective injection of single particle sensor into a target cell is in a great demand in single cell analysis. As I mentioned before, the optical tweezers can selectively manipulate a single small particle with high positioning accuracy. The trapping force of optical tweezers is used widely in trapping and transferring small particles and it is also expected to be used in the delivery of particle sensors into the target cell.

Table 1.1: Summary of approaches for cellular measurements

Method	Probe sensors	Fluorescent probes	Particle sensors
Schematic Image	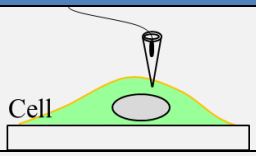	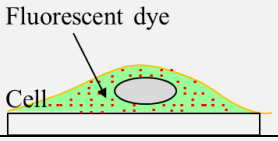	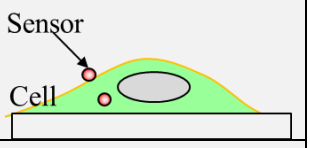
Principle	Thermopile Thermocouple pH electrode	Fluorescence, Color indicator	Fluorescence, Color indicator
Resolution	Good	Good	Good
Sensitivity	Good	Good	Good
Accuracy	Good	Fare	Fare
Intracellular measurement	Difficult	Possible	Possible
Individual cell measurement	Easy	Difficult	Easy
Damage to cell	Easy	Big stimulus to cell	Small
Multi-sensing	Possible	Difficult	Possible

Table 1.2: Summary of conventional approaches for sensor injection

Injection method	Micro injection	Endocytosis	Lipofection
Schematic Image	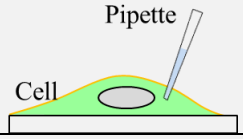	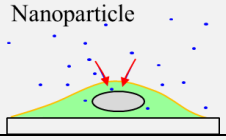	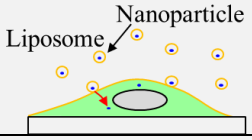
Principle	Micro-nano pipette	Endocytosis	Membrane fusion of lipid membrane
Injection of μm objects	Yes	Yes	Yes
Injection volume control	Yes	No	No
Damage to cell	Yes	No	No
Injection to individual cell	Yes	No	No

1.6.1 Research objectives

As I mentioned before, the key points and also the difficulties in micro environmental measurements of single cell are the novel sensor for multi-sensing of more than one parameters and an effective injection of single particle sensor into a target cell with small damage to cell. Therefore, our research purposes are as follows: (1) To fabricate a novel multi fluorescent sensor with high sensitivities and low interference between different fluorescent dyes. (2) To inject a single particle sensor selectively into a target cell without damage the cell.

1.6.2 Outline of this dissertation

This dissertation consists of six chapters, and proposes a novel multi fluorescent particle sensor for pH and temperature measurements and functionalization method of optical tweezers for single sensor injection into a target cell. In the last chapter, pillar sensors are also proposed for multi-sensing of three parameters (calcium, pH and Temp.)

The outline is described in Fig. 1.26.

Chapter 1 I introduce the background of the research and describe the research target in this chapter.

Chapter 2 I propose the fabrication of a novel multi fluorescent sensor based on polymeric microbeads which can simultaneously support pH and temperature-sensitive dye FITC and temperature- sensitive dye Rhodamine B to a single particle. The fluorescence responses of Rhodamine B and FITC to temperature and pH are detected. And the accuracy of the sensor is also verified in this chapter.

Chapter 3 I propose to use the multi fluorescent sensor to measure the pH and temperature changes of virus-infected and –uninfected cell on cell surface. The sensor is manipulated by optical tweezers to adhere on the cell surface. The fluorescence of the sensor is detected for several hours after adhesion on cell surface. The pH and temperature changes of virus-infected and –uninfected cell are calculated based on the fluorescence changes of the sensor.

Chapter 4 In order to apply the sensor for intracellular cell measurement, I propose the injection of a single particle sensor into a target cell by lipofection. The sensor is in advance encapsulated by liposome layers. Furthermore, I also propose vibration-assisted optical injection of a single fluorescent sensor into a target cell using optical tweezers. The optical tweezers is expected to promote the membrane fusion process for sensor injection.

Chapter 5 Except for the particle sensor, I also propose multi-fluorescence sensor pillars for multi-sensing in OCP analysis chip in this chapter. Microfluidic chip is designed for OCP analysis, and three kinds of sensor pillars with different sizes are designed to be fabricated in the chip. The sensors are sensitive to calcium, pH and

temperature, respectively. The responses of the sensor pillars to calcium, pH and temperature are detected. The calcium, pH and temperature changes are measured during OCP conversion using OCP analysis chip together with the sensor pillars in the chip.

Chapter 6 Summary of the dissertation and future work is discussed.

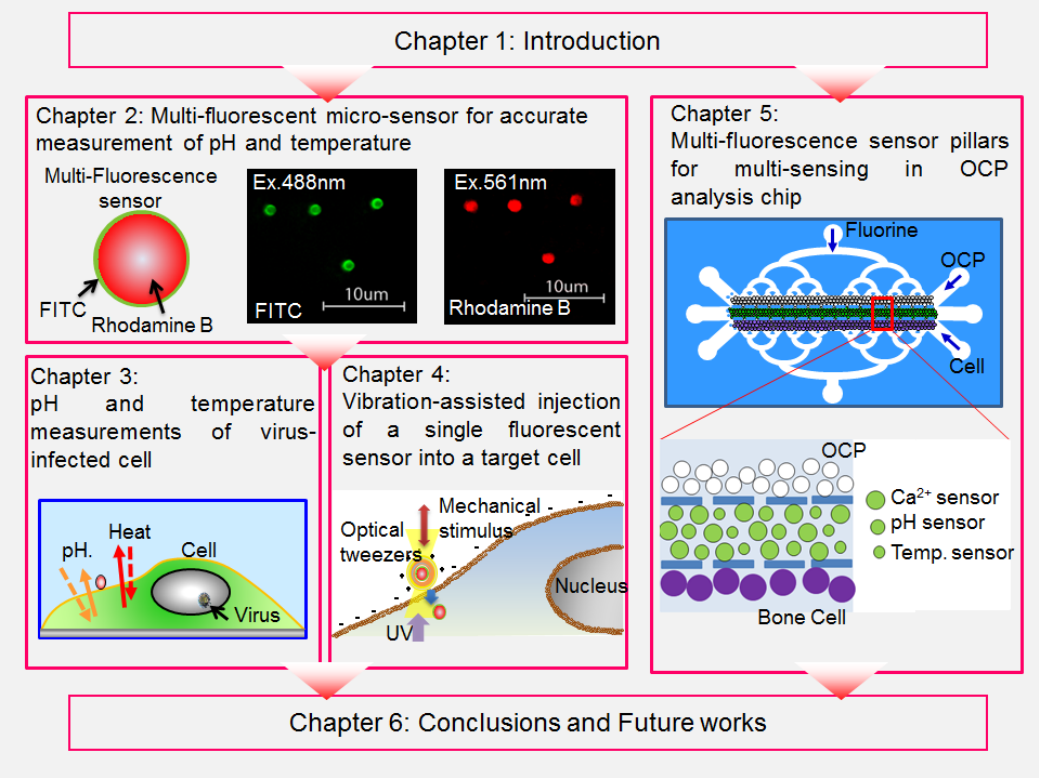

Figure 1.26: Outline of the dissertation

Chapter 2

Multi-fluorescent micro-sensor for accurate measurement of pH and temperature

2.1 Introduction

Temperature and pH levels play important roles in cell activities. As I introduced before, the development of micro- and bio-compatible sensors that can reveal temperature and pH changes in cells has become an urgent demand. Fluorescence-based microbeads have potential as sensors in medicine and biotechnology, especially since multiple indicators can be attached to a single particle. I have mentioned that many kinds of micro/nano sensors have been fabricated using different kinds of micro/nano particles together with fluorescent dyes. But very few fluorescent micro-sensors that can simultaneously detect pH and temperature changes in their surroundings have been reported. In our study, we proposed a synthesis method of a novel multi-fluorescent micro-sensor based on polymeric microbeads which can respond to both pH and temperature change of the surroundings. Two different kinds of fluorescent dyes

(Rhodamine B and FITC) are introduced to a single microbead simultaneously, but the positions of FITC and Rhodamine B are different. So any interference from each fluorescent dye is expected to be negligible by this method. Fluorescence microscopy is used to monitor fluorescent probes which can provide a high signal to noise ratio and a good spatial and temporal resolution. Fluorescence responses of Rhodamine B and FITC to both pH and temperature are studied and the temperature sensitivity and pH sensitivity of the micro-sensor are calibrated. In this research, the sensitivity of the micro sensor is defined as the change of its relative fluorescence intensity per unit temperature or pH. And then based on the sensitivities of the micro-sensor, temperature change and pH change of surroundings have been calibrated. Moreover, a method of temperature compensation for pH calibration is proposed and the accuracy of the micro-sensor for pH and temperature calibrations is also discussed.

2.2 Fabrication of multi-fluorescent micro-sensor

2.2.1 Material and synthesis process

Polystyrene (Ps) microbeads (1 μm in diameter) with amino group modified surfaces were used as the sensor carriers. Rhodamine B was embedded inside the amino-polystyrene beads, and FITC was modified on the surface of the beads as shown in Fig. 2.1. First, a solution of amino-polystyrene beads and 1 g/L Rhodamine B (in ethanol) (1:1 v/v) was stirred for 5 min and then washed with deionized (DI) water. The Ps beads swell in the presence of alcohol allowing Rhodamine B to get into and stain the beads inside. The expanded Ps beads shrink after washing with DI water. Then, the beads were added to a FITC saturated aqueous solution for 1 h and followed by three washes with DI water. FITC was immobilized on the surface of the amino-polystyrene beads through the chemical reaction shown in Fig. 2.2. The positions of FITC and

Rhodamine B are different so any interference from each fluorescent dye is expected to be negligible. Rhodamine B is one kind of fluorescence dye that is containing a xanthene ring. In high temperature, the twist motion of ethylamino in Rhodamine B molecular which leads to the twist of the xanthene ring will result in the decrease of fluorescence quantum yield. That's the reason why Rhodamine B is sensitive to temperature. In the strong acid solution (pH<3), ionization of carboxyl in Rhodamine B will be impeded which will change the ionic isomers of Rhodamine B. Then the fluorescence quantum yield of Rhodamine B will change. But in the pH range of 3 – 14, there is no change in the ionic isomers of Rhodamine B and Rhodamine B is stable in pH 3 – 14. That's why we choose Rhodamine B as the temperature sensitive fluorescence dye.

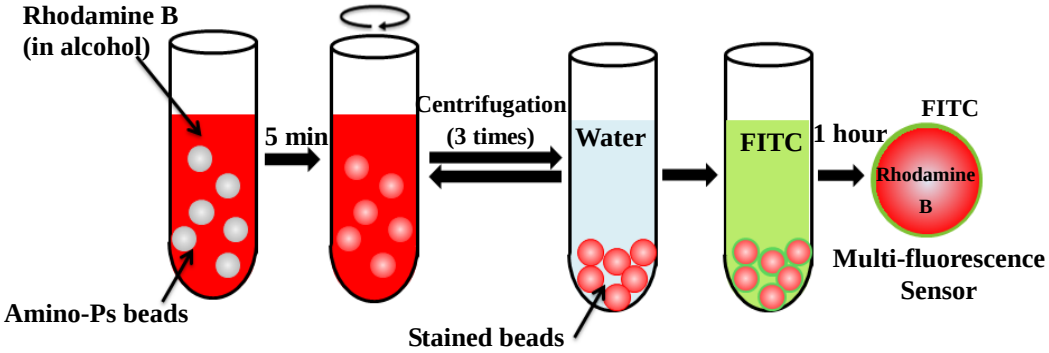

Figure 2.1: Schematic illustration of the synthetic process for the multi-fluorescent sensor.

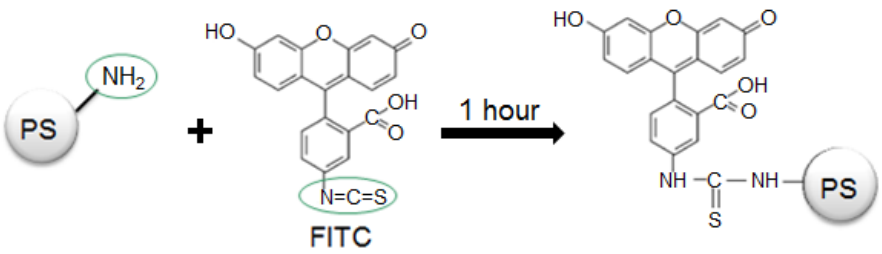

Figure 2.2: Process for FITC assembly on the amino-polystyrene beads.

2.2.2 Measurement methods of the micro-sensor

We studied the fluorescence responses of the micro-sensor to different pH values and temperatures. Buffer solutions with different pH values (pH = 5, 6, 7, 8) were prepared. The pH of surroundings was changed by changing the solutions with different pH. An incubation chamber was used to maintain the sample temperature, and the incubator chamber had four heaters (top heater, bath heater, stage heater, and lens heater). The temperature was controlled in the range of 32 – 38 ℃.

After the microbeads were stained with Rhodamine B and FITC, 3 mL of the bead solution was added to a glass dish and kept in the dark until the beads adhered to the bottom of the dish (almost 10 hours). Solution will be changed to remove the redundant floating beads. Then the dish was placed in the incubation chamber, and the top of incubation chamber was covered to avoid any interference from the lights. The fluorescence intensity of the beads was measured using a fluorescence microscope. The stability and fluorescence responses of the micro-sensor to pH and temperature, its fluorescence reversibility, and its endurance in the surrounding ionic strength were all detected. For the fluorescence measurements of the micro-sensor response to pH and temperature, the sample temperature was increased from 32 – 38 ℃ in a pH 5 solution. Then the pH was changed to 6, 7, 8, and the fluorescence responses to temperature (32 – 38 ℃) were repeatedly measured. We kept detecting the same beads during the experiments.

2.3 Experimental system setup

The fluorescent image of the target is obtained from an inverted confocal microscope (Ti-E Nikon) equipped with a high magnification lens (Plan Fluor 100x, Nikon) and CCD camera (iXon ultra, Andoe). The experimental system for fluorescence

measurement is shown in Fig. 2.3. The excitation wavelengths of FITC are in the range of 405 – 525 nm, and it always has a strong absorbance at 488 nm. Its emission wavelengths are 500 – 600nm with a peak emission of 520nm. The excitation wavelengths of Rhodamine B are 500 – 590 nm and it always has a strong absorbance at 561 nm. Its emission wavelengths are 550 – 650nm with a peak emission of 570nm. Therefore, wavelengths of 488 and 561 nm were selected as the excitation wavelengths for FITC and Rhodamine B, respectively.

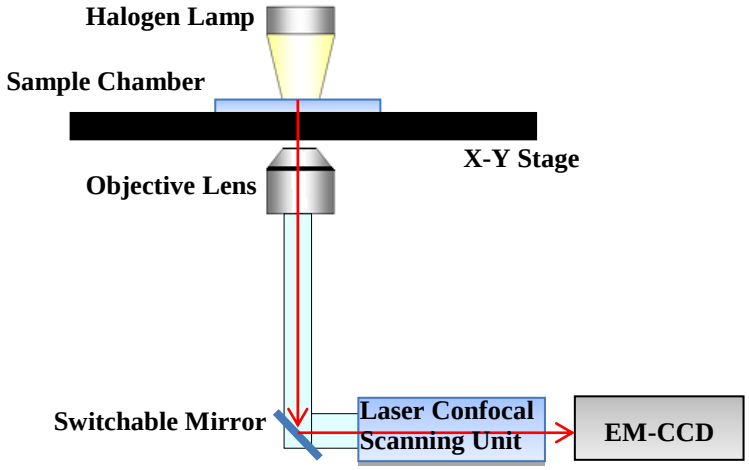

Figure 2.3: Schematic of the inverted confocal microscopy system.

Intensity based fluorescence measurements depend on many parameters, and the fluorescence intensity is represented in equation 2.1 [91].

$$I(t) = I'_0 C\Phi\varepsilon \exp(-\varepsilon x C) \cdot \exp(-t/\tau) \tag{2.1}$$

Where I [W/m^3] is the optical energy emitted from the fluorescent material per unit time, I_0' [W/m^3] is the excitation light flux on the fluorescent material, C [g/m^3] is the concentration of the fluorescent material, and Φ is the fluorescence quantum yield, and $\mathcal{E}$ is absorbance index. Φ decreases with environmental variation, whereas ε has low environmental dependence. x [m] is the propagation distance in the material. [s] is

fluorescence lifetime. t [s] is the excitation time.Φ is variable depending on environmental conditions such as temperature, pH, and ions.

The laser source is class 3B laser with a laser power of 50 mW and a high stability of±0.5％/h. The variation of dye amount from bead to bead is within 5%. It is based on the fluorescence intensity deviation of each beads comparing with the average value. Electron-multiplying gain is set to 200x, and the exposure time for one fluorescent image is 200 ms. So the fluorescence intensity measurement is mainly dependent on Φ. The lasers are controlled using a laser confocal scanning unit (CSU-X1, Yokogawa). The motorized filter changer model is available which make it easy to change the laser channel between 488 nm and 561 nm. The X-Y stage (BIOS-105T, Sigma Koki) of the microscope was controlled by the stepping motors, and the Z axis was controlled by the stepping motor.

2.4 The sensitivity calibration of the synthesized sensor

2.4.1 Stability

Figure 2.4 shows the fluorescent images of the micro-sensor. Green fluorescence detected at ex. 488 nm from FITC and red fluorescence detected at ex. 561 nm from Rhodamine B were observed. Before measuring the fluorescence responses of the micro-sensor to pH and temperature, the stability of the sensor was detected for 5 days. The pH value of the bead solution was 7.4 and the chamber temperature was set to 34 ℃. After the beads adhered to the bottom of the dish, the fluorescence intensity was detected every 24 hours for 5 days. We detected the same ten beads during the experiment and the fluorescence intensity results shown in Fig. 2.5 are the average values of the ten beads. There is almost no change in the fluorescence intensity for both Rhodamine B and FITC in 5 days, suggesting the bead possesses a high stability

without Rhodamine B diffusion in at least 5 days. Actually, we preserved the redundant sensor for more than two weeks and the fluorescence intensity of Rhodamine B was almost same as its initial value. The variation of intensity over different beads is within 5%.

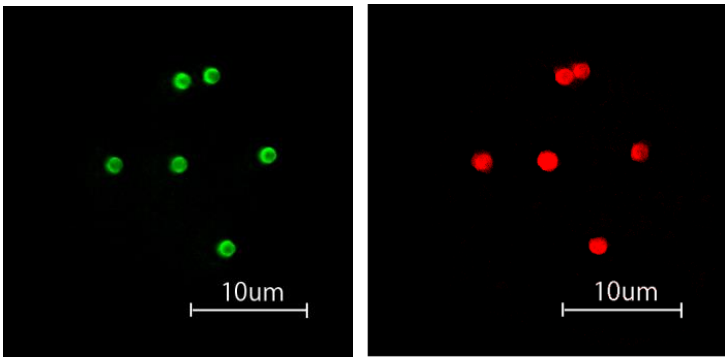

(a) (b)

Figure 2.4: Fluorescent images for indicators (a) FITC (excited at 488nm) and (b) Rhodamine B (excited at 561nm).

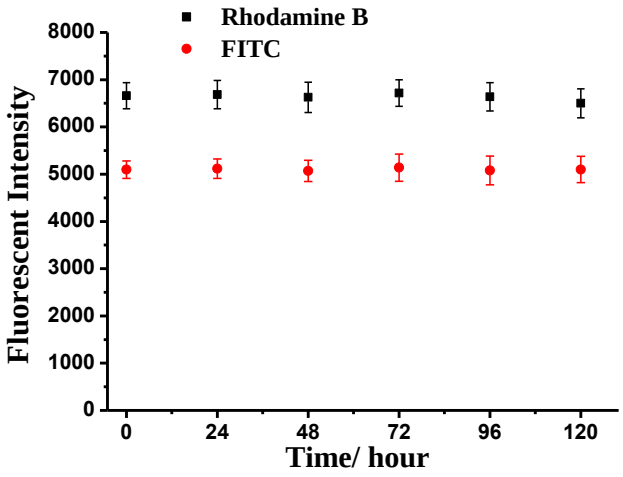

Figure 2.5: Fluorescence stability of the sensors over 5 days. (pH = 7.4, 34 ℃)

2.4.2 Responses of Rhodamine B to pH and temperature

The fluorescence responses of Rhodamine B to pH and temperature were measured in different pH solutions and at different temperatures. We define the fluorescence

intensity detected in a pH 5 solution at 32 ℃ as the basis point (F_0), and the relative fluorescence intensity (F) is the normalized value by comparing the measured fluorescence intensity (F_1) to the basis point (F_0). The unit of fluorescence intensity is arbitrary unit while the relative fluorescence intensity (F) is a non-dimensional value since it is the ratio of F_1 and F_0. ΔF is the change of relative fluorescence intensity (F), soΔF is also a non-dimensional value.

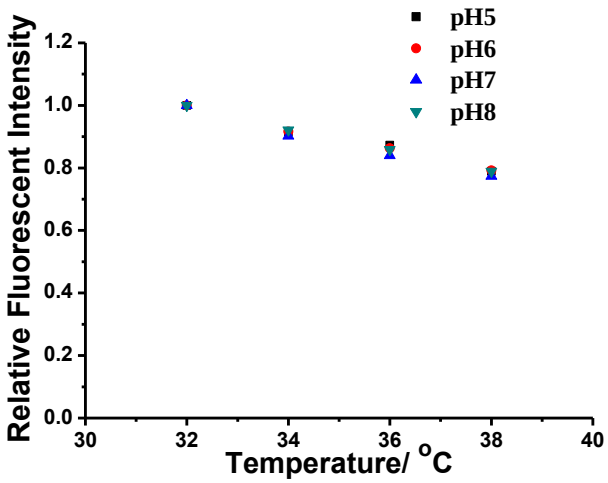

Figure 2.6: The response of Rhodamine B to temperature at different pH (5–8).

As shown in Fig. 2.6, the relative fluorescence intensity of Rhodamine B decreased as the temperature increased, and the sensitivities obtained in the different pH solutions were the same. It should be emphasized that Rhodamine B has an excellent linear relationship between its relative fluorescence intensity and temperature, and it is independent of pH [49]. Its relationship is shown in equation 2.2. The temperature information can be calibrated based on the fluorescence change in Rhodamine B using equation 2.2 and 2.3.

$$\Delta F_{R(Rho.B)} = -0.034 \cdot \Delta T \tag{2.2}$$

$$T_2 = {}^{\Delta F_{R(Rho.B)}}\!\!\diagup_{-0.034} + T_1 \tag{2.3}$$

T_1: the initial temperature, T_2: the temperature after change, ΔT: the temperature change

2.4.3 Responses of FITC to pH and temperature

According to the measurement procedure, the temperature of the chamber was increased from 32 to 38 ℃, and the fluorescence responses of FITC to temperature were measured in solutions with different pH values (5 – 8). Several curves of the relative fluorescence intensity based on the temperature in solutions with different pH values were obtained and are shown in Fig. 2.7. It can be seen in Fig. 2.7(a) that the relative fluorescence intensity of FITC decreases as the temperature increases in the range from 32 to 38 ℃, and a linear relationship between the relative fluorescence intensity and temperature was found and is expressed as equation 2.4. After a linear fitting of Fig. 2.7(a), the temperature sensitivities of FITC are shown in Fig. 2.7(b). It should also be noted that the temperature sensitivities of FITC are dependent on the pH, and the temperature sensitivity f (pH) in different pH is expressed by equation 2.5. It should be emphasized that FITC is dependent on both temperature and pH. The temperature sensitive of FITC is related with pH, and f (pH) is described as the temperature sensitivity of FITC in different pH.

Based on Fig. 2.7, the fluorescence responses of FITC to pH at different temperatures can also be obtained and are shown in Fig. 2.8. It is obvious that the pH sensitivity of FITC is also dependent on temperature. The pH information can be calibrated based on the relative fluorescence change of FITC using equation 2.6 and 2.8, and the pH sensitivity, g(T), related to temperature is expressed as equation 2.7. These linear relationships are necessary for the temperature compensation required for pH calibrations.

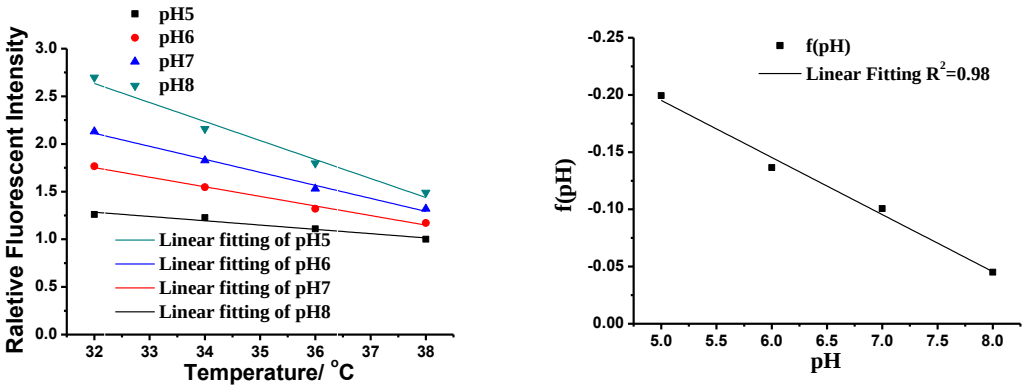

(a) (b)

Figure 2.7: (a) Responses of FITC to temperature at different pH values (5 – 8) (b) Temperature sensitivity of FITC at different pH values (5 – 8).

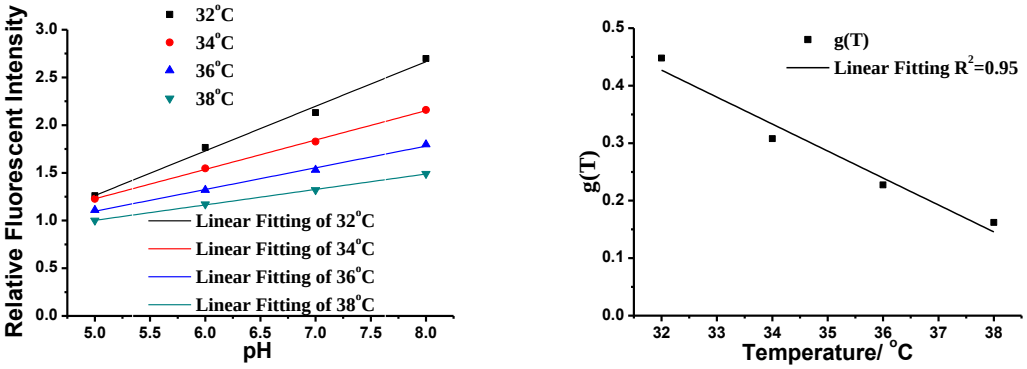

(a) (b)

Figure 2.8: (a) Responses of FITC to pH at different temperatures (32 – 38 ℃) (b) pH sensitivity of FITC at different temperatures (32 – 38 ℃).

$$\Delta F_{R(FITC)} = f(pH) * \Delta T \tag{2.4}$$

$$f(pH) = 0.0499 \cdot pH - 0.445 \tag{2.5}$$

$$\Delta F_{R(FITC)} = g(T) * \Delta pH \tag{2.6}$$

$$g(T) = -0.047 \cdot Temp. + 1.93 \tag{2.7}$$

$$pH_2 = \Delta pH + pH_1 = {}^{\Delta F_{R(FITC)}}\!/_{g(T)} + pH_1 \tag{2.8}$$

pH_1: the initial pH value, pH_2: pH value after change, ΔpH: the change in the pH value

2.4.4 Reversibility of FITC and Rhodamine B fluorescence responses to pH and temperature

We also detected the reversibility of FITC and Rhodamine B fluorescence responses to pH and temperature, respectively. The temperature was changed repeatedly by the heaters connected with the sample chamber, while the pH value of surroundings was changed by changing the buffer solutions of pH 5 and pH 8 repeatedly. For changing pH of surroundings, remove the original solution by micro pipet and then add new solution with different pH value by micro pipet. All the manipulations had to be done very slowly without washing away the adhered beads.

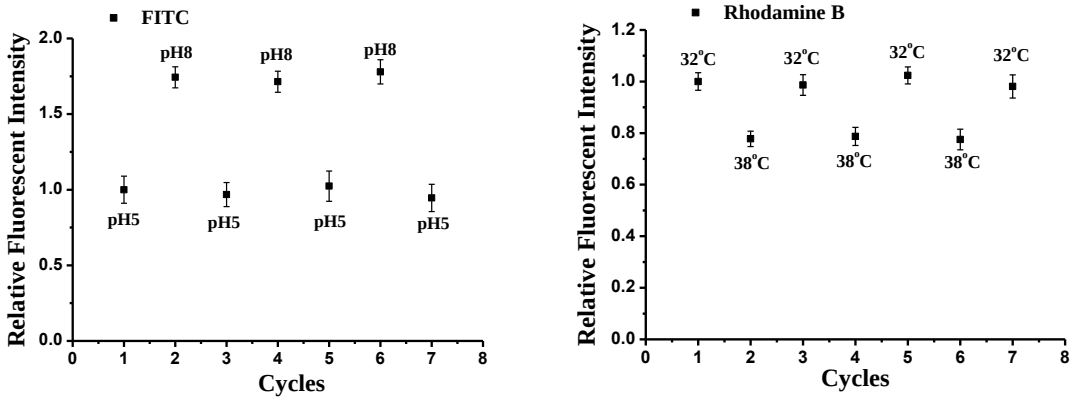

(a) (b)

Figure 2.9: Changes in the fluorescence intensity of the fluorescent sensor (a) for FITC (pH was repeatedly changed between 5 and 8 at 34 ℃) (b) for Rhodamine B (temperature was changed repeatedly between 32 and 38 ℃ in a pH 7.4 solution)

Fig. 2.9(a) shows the fluorescence intensity changes of FITC when the pH is repeatedly changed between 5 and 8. The results show that the fluorescence intensity of FITC reversibly changes based on the pH through at least four cycles. Similarly, Fig. 2.9(b) shows the fluorescence intensity change in Rhodamine B when the temperature is repeatedly changed between 32 and 38 ℃. The fluorescence intensity of Rhodamine B

is also reversibly changeable for a minimum of four cycles. This suggests that the fluorescent sensor possesses good reversibility towards pH and temperature changes.

2.4.5 Responses of the fluorescent micro-sensor to surrounding ionic strength

Salt concentrations have been reported to influence the absorbance and emission spectra of pH indicators [92]. To examine the effect of ionic strength on the optical properties of the fluorescent micro-sensor, the fluorescence intensity of FITC was measured in buffer solutions containing different concentrations of KCl (0, 100, 200, 300 mM) and NaCl (0, 100, 200, 300 mM). FITC, which is on the surface of the micro-sensor, is likely to be affected by the surrounding ionic strength. The responses of FITC to different ionic strength solutions were detected, and the results are shown in Fig. 2.10 as the average of ten beads. The results show that there were no significant changes in the relative fluorescence intensity of FITC in solutions with different concentrations of K^+ and Na^+. The optical properties of the fluorescent micro-sensor are not influenced by small changes in the ionic strength. This indicates that FITC is highly selective to pH and shows good applicability for pH sensing.

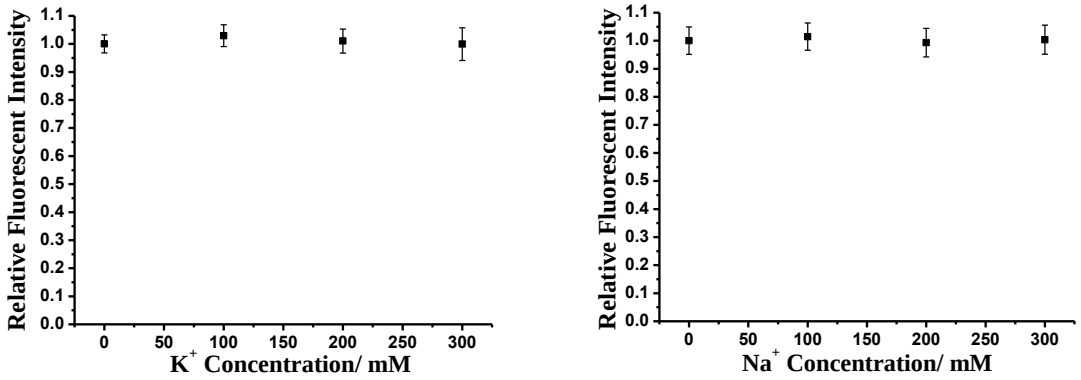

(a) (b)

Figure 2.10: Fluorescence responses of FITC in solutions (pH 7.4, 34 ℃) with different ionic strengths: (a) K^+: 0, 100, 200, 300 mM (b) Na^+: 0, 100, 200, 300 mM.

2.5 Applications of the micro-sensor

2.5.1 pH and temperature measurements by the micro-sensor using temperature compensation

In order to confirm the accuracy of the micro-sensor for pH and temperature change calibrations, the fluorescence responses of the sensor to changes in pH and temperature were measured. The pH values and temperature of the solution were changed as shown in Fig. 2.11 from (1) pH 8 and 32 ℃ to (7) pH 5 and 38 ℃ and then returned to (1) pH 8 and 32 ℃. The fluorescence responses of Rhodamine B and FITC to pH and temperature changes are shown in Fig. 2.12. Figure 2.12(a) shows that Rhodamine B only responds to temperature changes, which is consistent with the results in Fig. 2.6. Figure 2.12(b) also shows that a decrease in pH or increase in temperature can induce a decrease in the fluorescence intensity of FITC. Moreover, it can also be seen in Fig. 2.12 that the fluorescence intensities of Rhodamine B and FITC return to their original values after the pH and temperature parameters return to (1).

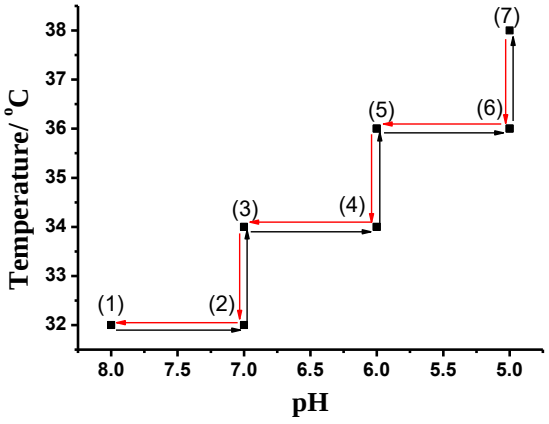

Figure 2.11: Experimental order: (1) pH 8 and 32 ℃, (2) pH 7 and 32 ℃, (3) pH 7 and 34 ℃, (4) pH 6 and 34 ℃,(5) pH 6 and 36 ℃, (6) pH 5 and 36 ℃, (7) pH 5 and 38 ℃, and the experimental cycle is changed from (1) to (7) and returned to (1).

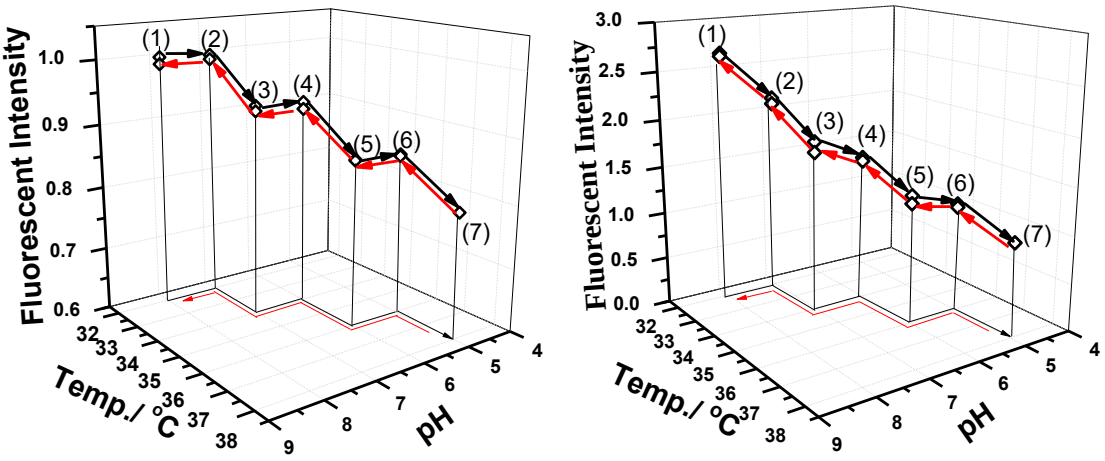

(a) (b)

Figure 2.12: Fluorescence responses of the sensor to pH and temperature changes (a) Rhodamine B (b) FITC (the experimental order is consistent with Fig. 2.11).

Based on the measured relative fluorescence intensity changes in Fig. 2.12 and equations 2.3 and 2.8, the temperature and pH values of the solutions can be calibrated. As shown in Fig. 2.13, based on the fluorescence changes in Rhodamine B (Fig. 2.13 (a)), the temperature was calibrated using equation 2.3. Figure 2.13(b) shows that the calibrated temperature values are consistent with the measured values, and the accuracy of the temperature calibration by Rhodamine B is within 0.1 ℃. For FITC, which can respond to both pH and temperature changes, temperature compensation was necessary for pH calibration to remove any interference from its temperature response. Its fluorescence change with pH and temperature is shown by the black data in Fig. 2.14(a). The fluorescence change of FITC caused by temperature changes can be calibrated using equation 2.4. Once the fluorescence change caused by the temperature was added to the black data, the fluorescence change of FITC with temperature compensation is shown as the red data. Based on the results of the relative fluorescence intensity changes in Fig. 2.14(a) and equation 2.8, the pH values of the solution, with and without

temperature compensation, were calibrated and are shown in Fig. 2.14(b).

We changed the experimental order and repeated the pH calibration. The pH value increased from 5 to 8 and then decreased back to 5, which was contrary to the pH change order in Fig. 2.11, and the temperature was increased from 32 to 38 ℃ and back to 32 ℃. The fluorescence responses of FITC to pH and temperature, with and without temperature compensation, are shown in Fig. 2.15(a), and the calibrated pH values based on the fluorescence changes of FITC are shown in Fig. 2.15(b). It is clear that the calibrated pH value with temperature compensation is consistent with the measured value. After temperature compensation by our proposed method, the pH accuracy based on the calibrated fluorescence change of FITC was improved from 1.5 to 0.2.

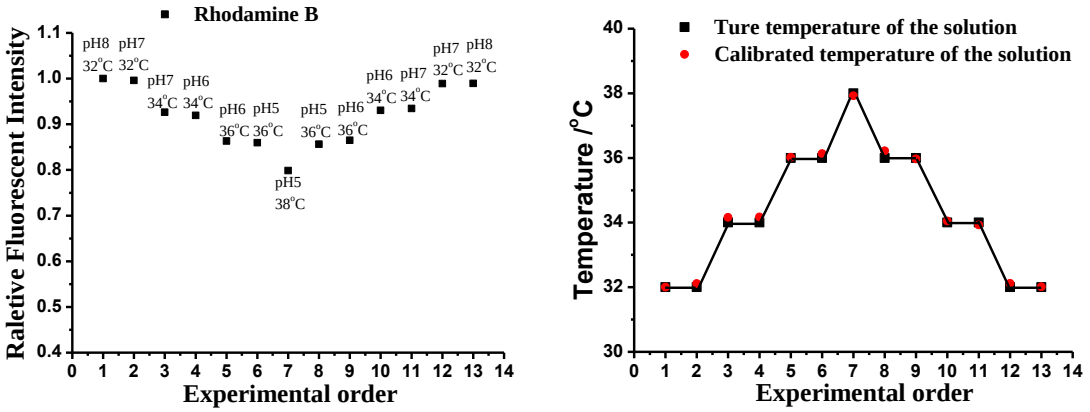

(a) (b)

Figure 2.13: (a) Fluorescence responses of Rhodamine B to temperature and pH (The experimental order is consistent with figure 2.11). (b) The measured and calibrated temperature values based on the fluorescence response results in (a).

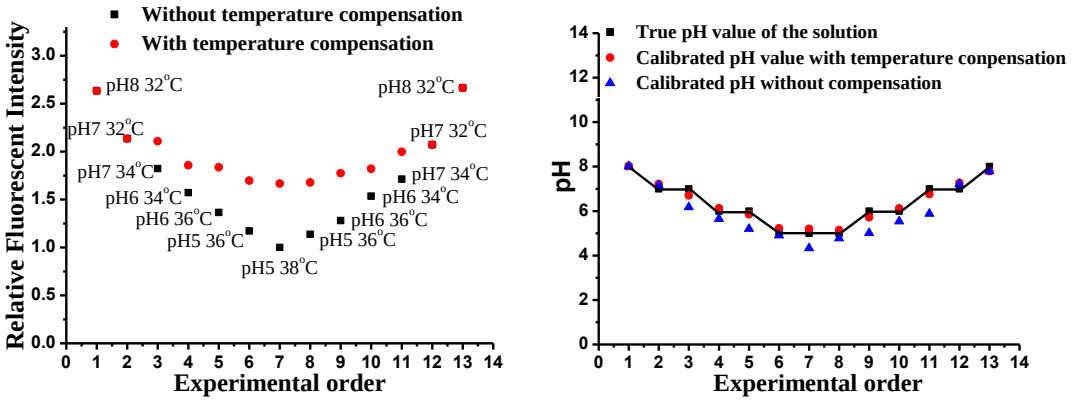

(a) (b)

Figure 2.14: (a) Fluorescence responses of FITC to temperature and pH (The experimental order is consistent with figure 2.11). (b) The measured and calibrated pH values based on the fluorescence response results in (a).

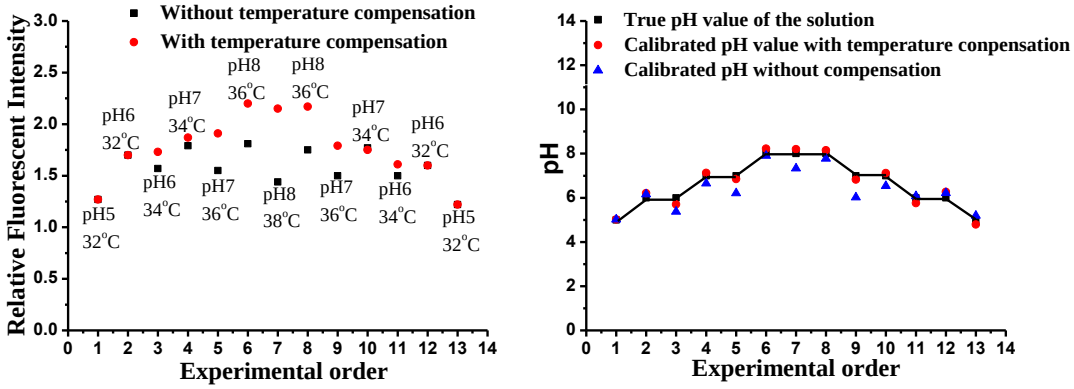

(a) (b)

Figure 2.15: (a) Fluorescence responses of FITC to temperature and pH. (The pH value increases from 5 to 8 and then decreases to 5, which is contrary to the order in figure 2.11). (b) The measured and calibrated pH values based on the fluorescence response results in (a).

2.5.2 The feasibility of applying the micro-sensor in cell measurement

As we know virus infected cells [93] show different pH value comparing with that of normal cells. So succeeding in measuring the temperature and pH changes of these cells

can help us to understand physiological and pathological processes of many diseases. In this paper, we propose that the fabricated multi-fluorescent micro-sensor based on polymeric microbeads can be applied in cell measurement in biological and medical applications.

In a real scenario, the sensor can be used in cells after sensitivity calibration. Firstly, a single sensor with a diameter of 1μm is successfully controlled and manipulated by optical tweezers. It can be transferred and adhere to the surface of a MDCK cell. In order to monitor the intracellular temperature and pH change, it is necessary to inject the sensor into a single cell. There are many technologies for sensor injection as I introduced in chapter one. So it is possible to measure the intracellular environmental changes. Actually, we always culture the cells in cell culture dish in incubator with a condition of 37 ℃ and CO_2 level of 5%. The medium pH as well as intracellular pH (cytoplasm) is about 7.4. So the initial condition of temperature and pH is already known before any changes happen in the cells. If any relative fluorescence change can be monitored, the temperature and pH changes can be calibrated. Furthermore, based on equation 2.3 and 2.8 which has been shown in the paper, the absolute temperatures and pH values can also be calibrated. It is anticipated to show cell measurement results in the near future.

2.6 Summary

We synthesized a novel multi-fluorescent micro-sensor based on polymeric microbeads that can simultaneously support pH and temperature sensitive FITC dye and temperature sensitive Rhodamine B dye on a single particle. Rhodamine B possesses high fluorescence emission at an excitation wavelength of 561 nm and shows good fluorescence responses to temperature in the range of 32 – 38 ℃. The calibrated

sensitivity of Rhodamine B is -3.4%/℃, with a temperature accuracy of 0.1 ℃. FITC possesses high fluorescence emission at an excitation wavelength of 488 nm and shows good fluorescence responses to solution pH. Because temperature can also affect the fluorescence change of FITC, we proposed a method to perform a temperature compensation for pH calibration. After the temperature compensation by our proposed method, the calibrated pH value based on the fluorescence change in FITC was consistent with the measured value. The pH accuracy was improved from 1.5 to 0.2. This micro-sensor has high selectivity for pH and temperature, good stability, and a high tolerance for ionic strength, making it suitable for cellular measurements. The sensor is based on a single microbead, which would only be a small stimulus to cells. For cell measurements, the biocompatibility of this sensor will be investigated in future. On the other hand, the novel fluorescent micro-sensor not only can be used in cell measurement, but also sensing in other close micro-environments, such as micro chamber and microfluidic chip. It can provide low contamination and high accuracy for local condition measurement in micro-environments.

Chapter 3

pH and temperature measurements of virus-infected cell by micro- sensors

3.1 Introduction

A virus must use cell processes to replicate. Figure 3.1 shows the viral infection steps in the virus replication cycle: the virus enters the cell, reproduction and assembly of viral components and new viruses leave the cell. Multiplication of the influenza virus requires metabolites (nucleotides, amino acids, etc.) and the cellular machinery to synthesize its genome and proteins, thereby producing viral particles. Infection by the influenza virus activates several metabolic systems in cells, which consume or generate large amounts of energy. Thus, it is considered that the viral multiplication processes involved in both genome replication and transcription require large numbers of nucleotides. The high level consumption of nucleotides generates large amounts of energy, some of which is converted into heat energy. Therefore, this heat energy may increase the temperature of cells. On the other hand, the M2 protein is a minor

component of the membrane of influenza A virus. Inhibition of the function of the M2 protein by amantadine can cause a conformational change in the haemagglutinin (HA) of H7 influenza A virus and the consequent expression of the low pH form of the glycoprotein on the surface of virus-infected cells [20]. To address this question, we propose to use the multi fluorescent micro sensor which can respond to pH and temperature changes to measure the temperature and pH changes of influenza virus-infected and uninfected cells on the surface.

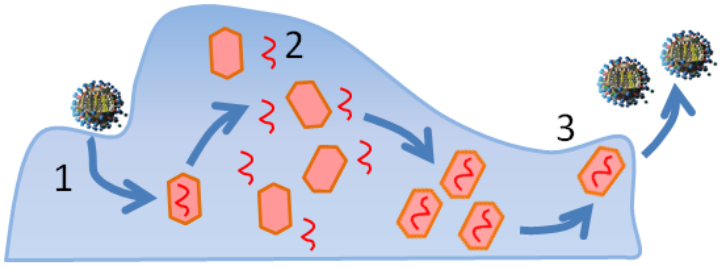

Figure 3.1: viral infection steps in the virus replication cycle. 1 the virus enters the cell, 2 reproduction and assembly of viral components, 3 new viruses leave the cell.

3.2 Materials and methods

3.2.1 Cell culture

Madin-Darby canine kidney (MDCK) cells were used for experiments. Before injection experiment, the cells are cultured in glass base dish (Φ3cm, ASAHI GLASS CO. LTD. JAPAN) in the incubator with a condition of 37 ℃ bubbled with 95% air, 5% CO_2 gas. Minimum essential medium eagle is used as cell medium containing 10% fetal bovine serum (FBS).

3.2.2 Fluorescent labeling of virus

Influenza virus A/PR/8/34 (wild type) was propagated in 10-day-old embryonated chicken eggs. The viral titer was determined using a plaque assay and by measuring the

hemagglutinin (HA) activity by titrating against chicken erythrocytes (Nippon Bio-Test Laboratories, Tokyo). Before they were used to label the virus particles, DiI and Syto21 (Invitrogen/Life Technologies, USA) were dissolved in dimethyl sulfoxide and diluted in phosphatebuffered saline (PBS) to a final concentration of 2 μg/mL. Influenza virus (in allantoic fluid) was incubated with either DiI or Syto21 for 30 min at room temperature. The virus solution was then applied to a spin column containing Sephadex G50 beads (Pharmacia, USA) and centrifuged for 2 min at 700 × g to remove excess dye. The flow-through fraction was then used in the subsequent experiments. Figure 3.2 shows the fluorescence of virus stained by Syto21 observed by a mercury lamp. The arrows are pointing at fluorescent virus. It suggests that the virus has been stained successfully.

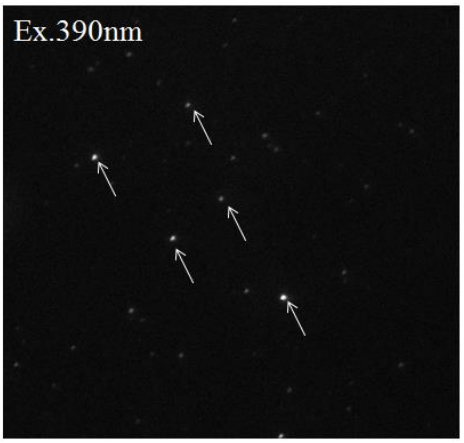

Figure 3.2: The fluorescent labeling result of virus by Syto21 observed by a mercury lamp. The arrows are pointing at fluorescent virus.

3.2.3 Virus infection and micro-sensor adhesion

Influenza viruses labeled with Syto21 at MOI of 1 were allowed to adhere to H292 cells for 15 min at 34℃ in serum-free medium. After 15 min, the virus had bound to the cell membrane but not all, and the serum-free medium was replaced with medium

containing serum.

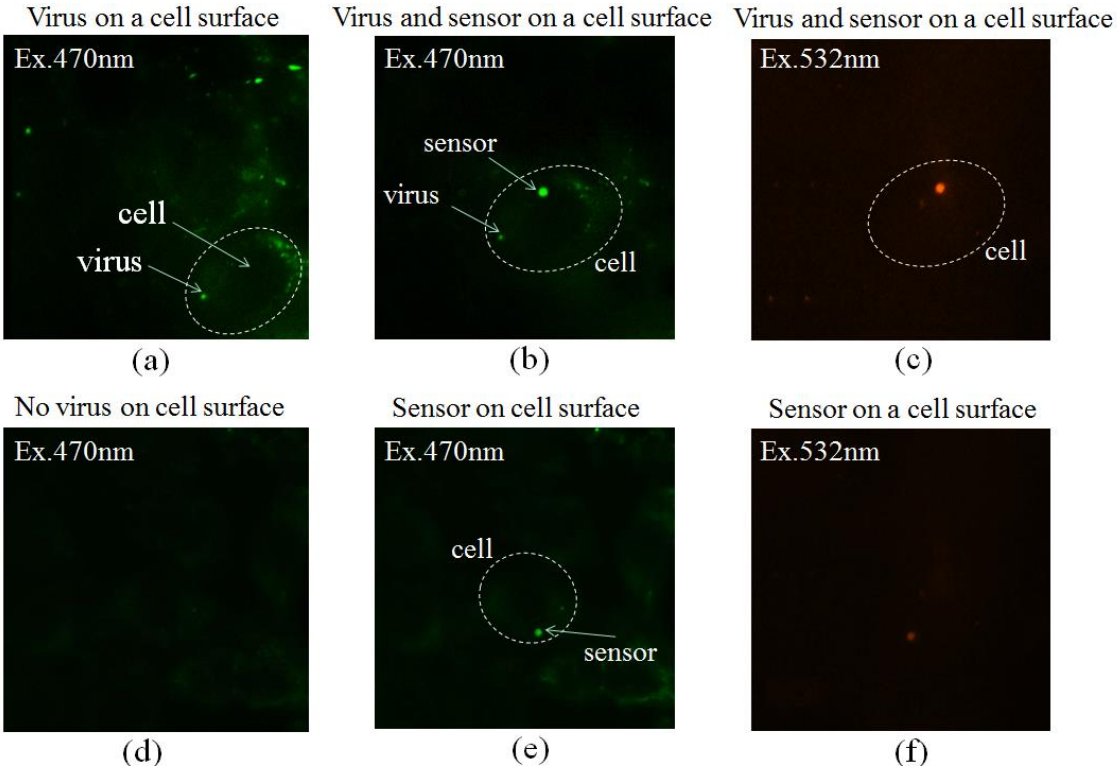

Figure 3.3: (a) Virus bound on cell surface. (b) A micro sensor adhered on the same cell with a virus on its surface, with an excitation of 470nm laser. (c) A micro sensor adhered on the same cell with a virus bound on its surface, with an excitation of 532nm laser. (d) Virus-unbound cell. (b) A micro sensor adhered on a virus-unbound cell, with an excitation of 470nm laser. (c) A micro sensor adhered on a virus-unbound cell, with an excitation of 532nm laser.

Figure 3.3 (a) and (d) show virus-bound and virus- unbound cells, respectively. The fluorescent sensor was then attached to virus-bound and virus- unbound cells using optical tweezers (Fig. 3.3 (b) and (e)), and the intensities of Rhodamine B and FITC fluorescence were measured using a Nikon TiE microscope fitted with a ×100 objective lens. All these experiments were carried out in the CO_2 incubator (Tokai Hit, Japan) setting on the stage of microscope. The sensor and virus that adhered on the surface of a same cell can be distinguished by not only their different size, but also that the sensor

can show fluorescence of Rhodamine B under excitation of 532nm while Syto 21 of virus cannot be excited by 532nm laser. Figure 3.3 (c) and (f) show the fluorescence of Rhodamine B contained in the sensor, at the same time, no fluorescence has been observed from virus.

3.3 Results

3.3.1 Temperature changes of cell after virus infection

The temperatures and pH in virus-bound cell (Fig. 3.3 (a)) and virus-unbound cell (Fig. 3.3 (d)) were determined using a fluorescence microscope by monitoring the changes in the intensity of fluorescence. The intensity was measured at the center of the sensor because the cells moved during the experiment. Figure 3.4 shows the fluorescence intensity changes of Rhodamine B of the sensor adhered on the surface of virus-bound cell and virus-unbound cell. The temperature changes can be calculated using equation 2.2 and 2.3. Figure 3.5 (a) shows that the temperatures of the virus-bound cells increased gradually with time. The temperature measured in influenza virus-bound cells increased by about 5℃ at 4 hour post infection (hpi). However, no increases were detected in the cell that did not bind influenza virus (Fig. 3.5 (b)).

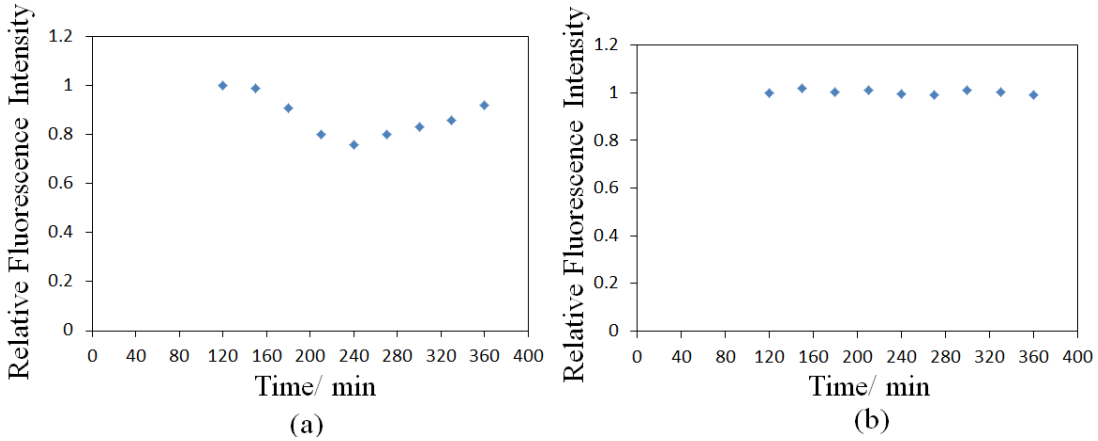

Figure 3.4: The fluorescence intensity changes of Rhodamine B started from 2 hpi of (a) virus-bound cell and (b) virus-unbound cell.

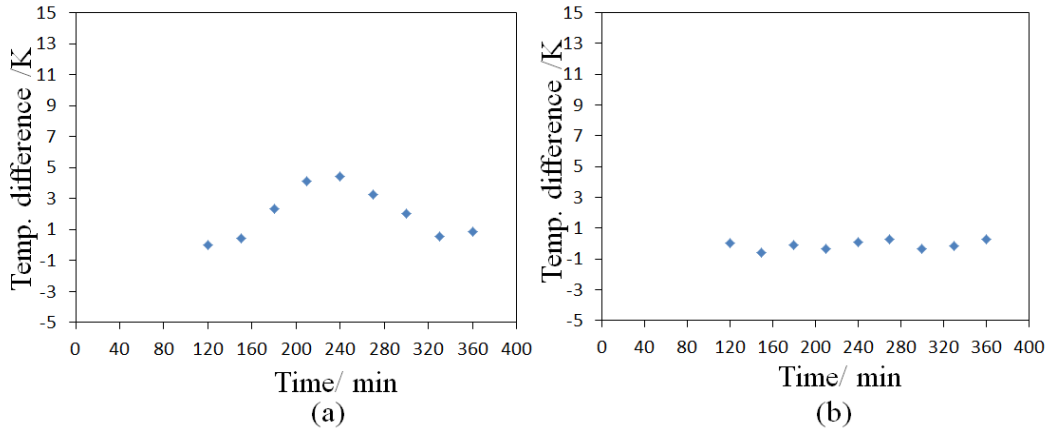

Figure 3.5: The surficial temperature changes of (a) virus-bound cell and (b) virus-unbound cell calculated from the fluorescence changes in Fig.3.4.

3.3.2 pH changes of cell after virus infection

Figure 3.6 shows the fluorescence intensity changes of FITC of the sensor adhered on the surface of virus-bound cell and virus-unbound cell. There is no obvious fluorescence change of FITC of the sensor adhered on virus-unbound cell as shown in Fig. 3.6 (b), and fluorescence changes of FITC have been detected of the sensor adhered on virus-bound cell (Fig. 3.6 (a)). As I discussed in chapter 1, both the changes of pH and temperature can induce the fluorescence intensity changes of FITC. So the fluorescence intensity changes of FITC in Fig. 3.6 (a) include two parts: the fluorescence changes induced by pH change and temperature change. pH changes of virus-bounded cell can be calculated based on the fluorescence changes result in Fig. 3.6 (a) by equation 2.7 and 2.8 with temperature compensation. The temperature information has been shown in Fig. 3.5 (a). After temperature compensation, the fluorescence change of FITC induced by temperature can be removed, and pH changes of the cell can be calculated as shown in Fig. 3.7. The pH measured in influenza virus-bound cells decreased by approximately 0.55 at 4 hour post infection (hpi). However, no decreases were detected

in the cells that did not bind influenza virus (Fig. 3.7 (b)). The temperatures and pH in each of 8 virus-bound and 10 -unbound cells have been determined by monitoring the changes in the intensity of fluorescence and the results are shown in Fig. 3.8. The temperature measured in influenza virus-bound cells increased by approximately 4.2 ℃ while the pH decreased by approximately 0.56 at 4 hour post infection (hpi). No obvious changes in temperature and pH have been detected on virus-unbound cells.

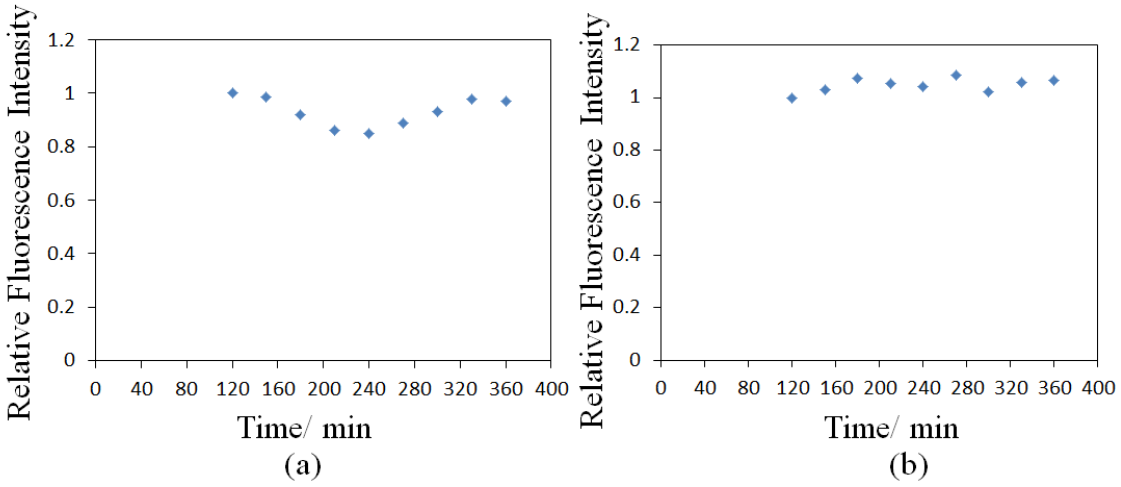

Figure 3.6: The fluorescence intensity changes of FITC started from 2 hpi of (a) virus-bound cell and (b) virus-unbound cell.

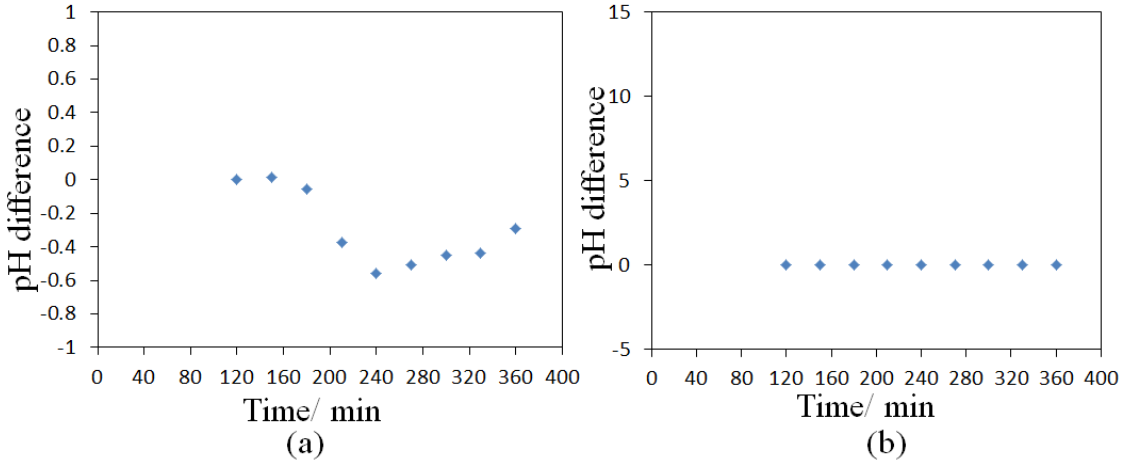

Figure 3.7: The surficial pH changes of (a) virus-bound cell and (b) virus-unbound cell calculated from the fluorescence changes in Fig.3.6.

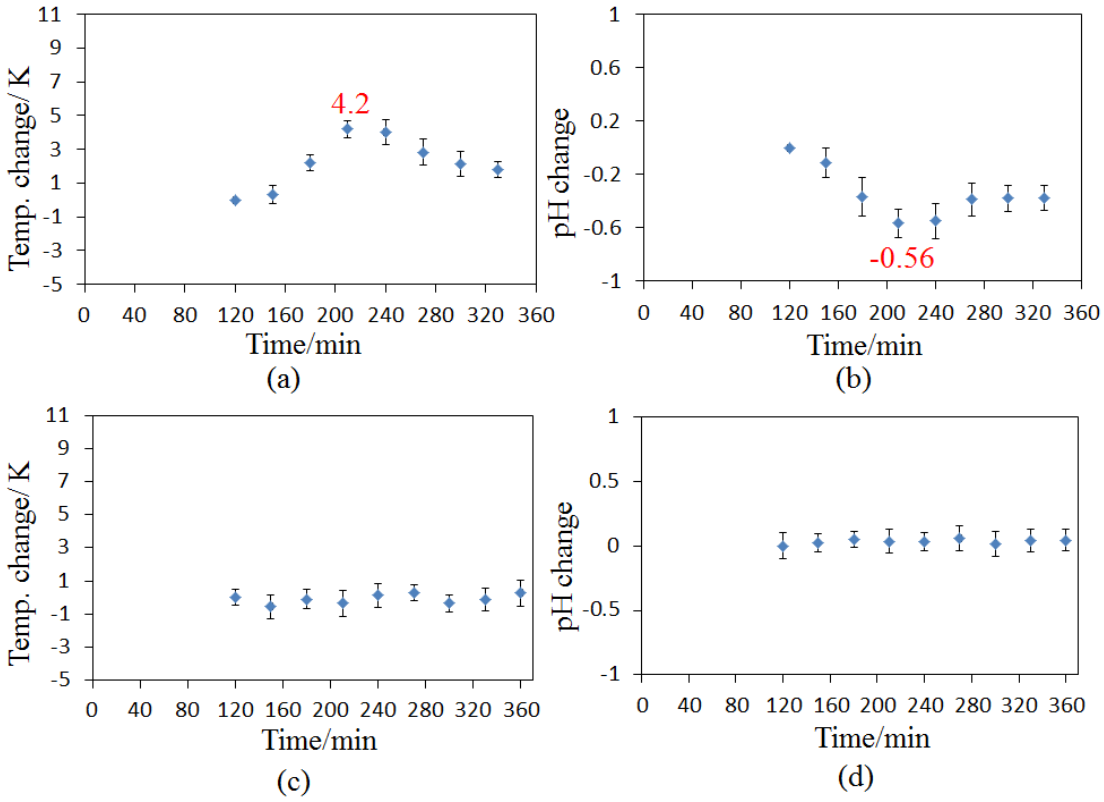

Figure 3.8: The average of pH and Temp. changes of virus-infected and –uninfected cell calculated by the fluorescence intensity changes of the fluorescent sensor adhered on cell surface, n=10. (a) Temperature changes of virus-infected cell. (b) pH changes of virus-infected cell. (c) Temperature changes of uninfected cell. (d) pH changes of uninfected cell.

3.4 Immunostaining of the cells

3.4.1 Methods

Cells with or without attached virus were immunostained with anti-PB1. In brief, 5 hours after measuring the intensity of fluorescence by the temperature sensor on the cells, the cells were washed three times with PBS, fixed with 4% paraformaldehyde solution at room temperature for 10 min, washed with PBS three times at room temperature, treated with 0.5% Triton X-100 for 5 min at room temperature, and blocked with 1% bovine serum albumin (BSA) in PBS. After blocking, the cells were

incubated with anti-PB1 antiserum for 1 h at 37 ℃, washed with 1% BSA/PBS solution, incubated with anti-rabbit IgG conjugated with Alexa 488 for 1 h at 37 ℃, and observed under a microscope fitted with a ×100 objective lens (Zeiss LSM 510 META).

3.4.2 Results

To confirm viral replication in the cells that changed the temperature and pH of cells, the cells were immunostained with anti-PB1 antiserum after measuring the cell temperature and pH. As shown in Fig. 3.9, we detected the PB1 subunit in the nucleus of cells that exhibited temperature and pH changes, but not in cells where the temperature and pH remained constant. These results suggest that influenza virus replication induces temperature and pH changes in cell. This system did not allow us to measure the temperature and pH inside the cell directly because we could not introduce the temperature sensor into the cytoplasm. At present, we are constructing a sensor that can be introduced into the cytoplasm. However, the data from the membrane-bound sensor clearly demonstrated that there was a difference in temperature and pH between the influenza virus-infected and uninfected cells. Thus, we performed a further experiment to understand the temperature increase and pH decrease in cells in which the influenza virus replicated.

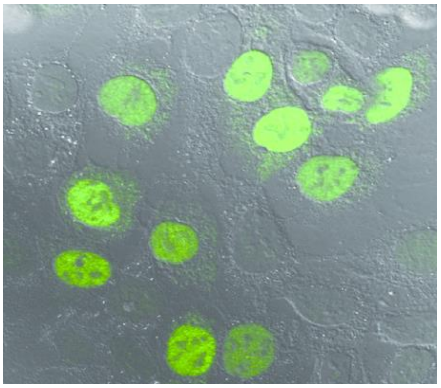

Figure 3.9: Immunostaining result: virus-infected and -uninfected cells were detected using anti-PB1 serum and an anti-rabbit IgG labeled with Alexa 488(Invitrogen, USA).

3.5 Discussions

In this study, we focused on the measurements of temperature and pH changes of influenza virus-infected cells. First, we found that the temperature of influenza virus-infected cells increased comparing with that of virus-uninfected cells. Many researches have studied that large amounts of RNA are synthesized within a short period after the influenza virus enters cell, and thus, the rate of ATP consumption should be higher in influenza virus-infected cells than that in uninfected cells. The multiplication of the virus requires large amounts of nucleotides to synthesize virus-related RNA, so the higher ATP consumption rate in influenza virus-infected cells may increase the temperature compared with that in uninfected cells, where the energy produced by ATP hydrolysis to synthesize RNA may increase the temperature rather than being used for metabolism. Liu Y et al. reported that intracellular mitochondria level and mitochondrial membrane potential is correlated [94]. Ando et al. recently showed that the ATP level in cells infected with hepatitis C virus (HCV) decreased in the cytoplasm according to an ATP indicator based on Föster resonance energy transfer. They observed a dot-like structure produced by enriched ATP. In HCV-infected cells, the ATP level decreased, and they concluded that HCV RNA replication consumed large amounts of ATP [95]. It is considered that a higher rate of ATP consumption compared with metabolism in the cell increases the temperature of the cell. Further studies will be required to determine whether the temperature differs among different cell organs during influenza virus infection.

We also found that the pH of influenza virus-infected cells decreased comparing with that of virus-uninfected cells. It should be related with the functions of the virus components in host-cell. Influenza A which was used in our research contains two major

envelope glycoproteins, haemagglutinin (HA) and neuraminidase (NA) [96]. Figure 3.10 shows the structure of the influenza virus A and virus replication cycle in host-cell. The HA and NA are important in the immune response against the virus. HA is responsible for infectious entry of the virus into cells, and it is also the virus' most important surface antigen. NA cleaves the sialic acid receptor, thus releasing progeny virus from the infected cell surface. Also embedded in the lipid membrane is the M2 protein, which is the target of the antiviral drugs – amantadine and rimantadine (Structure of the amantadine binding site of influenza M2 proton channels in lipid bilayers). Beneath the lipid membrane is a viral protein called M1, or matrix protein. This protein, which forms a shell, gives strength and rigidity to the lipid envelope. The well characterized M2 viroporin of influenza virus plays roles both during viral entry and egress. During entry, the M2 proton channel shunts H+ from the acidic endosome to the virion interior, leading to the membrane fusion and then release of the genome as well as H^+ initiating. With the release of H^+ to cytoplasm, it always results in pH decrease in cytoplasm. In certain subtypes, M2 also equilibrates the intraluminal pH of the trans-Golgi network with the cytoplasm, preventing premature conformational changes in the viral haemagglutinin (HA) during exit [97]–[99]. It always leads to pH increase inside trans-Golgi network and pH decrease in cytoplasm. As a conclusion, the M2 protein is largely responsible for the reduction in intracellular pH of virus-infected cells.

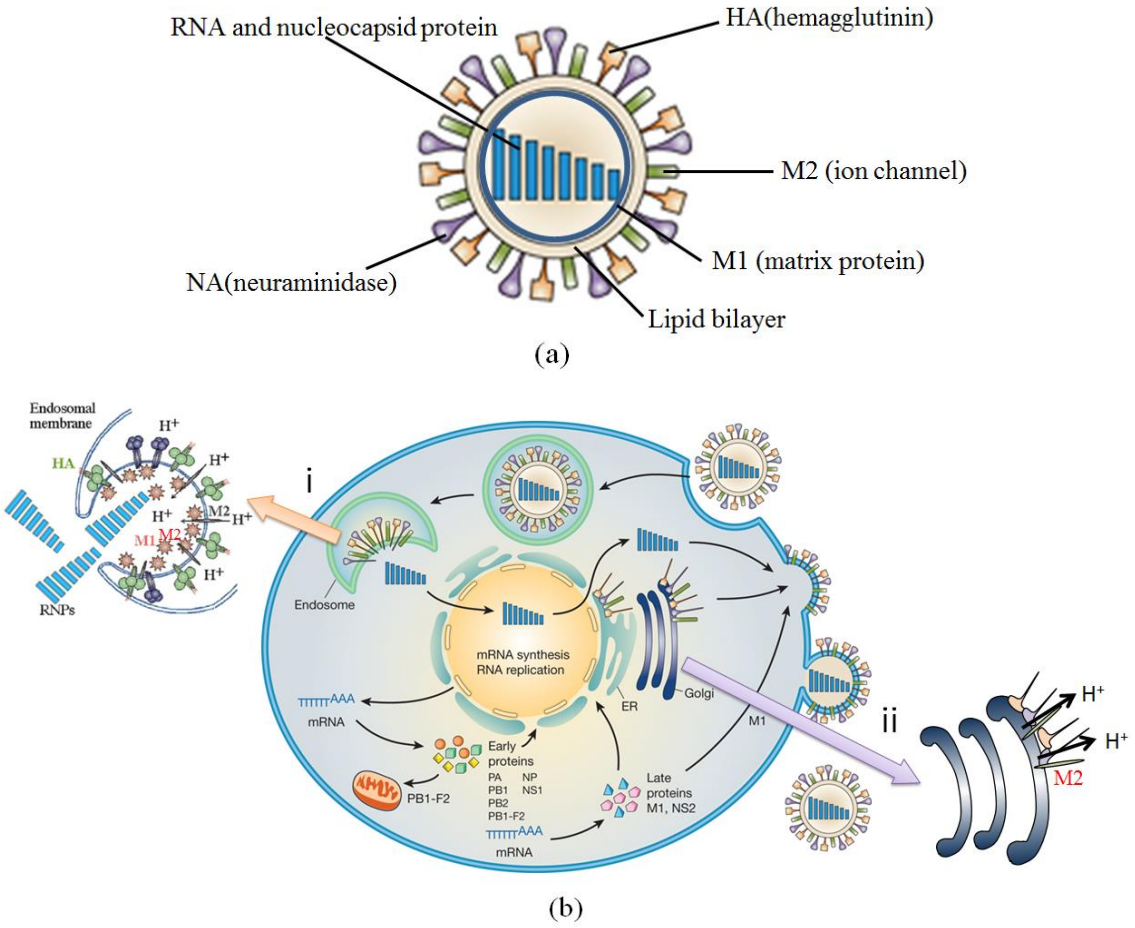

Figure 3.10: (a) Structure of influenza virus A, (b) Virus infection into a cell and virus replication cycle, i: M2 proton channel transfers H+ from the acidic endosome to the virion interior, ii: M2 also equilibrates the intraluminal pH of the trans-Golgi network with the cytoplasm. [100]

Okabe et al. recently showed that the intracellular temperature differs among organs by using a fluorescent polymeric thermometer and fluorescence lifetime imaging microscopy to map the temperature inside cells [16]. This system involves increasing the temperature outside cell and measuring the rise in the temperature inside the cell. The temperature outside cells did not have equal effects inside the cell, and it was suggested that the difference of temperature among organs was influenced by fundamental of cell processes. Unfortunately, the multi sensor that was used in our

experiments was placed on the cell membrane, so the results cannot describe the cell activities inside the cell accurately. Therefore as mentioned earlier, it is necessary to develop a system that can measure the temperature and pH in the cytoplasm. On the basis of our discovery that the temperature increases and pH decreases in influenza virus-infected cells, we can also examine the temperature and pH of other virus-infected cells. We consider that the temperature and pH changes in virus-infected cells may differ among viruses. Thus, further studies will be required to understand the virus specificity of temperature increases.

3.6 Summary

We prepared a tool based on Rhodamine B fluorescence, and we successfully used to measure the temperature and pH of influenza virus-infected and uninfected cells. The fluorescent sensor was attached to virus-bound and virus-unbound cells. The temperatures and pH in virus-bound cell (Fig. 3.3 (a)) and virus-unbound cell (Fig. 3.3 (d)) were determined using a fluorescence microscope by monitoring the changes in the intensity of fluorescence. We found that influenza virus multiplication increased the temperature of cells by approximately 4–5℃ and decreased the pH of cells by approximately 0.5-0.6. The increase in cellular temperature during infection by influenza virus may be due to the massive consumption of ATP over a short period. The decrease in pH should be related with the functions of the virus components in host-cell. Especially, M2 protein on virus surface plays an important role in both during viral entry and egress and is closely related with the pH decrease in cytoplasm.

Chapter 4

Vibration-assisted optical injection of a single fluorescent sensor into a target cell

4.1 Introduction

The multi sensors have been placed on the membrane of virus-infected and virus-uninfected cells to measure the temperature and pH changes of the cells, but the results cannot describe the cell activities inside the cell accurately. Therefore it is necessary to develop a system that can measure the temperature and pH in the cytoplasm. An accurate method of measuring intracellular temperature and pH could thus help clarify intricate cellular processes and develop new applications in biology and medicine. In order to pass through the cell membrane and measure local intracellular conditions, effective and rapid injection technologies with low stimulus to the target cell are in great demand.

Spiropyran is a type of organic chemical compound, known for photochromic properties that provide this molecule with the ability of being used in medical and

technological areas. There have been many studies on photochromism in spiropyrans [101]. Optical tweezers, which are arguably the most versatile single-molecule manipulation technique, are widely used in single-molecule measurements, optical injection of small particles, and cell palpation. In order to realize selective adhesion and quantitative injection of a single sensor on cell surface, in this study, we introduced liposome layers containing photochromic material (spiropyran) on the surface of the micro-sensor. Zeta potential of the liposome layers can be switched between negative and positive by photoisomerization of spiropyran. Then we propose rapid injection of fluorescence sensors into a target cell by applying local vibration stimulus using optical tweezers. We also compare the results of rapid injection with those of injection without any stimulus on the cell membrane.

4.2 Concept of rapid injection by optical tweezers with local vibration stimulus

Figure 4.1 shows the principle of the rapid optical injection of a single sensor into a cell using optical tweezers. Before the injection experiment, the surface of the sensor was modified by functional liposome layers. Lipofection, as shown in Fig. 1.12, is a technique used to inject biological particles into a cell by means of liposomes, which can easily merge with the cell membrane since they are both made of a phospholipid bilayer. So the sensor encapsulated in liposome could be delivered into cytoplasm by lipofection. Furthermore, we applied vibration stimulus using optical tweezers on the liposome-encapsulated sensor to promote the membrane fusion process. In the optical tweezers, a small object is trapped by the force of radiation pressure exerted by a focused laser beam [102]. Radiation force can hold the object and translate it with high

spatial resolution in the sub-micrometer scale. We took advantage of the optical tweezers and drove them to move up and down circularly near the sensor, which has adhered to the cell membrane. A periodic trapping force was experienced by the sensor, which was similar to a vibration on the sensor and cell membrane. G. Apodaca and the coworkers had done the research on the mechanical stretch-regulated exocytosis/endocytosis in bladder [103]. They found that the stretch on umbrella cell membrane could enhance both exocytosis and incorporation of vesicle cargo into the apical membrane. So the vibration stimulus on the sensor and local cell membrane in our study could probably promote lipid fusion between liposome layers on the sensor and cell membrane and induce a rapid injection of the sensor into the cell.

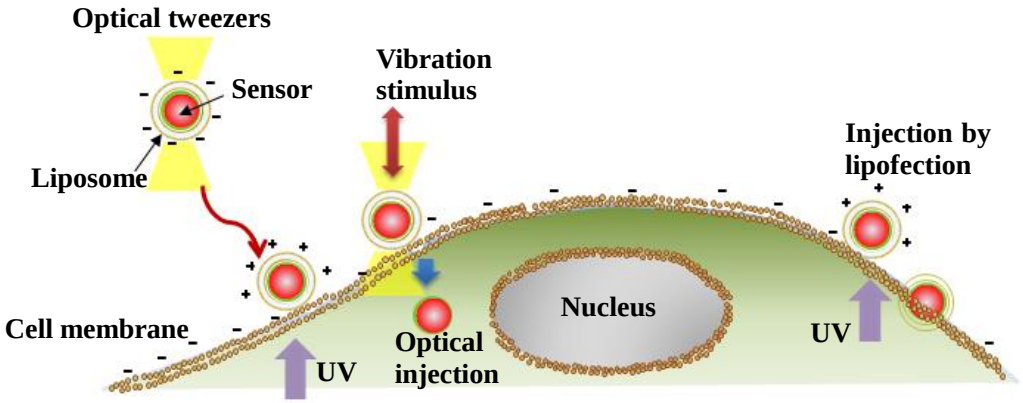

Figure 4.1: A schematic diagram of selective adhesion and rapid injection of a fluorescent sensor into a target cell using local mechanical stimulus applied by optical tweezers.

4.3 Encapsulation of the micro-sensor by functional liposomes

4.3.1 Materials

Polystyrene (PS) microbeads with amino group-modified surfaces (1 μm in diameter, manufactured by Polysciences Inc.) were used as the sensor carriers. Two indicators (Rhodamine B and FITC) were used to stain the PS microbeads. 1,2-dipalmitoyl-sn-glycero-3-phosphatidylcholine (DPPC) and 1,2-dipalmitoyl-sn-

glycero-3- phosphatidylglycerol (DPPG) were used as liposomes (manufactured by NOF CORPORATION). DPPC is a cationic liposome and DPPG is an anionic liposome. 1',3',3'-Trimethyl-6-nitrospiro [1(2H)-benzopyran-2,2'-indoline] (SP) (Tokyo Chemical Industry Co., Ltd.) was used as the photochromic material that was mixed with the liposomes.

Madin-Darby canine kidney (MDCK) cells were used for experiments. Before injection experiment, the cells are cultured in glass base dish (Φ3cm, ASAHI GLASS CO. LTD. JAPAN) in the incubator with a condition of 37 ℃ bubbled with 95% air, 5% CO_2 gas. Minimum essential medium eagle is used as cell medium containing 10% fetal bovine serum (FBS). For injection experiment, the glass dish containing cells is moved to experimental chamber in the experimental system. The temperature in the chamber is controlled to 37 ℃ with a gas injection of CO_2. The condition in the chamber is suitable for cell culture which makes it possible to be used for experiment.

4.3.2 Preparation of lipid vesicles

In order to encapsulate the sensor using liposome layers, we first prepared lipid vesicles as follows. The lipids and spiropyran (SP) were first mixed in test tubes with chloroform solutions (C_{lipids} = 0.2 mM, C_{SP} = 0.04 mM). To form dry lipid films, the mixtures were dried in an evaporator under a water-heating temperature of 40 ℃. The thoroughly dried lipid films were hydrated in deionized (DI) water to form multi-lamellar vesicles (MLVs) and then transformed into small unilamellar vesicles (SUVs) by sonication (60 min, 50 W, 0.4 s pulse). The resulting solution was strained through a filter with a pore size of 0.4 μm.

4.3.3 Encapsulation of the micro-sensor by functional liposomes

Figure 4.2 shows the encapsulation process of the individual sensor in lipid layers

fabricated via the layer-by-layer method. Bilayers were assembled on the beads via the same vesicle adsorbing/spreading process as reported by J.T. Groves and coworkers [104]. The fabricated fluorescent sensors were suspended in DI water with a final concentration of 0.5 wt%. The sensor (100 μL in volume) and the SUV solution (900 μL in volume) were combined in a small centrifuge tube, and the mixture was subjected to pulse vortex. Excess vesicles were removed by rinsing several times with DI water. After removing all of the DI water, 1 mL of $CaCl_2$ solution (100 mM) was added to the same tube, as calcium ions could induce the fusion of SUVs, and a solid supported membrane was formed on the beads. A double-lamellar layer of positively charged DPPC was first prepared on the surface of the sensor, and then negatively charged DPPG was coated on the outside of DPPC, as shown in Fig. 4.2.

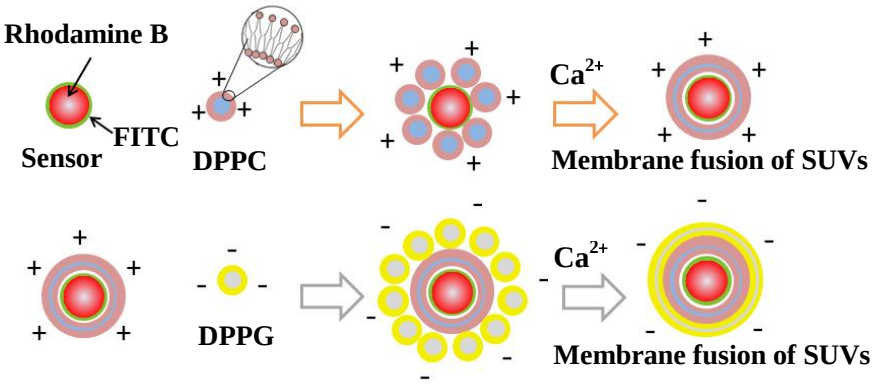

Figure 4.2: Encapsulation of the sensor into the liposomes.

4.3.4 Surface charge control of the sensor by photoreaction of spiropyran

We used the zeta potential control for selective adhesion of sensors to the cell membrane, not for cell injection experiment. If the sensor was encapsulated by positive-charged DPPC liposome, many DPPC-coated sensors will adhered on negative-charged cell membrane without control. So in our research, we have coated the

sensors with negative-charged DPPG liposome which is also containing spiropyran. Spiropyran (SP), which is a type of photochromic material [105], was included in the lipid layers. While SP was isomerized into a colored zwitterionic structure (merocyanine, MC type) by UV illumination, the isomerized SP was isomerized back into a colorless non-ionic structure (SP type) by visible light illumination, as shown in Fig. 4.3 (a).

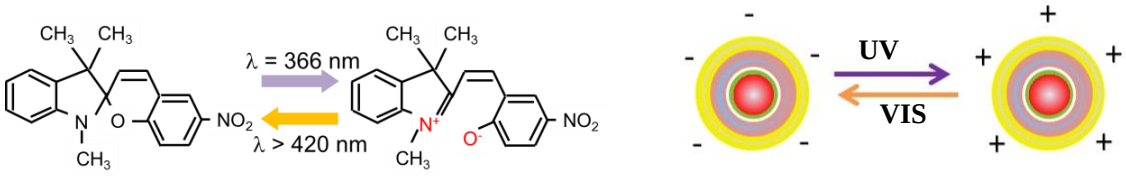

(a) (b)

Figure 4.3: Optical control of surface charge of liposomes by photo-isomerization action. (a) Isomerization of spiropyran by UV/VIS illumination. (b) Control of the surface charge of liposomes by UV/VIS illumination.

The widespread utility of the spiropyran switch lies in the fact that the SP and MC isomers have vastly different physicochemical properties. This structural change facilitated the optical control of zeta potential. The zeta potential of the liposome layers can be switched from negative to positive under UV irradiation as shown in Fig. 4.3 (b). After transform a single sensor to the surface of the cell and irradiate the sensor by UV, the UV-irradiated-DPPG-coated positively charged beads can adhere on the negatively charged cell membrane. Selective adhesion of sensor on cell membrane can be realized by this method without excess sensor adhesion. Most animal cells, for example Madin-Darby canine kidney (MDCK) cells [106], possess negative surface potential. Therefore, we could regulate the adhesion of a single sensor to the cell surface via the optical control of zeta potential. In our study, we measured the zeta potential of PS beads, amino-PS beads, DPPC liposomes with SP, and DPPG liposomes with SP using a

zeta potential analyzer at an illumination wavelength of 600 nm (Zetasizer Nano ZS, Malvern).

4.3.5 Mechanism of fluorescence resonance energy transfer (FRET)

Fluorescence resonance energy transfer (FRET) is the physical phenomenon of the radiationless transfer of energy between two light-sensitive molecules [107]. Fluorescence energy transfer occurs via the overlapping of the spectrum of a fluorophore (donor) with the absorption spectrum of a molecule (acceptor), as shown in Fig. 4.4. The excited donor fluorophore emits a virtual photon that is instantly absorbed by the acceptor molecule. According to the theory of fluorescence resonance energy transfer [107], the transfer energy is very sensitive to the distance between the donor and the acceptor, as described in equation 4.1.

$$E = 1 - \frac{F}{F_o} = \frac{R_o^6}{R_o^6 + r_o^6} \tag{4.1}$$

F and F_0 are the fluorescence intensities of the donor in the presence and absence of a quencher, respectively, r_0 is the distance between the acceptor and the donor, and R_0 is the critical distance when the transfer efficiency is 50%. The distance between the donor and the acceptor is typically in the range of 1–10 nm. In our research, the FRET method was used to observe the contact area between the adhered sensor and the cell membrane. The cell membrane could be excited by the fluorescent emission of the sensor, which has adhered to the cell membrane.

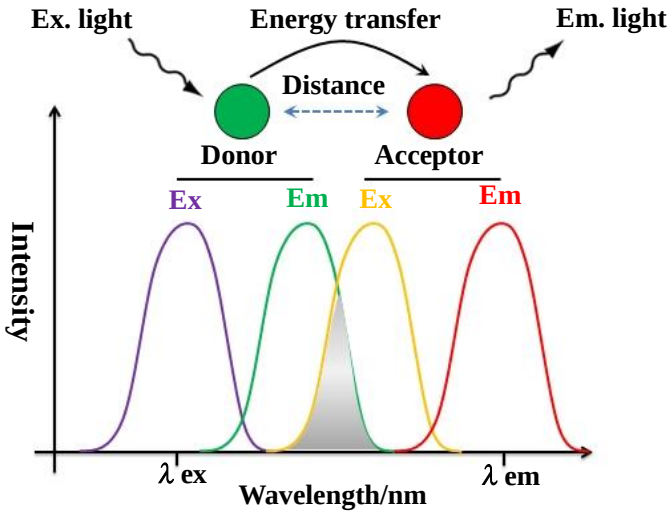

Figure 4.4: The mechanism of fluorescence resonance energy transfer (FRET).

4.4 Experiments

4.4.1 Experimental setup

We constructed an optical system based on a commercial inverted microscope (IX71, Olympus), consisting of holographic optical tweezers (HOT) and a laser confocal scanning system as shown in Fig. 4.5. The HOT system has been designed and reported in our previous work [108]. An infrared laser (YLM-10-1064, IPG PHOTONICS, maximum power: 10 W, wavelength: 1064 nm) was used as a light source. The laser beam was modulated with a spatial light modulator (SLM: Hamamatsu Photonics X10468-03, frame rate: 60 Hz) [109], which displayed a Kinoform hologram. Then the laser beam was transferred to the back focal plane of the microscope objective lens (Olympus, UPLSAPO 100XO, 100×, numerical aperture: 1.40, working distance: 130 μm. The laser spot was generated on the focal plane of the objective lens and the target object was trapped at the laser spot.

The Z piezo stage was fixed to the objective lens so that the movements of the laser spot and the objective lens could be controlled by the Z piezo stage. The manipulation

of the trap point of one bead to vibrate near a certain region of the cell membrane was applied by the HOT system, and the manipulation was observed with an analog CCD camera (WAT-221S, Watec. Co. Ltd.). Three-dimensional fluorescent images were taken using a laser confocal scanning system (CSU-X1, Yokogawa. Co. Ltd.) with two excitation lasers at 488 nm and 561 nm and an electron-multiplying charge-coupled device (EM-CCD) (iXon, Andor). A Z stage for the objective lens (P-E662, Physik Instrumente GmbH Co.) was used to acquire 3D slice images. A fluorescence system equipped with a mercury lamp was also used to induce photo-isomerization by UV illumination.

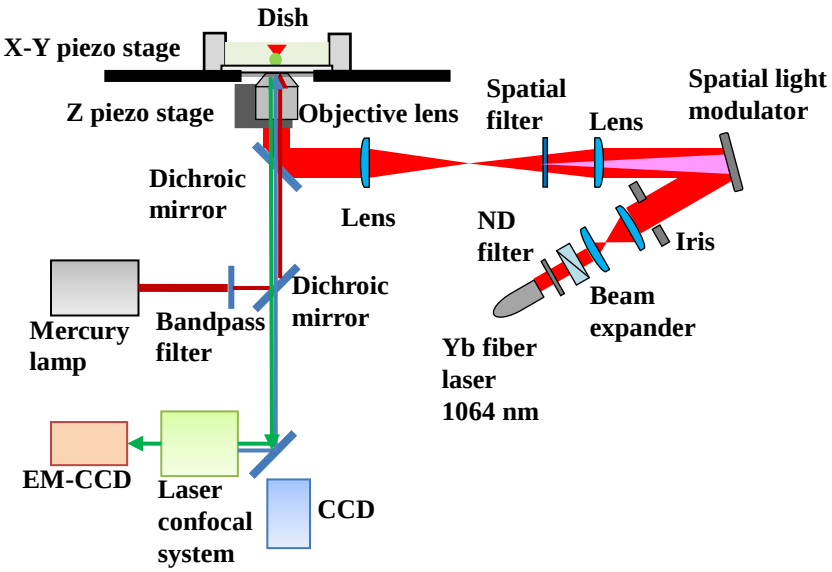

Figure 4.5: Setup of optical tweezers system and inverted confocal microscopy system.

4.4.2 Selective adhesion of liposomes to the cell membrane using optical manipulation

The sensor-encapsulated lipid layers were trapped by the optical tweezers and placed in contact with the cell surface under visible light (VIS). The sensor was then illuminated by ultraviolet (UV) light for 1 min, and the zeta potential of the liposomes could be switched from negative to positive via the photo-isomerization of SP. In this

experiment, the UV light power was 3.5 mW/cm^2 and the VIS power was 5.4 mW/cm^2. During the UV illumination, the positively charged lipid was able to adhere to the cell membrane.

4.4.3 Vertical vibration stimulus on the adhered sensor using optical tweezers for rapid injection

As shown in Fig. 4.6 (a), after two sensors adhered to the same cell surface, we applied optical tweezers on one of the sensors to move it up and down circularly in sine mode below the sensor. In our experimental system, the laser spot of the optical tweezers was on the same plane as the focus plane of the objective lens, which was fixed to a Z piezo stage, so that the displacement and frequency of the moving optical tweezers could be controlled by the input voltage of the Z piezo stage. In our experiment, the frequency of the moving focal point of the laser was 1 Hz and the maximum displacement (ΔZ) was 4 μm. The displacement curve of the optical tweezers in sine mode is shown in Fig. 4.6 (b).

The cyclic vertical movement of the focal point of the laser provided a persistent vibration stimulus on the sensor. In the vibration experiment, the peak position of the focal point of the laser was the same as the position of the adhered sensor. Therefore, the trapping force of the sensor was downward on the cell membrane when the focal point moved to a position below the sensor. After the application of the vibration stimulus, a laser confocal microscope was used to take Z slice images with a scanning distance of 10 μm. The exact position of the sensor before and after the application of the vibration stimulus could be observed in the 3D fluorescent images.

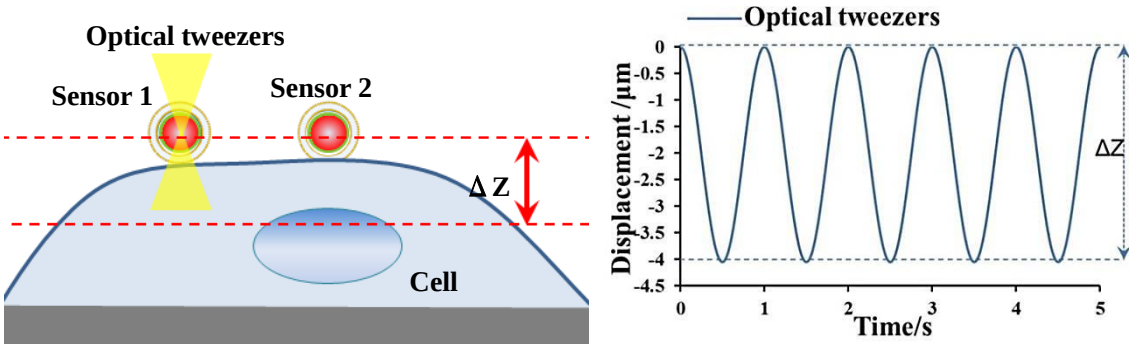

(a) (b)

Figure 4.6: Vertical vibration stimulus on the adhered rapid injection sensor. (a) Schematic diagram of the local injection of a sensor with vibration stimulus applied by optical tweezers. (b) The displacement curve of the laser focal point in 5 cycles in sine mode with a frequency of 1 Hz and ΔZ of 4 μm.

4.4.4 Observation of the contact area between the adhered sensor and the cell membrane by FRET

We used the FRET method to detect the change in contact area between the adhered sensor and the cell membrane after vibration. The microbead (Φ 5 μm) was encapsulated by liposomes, which was stained by quantum dots (Lumidot™ CdSe/ZnS 510, ex. 366 nm, em. 510 nm) as the donor, as shown in Fig. 4.7. When fabricating liposome layers on the surface of the microbeads using layer by layer method as introduced in section 4.3.3, quantum dots solution was added in the lipids. The quantum dots target the liposome layers on sensor surface because it has a strong affinity for the phospholipids in the liposome layers. The cell membrane was stained by CellMask™ as the acceptor. The CellMask™ plasma membrane stains are amphipathic molecules providing a lipophilic moiety for excellent membrane loading and a negatively charged hydrophilic dye for “anchoring” of the probe in the plasma membrane. So both the stain of the sensor by quantum dots and the stain of the cell are on the surfaces of the samples.

The overlap of the absorption spectrum of CellMask™ with the fluorescence emission spectrum of Lumidot™ 510 is shown in Fig. 4.8 (a). The experimental setup is shown in Fig. 4.8 (b). UV was illuminated by a mercury lamp, and an EM-CCD equipped with a barrier filter (590 nm) was used to observe the fluorescence emission from the cell membrane.

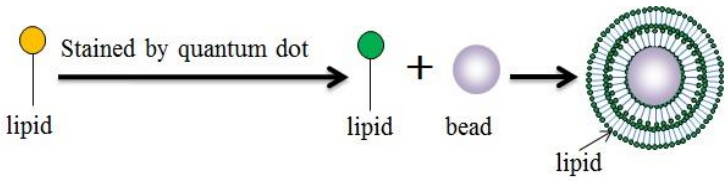

Figure 4.7: The fabrication of a fluorescent microbead encapsulated by a lipid membrane, stained by quantum dots (Lumidot™ CdSe/ZnS 510, ex. 366 nm, em. 510 nm).

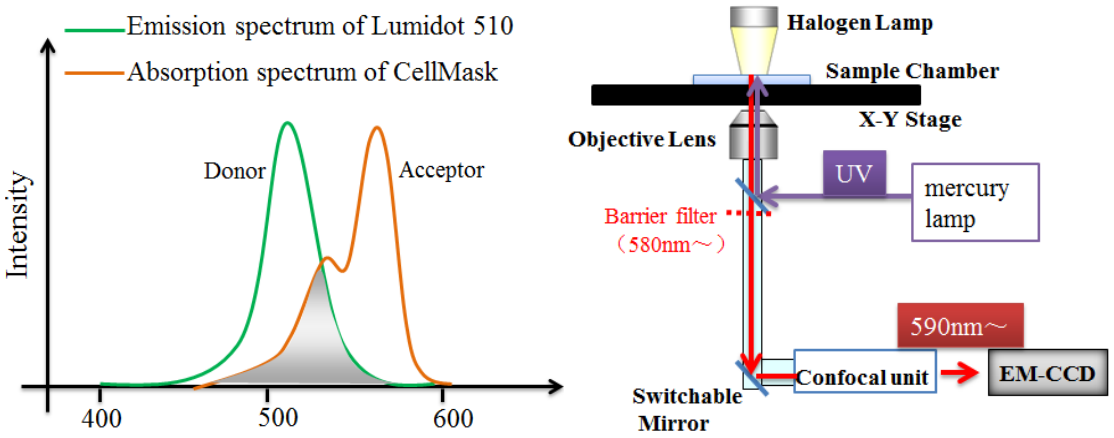

Figure 4.8: FRET experiment system. (a) Overlap of the UV absorption spectrum of CellMask™ with the fluorescence emission spectrum of Lumidot™ CdSe/ZnS 510. (b) Experimental system for FRET observation.

Figure 4.9 shows our schematic design of the FRET experiment between a single sensor and the cell membrane. The adhered sensor, which was stained by Lumidot™ 510, could be excited by UV illumination. The cell membrane could absorb the fluorescence emission from the adhered sensor, in turn emitting fluorescence at a longer wavelength. Therefore, the emission, which was excited by FRET, should be very weak.

In order to successfully observe the emission by FRET, we used microbeads with a larger size (Φ 5 μm) than those used in the injection experiment (Φ 1 μm). We applied the same vibration stimulus on the sensor in the FRET experiment.

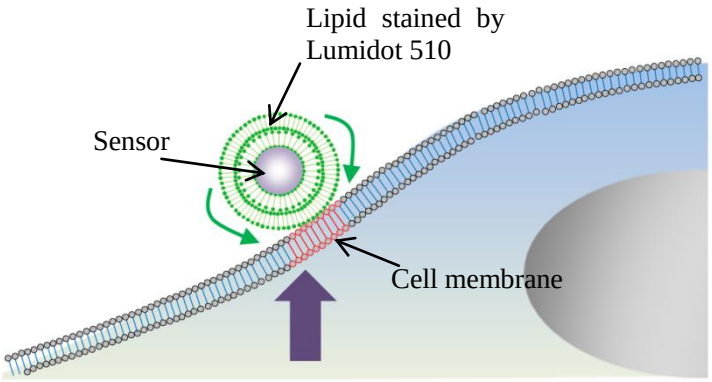

Figure 4.9: Schematic design of FRET experiment between a single sensor and the cell membrane.

4.5 Results

4.5.1 Control of zeta potential of liposomes containing photochromic material

We measured the zeta potential of PS beads, amino-PS beads, DPPC liposomes with SP, and DPPG liposomes with SP using a zeta potential analyzer under illumination at 600 nm (Zetasizer Nano ZS, Malvern), and the results are shown in Table I. In table I, the measured zeta potential of DPPC is positive while that of DPPG is negative. We also examined the amount of surface charge in each material by evaluating the duration of the particle passage (the time it took for a particle to go through a pore) using a nanoparticle analysis system (qNANO, iZON). The duration increases with the zeta potential in this equipment. Figure 4.10 shows the calibration curve of zeta potential and the duration of passage. From this result, the relationship between the zeta potential and the duration of passage is represented in equation 4.2.

$$V_Z = 30.6 \cdot D - 156 \tag{4.2}$$

V_z is the zeta potential [mV] and D is the time [ms] it took the particles to pass through the pore during the particle charge analysis. In our experiment, DPPG with SP was located at the surface of the sensor. The measured duration of passage of the DPPG liposome under UV illumination was 5.67 ms. From equation 4.2, the zeta potential of the UV-illuminated DPPG liposome was calculated to be 17.4 mV, suggesting that we have succeeded in switching the zeta potential of the liposome-containing sensor from negative (-73.2) to positive (17.4). Actually, the photoisomerization of spiropyran is reversible. After UV was removed, the zeta potential of the liposome-containing sensor was change to negative again.

Table 4.1 Zeta potential of each material measured by zeta potential analyzer

		Material and condition			
		PS bead	Amino-PS bead	DPPC (VIS)	DPPG (VIS)
Zeta potential	**mV**	-54	-47.4	10.4	-73.2

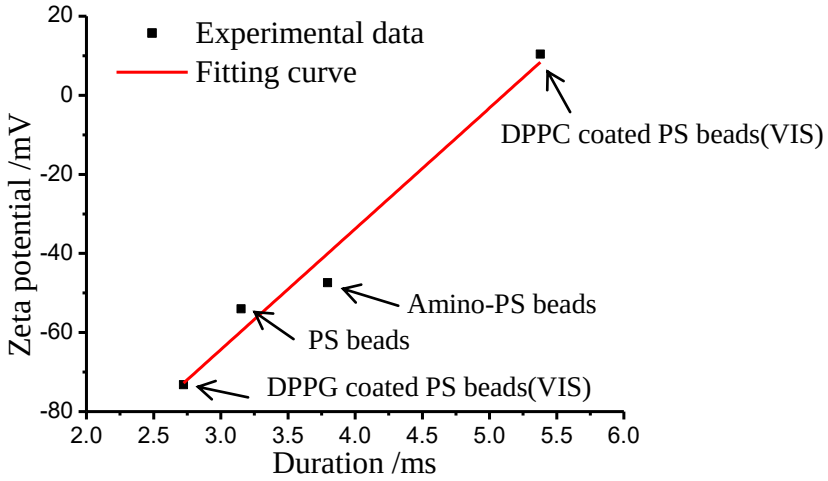

Figure 4.10: Calibration result of the relationship between zeta potential and duration of particles passing through the pore in particle charge analysis.

4.5.2 Selective adhesion of liposomes to the cell membrane

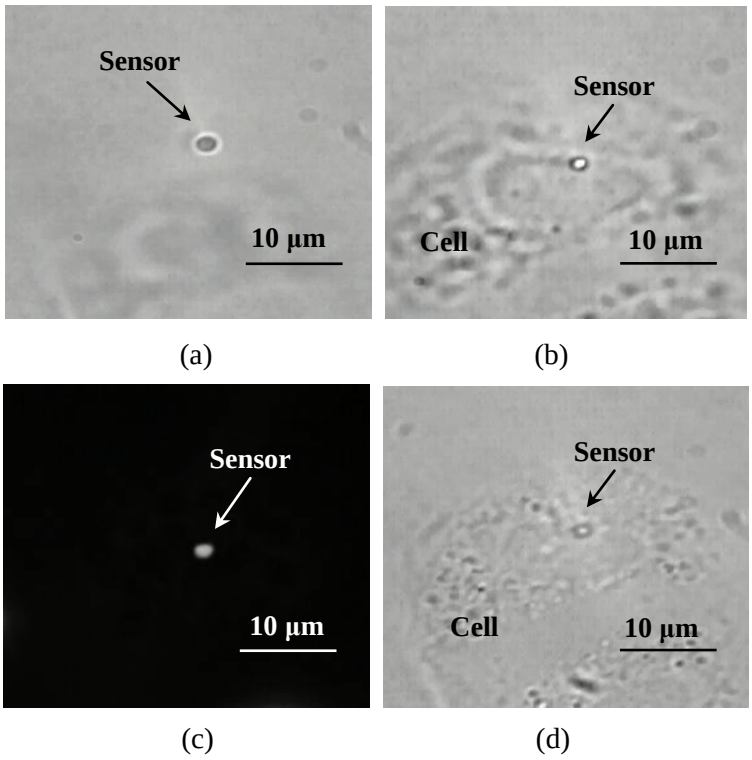

Figure 4.11: Selective adhesion of a single sensor to the cell membrane by photo-isomerization. (a) A single sensor trapped by optical tweezers. (b) Transfer of the sensor to the surface of an MDCK cell. (c) UV illumination of the sensor for adhesion. (d) Sensor adhesion on the cell surface after UV illumination.

We succeeded in the adhesion of a single sensor to the cell membrane by photo-isomerization, as shown in Fig. 4.11. A single sensor could be trapped and manipulated by optical tweezers and transferred to the cell surface (Fig. 4.11 (a) and (b)). The sensor has been encapsulated by liposome layers containing the photochromic material, spiropyran. Then the sensor was exposed to UV illumination for 1 min, and adhered to the cell membrane based on the change in surface charge induced by photo-isomerization (Fig. 4.11 (c) and (d)). When the focal point of the laser was removed from the sensor, the sensor still adhered to the cell surface. Based on our

experiment results, without UV illumination, after the sensor was transferred to cell membrane, the sensor escaped from cell surface after removing the laser point.

4.5.3 Sensor injection by lipofection without vibration stimulus

Before the injection experiment, the cell membrane of MDCK cells was stained by CellMask™, which shows red fluorescence at ex. 561 nm as seen in Fig. 4.12. Figure 4.12 (a) shows the fluorescence emission spectra of CellMask™ Orange plasma membrane stains with an excitation peak at 550 nm. Figure 4.12 (b) shows a 3D fluorescent image of the cell membrane taken by Z slicing with steps of 0.2 μm and a scanning distance of 10 μm. In order to investigate the different effects of injection with and without vibration stimulus, before applying the vibration stimulus on the sensor, we detected the injection results of lipofection without any stimulus on the sensor, which are shown in Fig. 4.13. In the 3D fluorescent image in Fig. 4.13 (a), we observed the position of the sensor, which adhered to the surface of a cell. Lipofection is based on membrane fusion between the cell membrane and the liposome layers of the sensor. The cross section images of Fig. 4.13 (a) taken at different times after sensor adhesion are shown in Fig. 4.13 (b). The results show that within 3 h after adhesion, the sensor was embedded in the cell membrane, indicating that membrane fusion occurred during lipofection. It took almost 5 hours for the sensor (Φ 1 μm) to be completely injected into the cell, as shown in Fig. 4.13 (b). Of the ten sensors that adhered to different cell surfaces, only four were injected into the cells in 5 hours. Therefore, the injection time of lipofection was 5 hours at an injection rate of 40%.

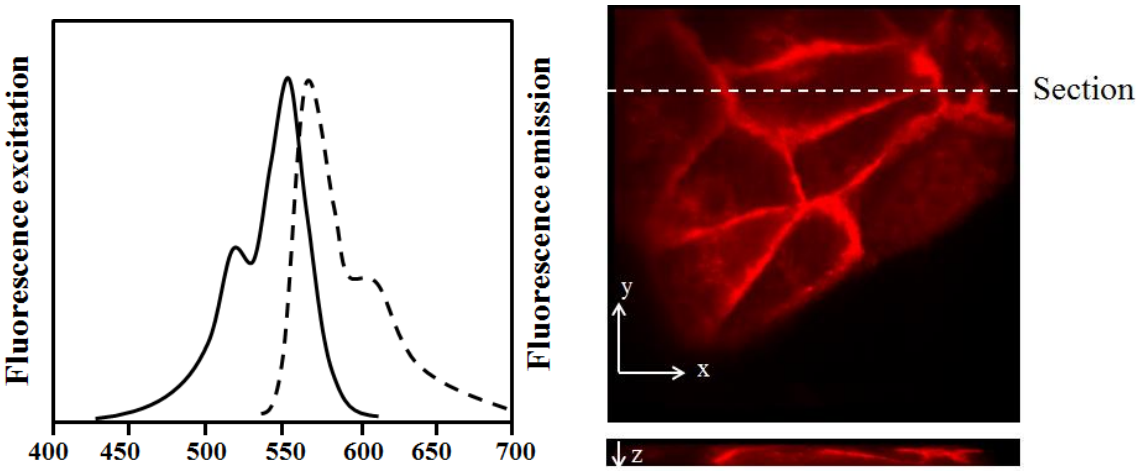

(a) (b)

Figure 4.12: Fluorescence image of cell membrane stained by CellMask™. (a) The fluorescence emission spectra of CellMask™ Orange plasma membrane stains. (b) 3D fluorescence image of cell membrane (ex. 561 nm).

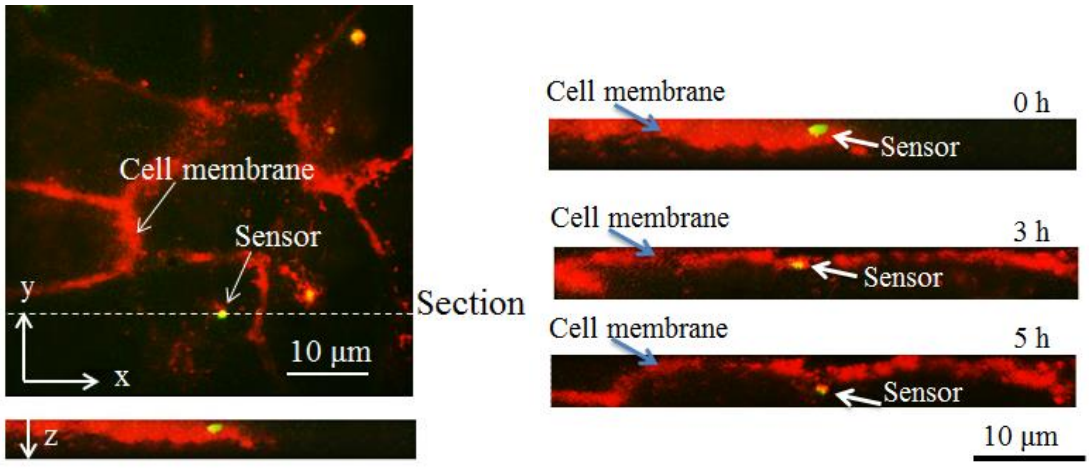

(a) (b)

Figure 4.13: Injection result based on lipofection without vibration stimulus on the sensor. (a) 3D fluorescent image of a single sensor (Φ 1 μm) adhered to the cell membrane before injection. (b) The cross section images of (a) taken at different times after sensor adhesion.

4.5.4 Rapid injection by optical tweezers with local vibration stimulus

4.5.4.1 Contact area change between sensor and cell membrane

The sensor was encapsulated by lipid layers that were stained by quantum dots (Lumidot™ CdSe-ZnS 510, ex. 366 nm, em. 510 nm) and a fluorescent image of the sensor is shown in Fig. 4.14. Figure 4.14 (a) shows the typical absorption and photoluminescence spectra of Lumidot™ 510. The quantum dots can be excited by UV light (366 nm) and shows fluorescent emission in the region of 450 nm to 550 nm, as shown in Fig. 4.14 (c). They show no emission at wavelengths that are longer than 590 nm, as shown in Fig. 4.14 (d).

The FRET results are shown in Fig. 4.15, where we observed three sensors in Fig. 4.15 (a). Sensor 1 and sensor 2 adhered to the cell membrane and sensor 1 was later vibrated by optical tweezers. Sensor 3 adhered to the glass dish. In the FRET experiment, UV illumination was used to excite the sensor to emit fluorescence, which could be absorbed by the cell membrane. EM-CCD equipped with a barrier filter (590 nm) was used to observe the emission fluorescence of the cell membrane. Figure 4.15 (b) shows the fluorescent image of the cell membrane excited by FRET before the vibration experiment. The red fluorescence in Fig. 4.15 (b) was expressed by the cell membrane, which was excited by the sensor that adhered to it.

d_1 and d_2 show the diameters of the fluorescent membrane in the positions of Sensor 1 and Sensor 2, respectively. d_1 and d_2 were almost same (d_1 = 1.76 μm, d_2 = 1.83 μm) before vibration was applied on Sensor 1. d_1 increased to 3.64 μm while a very small change occurred on d_2 (1.97 μm) after vibration was applied on Sensor 1 for 20 min, as shown in Fig. 4.15 (c). These observations suggest that the vibration on Sensor 1 could push down the sensor and induce a downward displacement. As shown in the upper

diagram in Fig. 4.15 (c), the downward displacement of the sensor induced a corresponding deformation of the cell membrane, which increased the contact area between the sensor and the cell membrane, resulting in the increase in d_1.

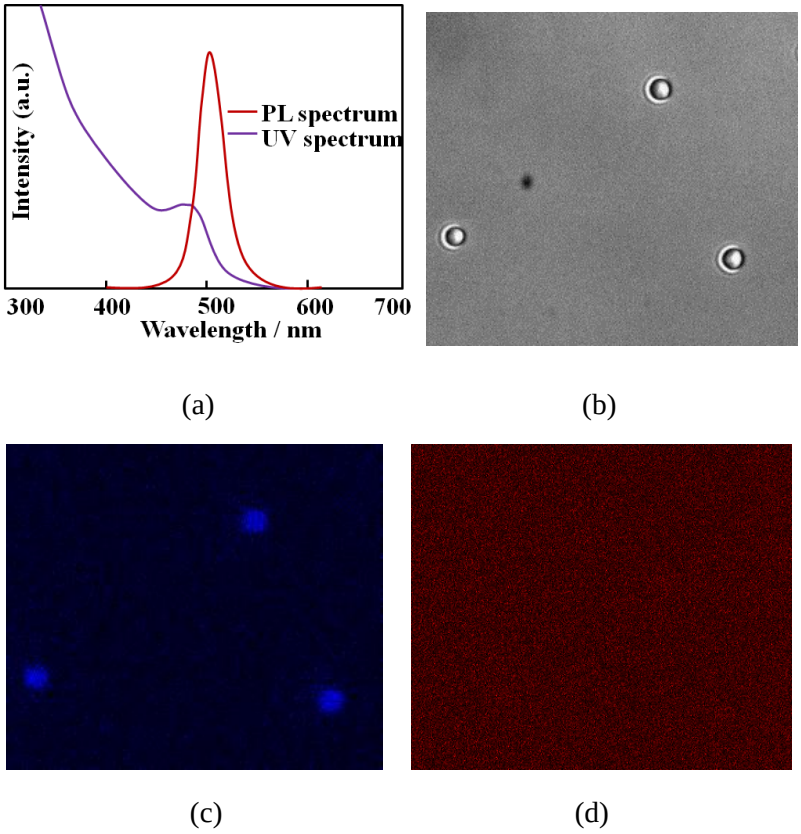

Figure 4.14: Observation of the sensor (Φ 5μm) stained by quantum dots. (a) Typical absorption and photoluminescence spectra of quantum dots (Lumidot™ CdSe-ZnS 510, ex. 366 nm, em. 510 nm). (b) Optical image of sensor observed under bright-field. (c) Fluorescent image of sensor (ex. 366 nm, em. 420 nm). (d) Fluorescent image of sensor (ex. 366 nm, em. 590 nm).

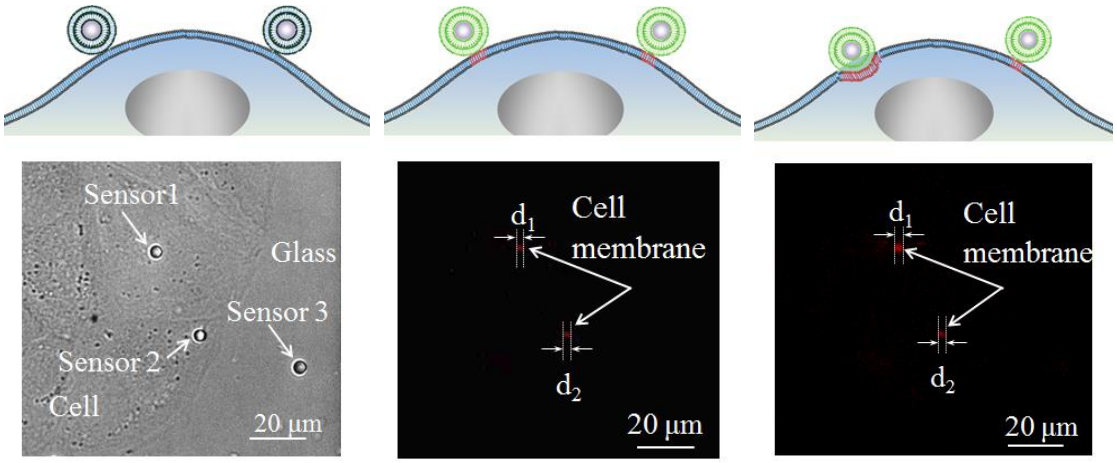

(a) (b) (c)

Figure 4.15: FRET experiment. (a) Bright-field image of the sensors. Sensor 1 and Sensor 2 adhered to the cell surface and Sensor 1 was later vibrated by optical tweezers. Sensor 3 adhered to the glass dish. (b) Fluorescent image of the cell membrane excited by FRET before vibration experiment. (c) Fluorescent image of the cell membrane excited by FRET after vibration experiment. d_1 and d_2 are the diameters of the fluorescent membrane in the positions of Sensor 1 and Sensor 2, respectively.

4.5.4.2 Rapid injection results

Figure 4.16 shows the results of rapid sensor injection by applying a vibration stimulus using optical tweezers. Figures 4.16 (a)–(c) are bright-field images and Fig. 4.16 (d)–(f) are 3D fluorescent images taken in multi-channels of red and green. In our experimental system, the focal point of the laser moved with the Z piezo stage in sine mode with a frequency of 1 Hz and an amplitude of 4 μm. The displacement and frequency of the focal point could be controlled by the input voltage of the Z piezo stage. Two sensors adhered to the cell surface before vibration, as shown in Fig. 4.16 (a) and (d). The cell membrane shows fluorescence in the red channel (ex. 561 nm, em. 590 nm) and the sensor shows fluorescence in the green channel (ex. 488 nm, em. 510 nm).

After applying vibration stimulus for 20 min on Sensor 1 and also 10 min after vibration, the bright-field images in Fig. 4.16 (b) and (c) show an apparent difference in the vertical position of the two sensors, suggesting that a displacement between Sensor 1 and Sensor 2 was induced by the vibration.

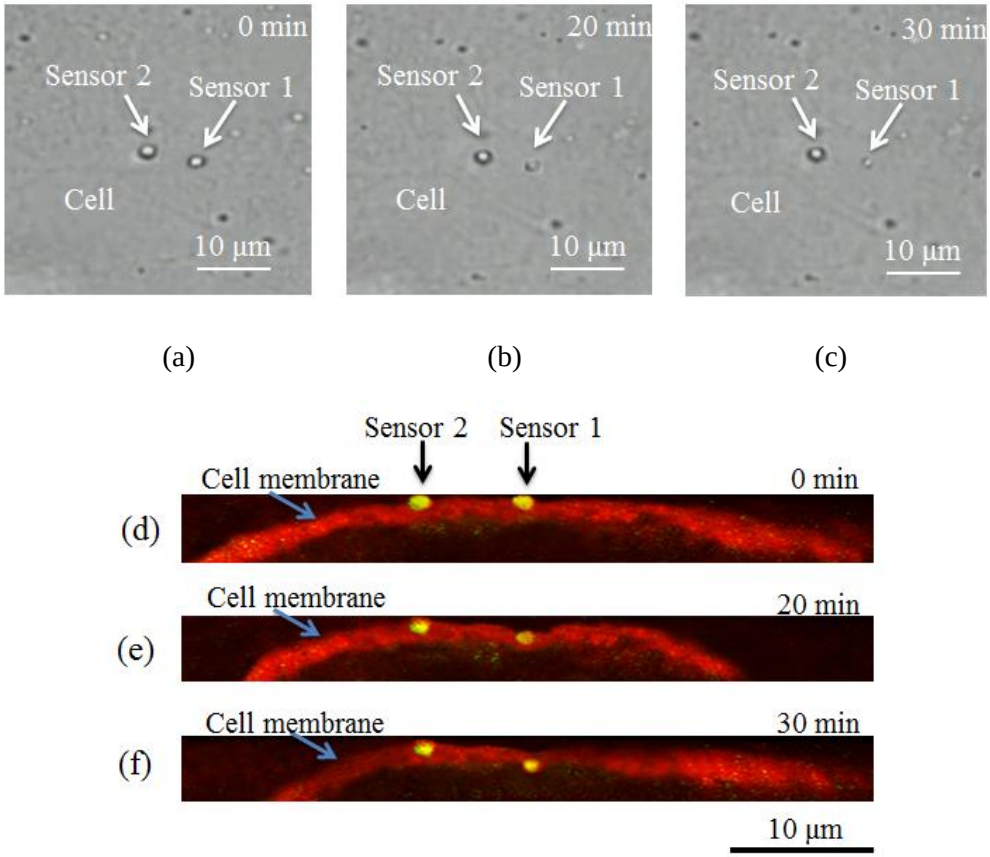

Figure 4.16: Local injection of individual sensor into a single cell with vibration stimulus applied by optical tweezers. (a–c) Bright-field images of sensors taken at different times: before applying the stimulus, after applying vibration for 20 min on Sensor 1, and 10 min after vibration, respectively. (d–f) Cross section images (in multi-channels of red and green) taken at different time: before applying the stimulus, after applying vibration for 20 min on Sensor 1, and 10 min after vibration, respectively. Green channel: ex. 488 nm, em. 510 nm, Red channel: ex. 561 nm, em. 590 nm.

Figure 4.16 (d) – (f) are the cross section images taken at different time. In the 3D fluorescent image in Fig. 4.16 (e), Sensor 1 has been pushed down by the optical tweezers compared with Sensor 2. The displacement of Sensor 1 induced a corresponding deformation of the cell membrane, but the sensor was still on the cell surface. Figure 4.16 (f) shows that 10 min after the vibration was applied, the sensor was totally injected into the cytoplasm. In the 3D fluorescent image of Fig. 4.16 (f), it is clear that Sensor 1 was below the cell membrane while Sensor 2 was still on the cell surface. In fact, we observed ten sensors that adhered to different cell surfaces, and eight of them were injected into the cytoplasm in 30 min. Thus, in comparison with the lipofection method, which had an injection time of 5 hours, the presence of local vibration stimulus on the sensors shortened the injection time to 30 min. Additionally, the injection rate was also increased to 80% compared with that of lipofection (40%).

4.6 Discussions

In our research, we succeeded in the selective adhesion and rapid injection of a single micro-sensor into a target cell. Comparing with the nano-sensors which have been studied by many researchers, the injection of micro-sensors into target cells has several merits. For the polymeric nanoparticles, it can always pass through the cell membrane by diffusion and endocytosis after incubating the cells with the nanoparticles [16], [110]. It not only takes several hours for the delivery of the nanoparticles into cytoplasm but also non – quantitative. For the nanoparticles modified by some metal particle, it is commonly delivered into cell by optical methods [57], [111]. The optical injection of metallic nanoparticles can provide a very short injection time (as short as several seconds), however it also leads to localized heating-up on cell membrane. The heating-up on cell membrane is a big interference especially during the temperature

measurement of the cell. Using our proposed method, we can control the number of sensors introduced to cells which can be as small as a single sensor. The very low stimulus to the cell during the injection is thinkable based on the small injection number of sensors and the very weak force of optical tweezers. And no heat is produced by optical operation since our sensor is based on polymeric material. What we want to mention here is that our established optical system is consisting a holographic optical tweezers (HOT) which makes it possible to manipulate several micro-sensors as same time. Then the micro-sensors can be transferred to different regions on cell membrane and then be injected into the cell. As it is considered that pH and temperature of different organs in a cell are not same, injection of several micro-sensors into different places in cytoplasm will be convincing. The number of injected sensors for detection is really small, so the sensor in micro scale will be easy for fluorescence detection after injected in cytoplasm.

G. Apodaca et al. cited on the role of mechanical forces on endocytosis [18]. They reported that mechanical stretch stimulates apical endocytosis in bladder umbrella cells. In our study, the mechanical stimulus was driven by optical tweezers which was weak a lot comparing with stretch. And MDCK cells that we used are totally different with bladder umbrella cells. The membrane area of MDCK cell cannot expand as large scale as that of bladder umbrella cells. So in our case, the mechanical force-induced endocytosis is only to a limited extent. The fluorescent sensor that we used was encapsulated in liposome layers which had been used widely for lipofection delivery of biological particles [112], [113]. The liposome layers can easily merge with the cell membrane since they are both made of a phospholipid bilayer. In our previous work, nano-sensors encapsulated in liposome layers have been transfected into cell nucleus by

lipofection [66]. Actually not only stretch-induced endocytosis had been noted by G. Apodaca et al., it had been also demonstrated that mechanical stretch on cell membrane also resulted in the delivery and incorporation of vesicle cargo into the apical membrane [103]. Our research results are coincident with that mechanism. The mechanical force driven by optical tweezers increased the liposome merging with cell membrane. So the injection of sensor into cell by lipofection was enhanced by mechanical force.

In the fluorescent image of the sensor after injection into cytoplasm, the sensor also shows good fluorescence which makes it possible to track and observe the sensor. It had been proved that our fabricated fluorescent sensor could endure low pH (pH=4), and can also respond to low pH repeatedly. So the sensor will be an effective mean for intracellular measurement even in acidic organs. The observation of sensor location and measurements in cytoplasm after sensor injection will be urgent works in future. The sensor is expected for its applications in intracellular measurement in different organs.

4.7 Summary

A novel multi-fluorescent sensor has been synthesized based on amino-polystyrene microbeads using Rhodamine B and FITC. It was able to respond to changes in both temperature and pH. A single sensor was successfully manipulated by optical tweezers and adhered selectively to the cell surface via the optical control of the zeta potential of spiropyran. Rapid sensor injection was achieved with an injection time of approximately 30 min by applying cyclic vibration stimulus using optical tweezers. With the vibration method, the injection rate was also increased to 80% compared with that observed in the lipofection method. This study is fundamentally helpful in the delivery of micro-nano particles used in biomedical applications, such as delivery of drugs, genes, or contrast agents for biomedical imaging and therapy. At the moment, we are seeking to extend

this injection method to other cell lines. Since the membranes of most cell types are constructed from similar lipids, we expect that the rapid injection method will work for most cell lines. This technique also makes it possible to measure intracellular pH and temperature, which will be a great contribution to cell biology.

Influenza, one of the most common infectious diseases, is a highly contagious airborne disease that occurs in seasonal epidemics. Our proposed micro sensor and injection method can be applied to transfer the sensors to different parts of a single cell with high positioning accuracy applied by optical tweezers (≈100 nm). Then the pH and temperature of different organelles in a cell (such as nucleus, mitochondria, endoplasmic reticulum which are the important organelles for virus proliferation) can be measured and compared. As a result, we can understand the heterogeneity in a single cell and also the production and transference of heat in cell. It will help us to understand the virus infection process to a host cell and the responses of the cell to the infection. We believe that our work will support breakthroughs in the development of new medicine and drug therapy in cancers and viral diseases.

Chapter 5

Multi-fluorescence sensor pillars for multi-sensing in OCP analysis chip

5.1 Introduction

Temperature, pH, and surrounding ion concentration are fundamental parameters that affect much cellular activity, namely proliferation, and differentiation. Analysis of interactions between these parameters and cell conditions are of great concern. For example, in bone regeneration, octacalcium phosphate (OCP) is used widely as biological scaffold material since it can enhance bone regeneration and tend to be replaced with newly formed bone [114]–[116]. OCP, which is a precursor of hydroxylapatite (HA), has been reported to have high affinity to F^- [117]. Fluoride ion (F^-) is known to stimulate osteoblastic cell proliferation and differentiation in vitro [118] and promote fluoridated hydroxyapatite (FHA) formation rather than hydroxyapatite (HA) formation [119]. F^- is recognized as an important element in bone and tooth mineralization. However, the effect of F^- on the growth and physicochemical properties

of OCP crystals, remains unclear.

The transformation of OCP to (F)HA has been examined [120]–[122] as show in Fig. 5.1. During OCP conversion, there is always a decrease in pH [123] and change of Ca/P ratio [124] after OCP transformation. Measurement of multi parameters such as pH and Ca/P ratio was important issues for interaction analysis. However, simultaneous measurement of multi parameters is still a big challenge. Conventionally, fluorescence measurement was used for on-chip measurement. However, sensible number of parameters was limited by the number of usable fluorescence wavelength. And interference of multi fluorescence dye in the same carrier was also a serious problem. In our research, we propose multi fluorescence micro sensor pillars with different sizes for calcium, pH and temperature sensing respectively in microfluidic chip. The fluorescence responses of the sensor pillars have been detected using a laser confocal microscopy.

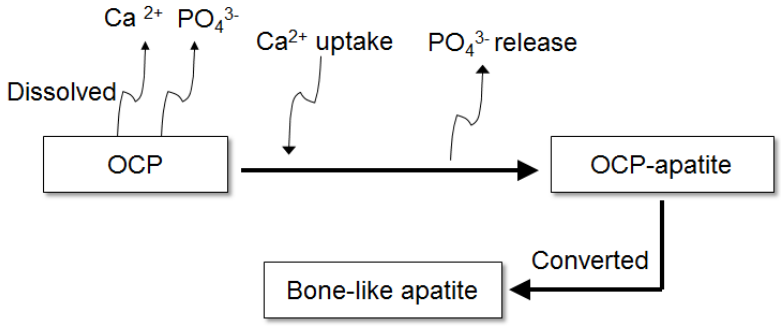

Figure 5.1: The transformation and biomineralization process of OCP in vivo

5.2 OCP analysis chip

5.2.1 Concept of OCP analysis chip

Figure 5.2(a) shows the concept of OCP analysis chip for multi-sensing of calcium, pH and temperature simultaneously during OCP conversion. There are three micro-channels in the chip for OCP, sensors, and cells respectively. They are interlinked

through the holes of PDMS walls. So the sensors in the middle channel can respond to the changes of surroundings in the chip. The OCP slurry and cells can be injected into micro-channels through inlet of every micro-channel by syringe pump and stopped by the PDMS pillars near the outlet.

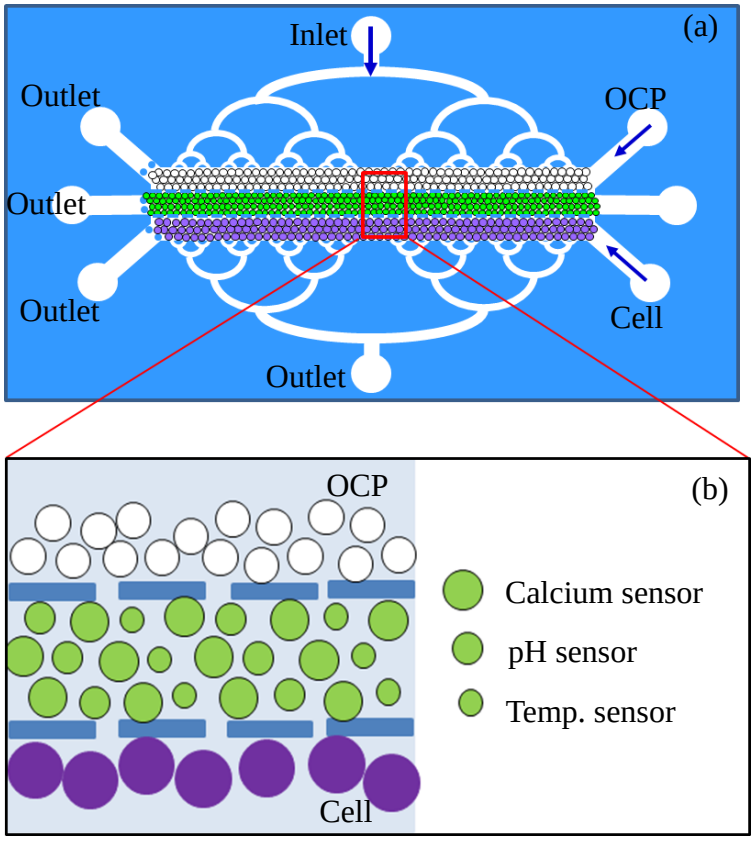

Figure 5.2: Concept of OCP analysis chip (a) schematic diagram of OCP chip (b) the arrangement of multi-sensor pillars in micro-channel. calcium sensor: Φ20μm, pH sensor: Φ15μm, temperature sensor: Φ10μm.

5.2.2 The design of multi sensor pillars

As shown in Fig. 5.2 (b), three kinds of sensor pillars with different size (Φ20 μm, Φ15 μm and Φ10 μm) are designed to be fabricated in the micro-channel. The sensor pillars are containing different fluorescence dyes which can respond to calcium, pH and temperature changes respectively. The different sensor pillars can be recognized from

each other by their different sizes. The surrounding changes can be studied through the fluorescence changes of the sensor pillars. Table 5.1 shows the advantages of the pillar sensors with same fluorescence compared with other designs. All of the fluorescent pillars can be excited by same laser source making the detection system easy. Compact arrangement of pillar sensors with different sizes can be realized by MEMS technology.

Table 5.1: The comparison of different design of pillar sensor on chip for multi-sensing.

Layout method	Bead sensors with different fluorescence	Pillar sensors with different fluorescence	Pillar sensors with same fluorescence
Concept	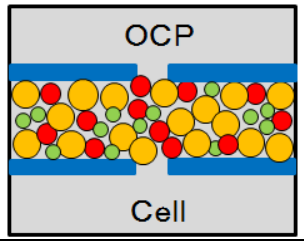	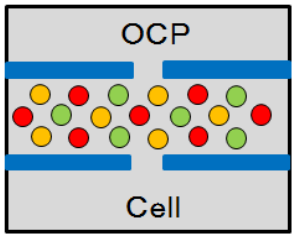	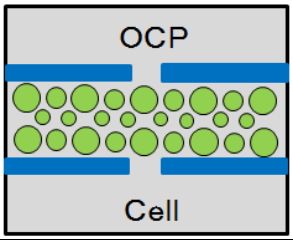
Temp. sensor	Rhodamine B	Rhodamine B	Lumidot 480
pH sensor	FITC	FITC	FITC
Ca^{2+} sensor	Fura-2	Fura-2	Fluo-3
Simultaneous measurement	No (Exchange of Ex.)	No (Exchange of Ex.)	Yes (Same Ex. laser)
System	Complex	Complex	Easy (one excitation)
Feature	Compact arrangement of sensor	Application of MEMS	Compact arrangement of sensor by MEMS

5.2.3 Chip functions

The OCP analysis chip possesses several functions. Firstly, our designed OCP analysis chip provides a culture device for OCP and cells. OCP and cells can be injected and cultured together in one OCP chip. Secondly, simultaneous multi-sensing (Ca^{2+}, pH, Temp.) can be done by sensor pillars in microfluidic chip during OCP conversion. Lastly, the interactions between OCP conversion and cell activities related with environmental changes can be detected.

5.3 Fabrication of OCP chip

The fabrication process of OCP chip is shown in Fig. 5.3 (a). The process consists of bioresist patterning, PDMS molding, bonding with glass. The detailed process flow is explained as follows:

1) Spin coating SU-8 on silicon wafer

2) Exposure and development of SU-8 as OCP device

3) Molding by PDMS

4) Bonding PDMS chip with glass substrate

A fabricated chip photograph and optical image are shown in Figs. 5.3 (b) and (c), respectively. We succeeded in fabricating the OCP chip.

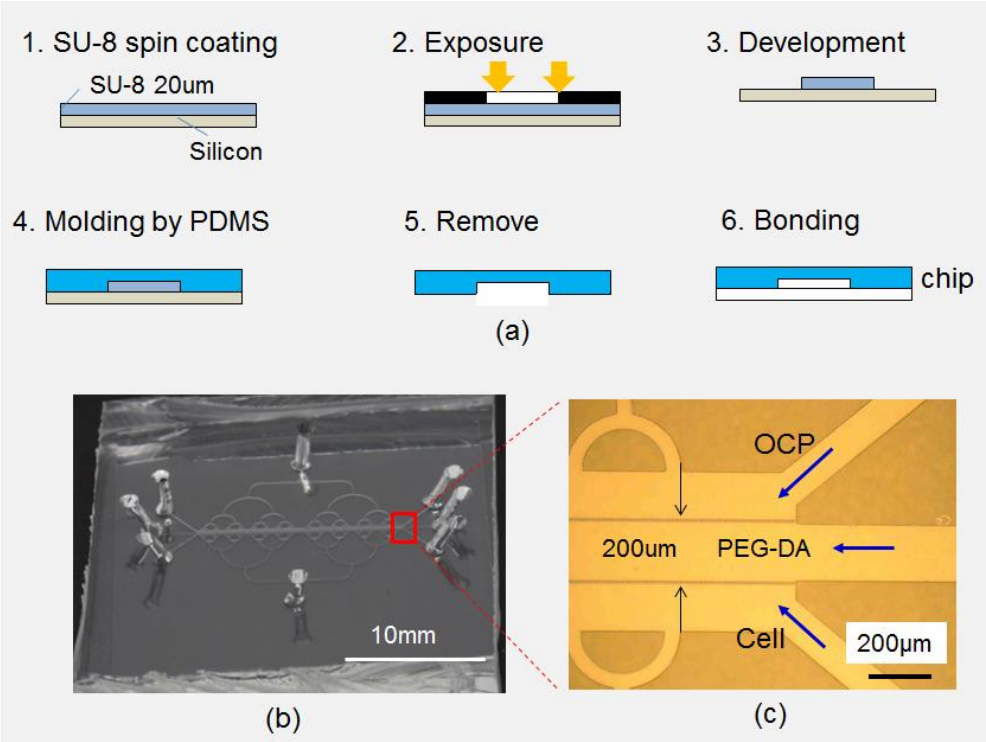

Figure 5.3: (a) Fabrication process of OCP analysis chip. (b) The photo of fabricated chip. (c) Local optical image of OCP chip.

5.4 Fabrication of muiti-fluorescent sensor pillars

5.4.1 Materials

Polyethylene (glycol)-diacrylate (PEG-DA) is used as the material of sensor pillar. It is a blank slate hydrogel that gels rapidly at room temperature in the presence of a photo-initiator and UV light [125]–[127]. It is used widely as the materials of biosensors [128], microfluidic chips [129], micro chambers[130]. DAROCUR 1173 is used as photo-initiator and mixed with PEG-DA with a ratio of 5%. Fluo-3, FITC and Lumidot 480 are selected as the responsive fluorescence dyes for calcium, pH and temperature, respectively. All the fluorescence dyes can be excited with same laser source (488nm).

5.4.2 Fabrication process

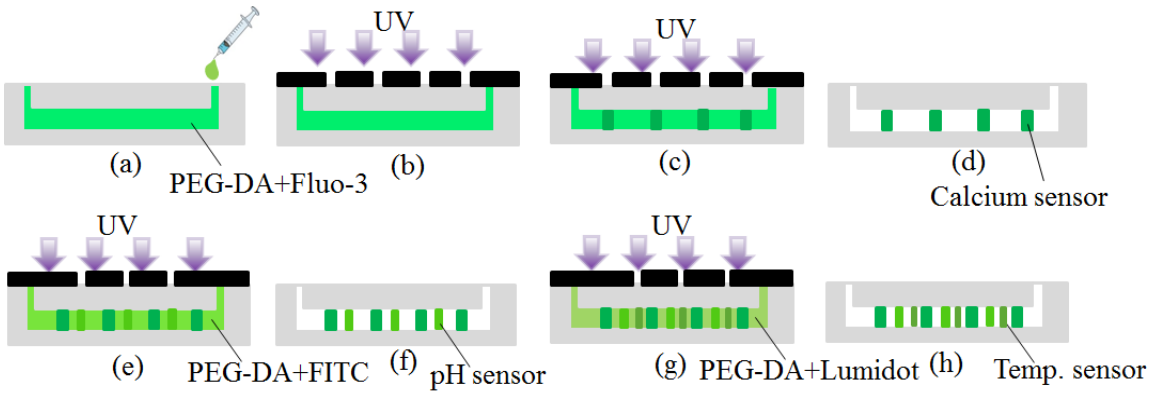

Figure 5.4: Fabrication process of multi sensor pillar in the chip: (a) injection of PEG-DA mixed with fluo-3 into the channel of the chip (b) exposure to UV light (c) the formation of calcium sensor pillars in the channel (d) rinse by DI water (e-f) the fabrication of pH sensor pillars (g-h) the fabrication of Temp. sensor pillars.

The fabrication process of multi-sensor pillars in micro-channel is shown in Fig. 5.4. First, PEG-DA mixed with Fluo-3 in DMSO solution (v/v: 10/1) is injected in the chip. Then expose to UV light with mask and calcium sensor pillar array (Φ20 μm) can be fabricated by photolithography. The unexposed PEG-DA is removed by DI water. Then

PEG-DA mixed with FITC in alcohol (v/v: 10/1) is injected in the chip. After exposure to UV light with mask and rinse by DI water, pH sensor pillar array (Φ15 μm) can be fabricated. Temperature sensor pillars can be fabricated by the same fabrication method using PEG-DA mixed with Lumidot 480.

5.4.3 Fluorescence of fabricated sensor pillars

As shown in Fig. 5.5, three kinds of sensor pillars with different sizes have been fabricated in microfluidic chip (calcium sensor: Φ20 μm, pH sensor: Φ15 μm, temp. sensor: Φ10 μm). All the sensor pillars can be excited simultaneously and show fluorescence by exposure to 488nm laser. They can be distinguished with each other by their different size.

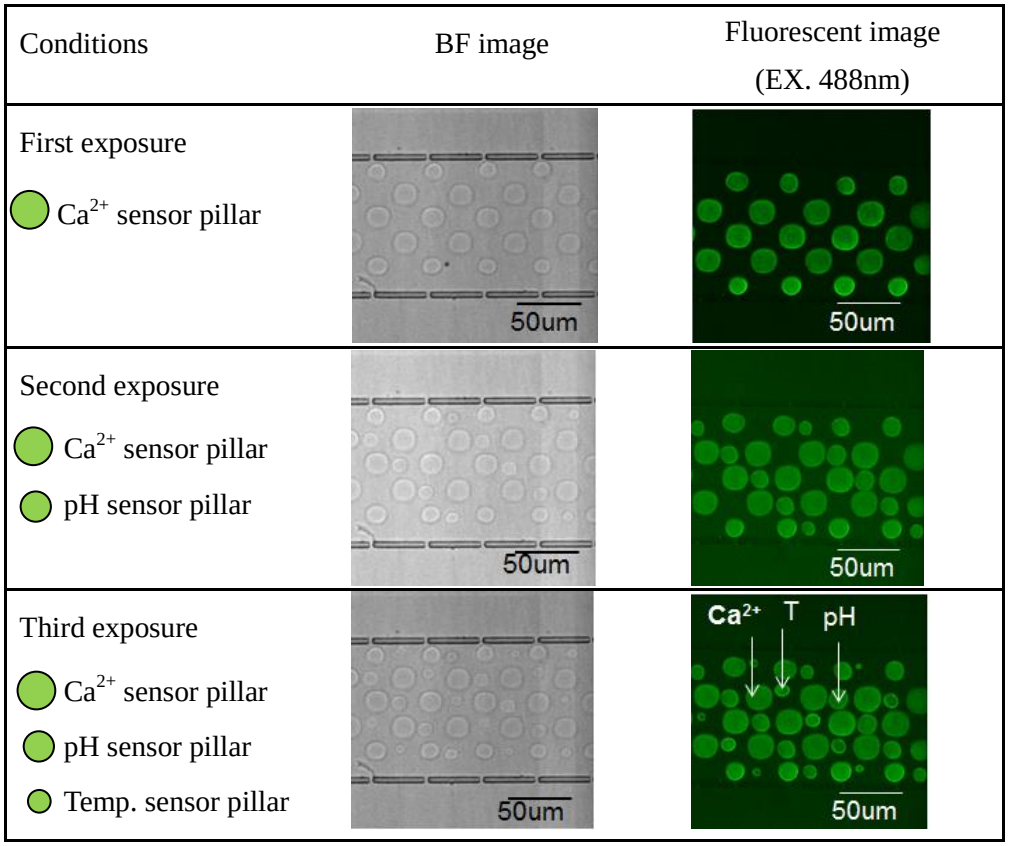

Figure 5.5: The images of the fabricated multi sensor pillars in micro channel: Calcium sensor (Φ20 μm), pH sensor (Φ15 μm), Temp. sensor (Φ10 μm).

5.5 Experiments and results

5.5.1 Sensitivity calibration

The results of the fluorescence responses to calcium and pH changes are shown in Fig. 5.6. The calcium solution with a concentration of 200 nM was injected into chip in which the original calcium concentration was 0 nM. The result in Fig. 5.6 (a) shows the fluorescence intensities of calcium sensor increase with time after calcium solution injection and become stable in less than 1 min. The solution with a pH value of 8 was injected into chip in which the original pH value was 5. The result in Fig. 5.6 (b) shows the fluorescence intensities of pH sensor increase with time after new pH solution (pH=8) injection and become stable in less than 1 min.

The calibration results of the sensitivities of different sensor pillars are shown in Fig. 5.7. Figure 5.7 (a) shows the fluorescence intensities of calcium sensor pillars under different calcium concentrations. The fluorescence intensities of pH and temperature sensor pillars do not change with the calcium. Figure 5.7 (b) shows the fluorescence intensities of pH sensor pillars under different pH values, while no changes are observed in the fluorescence intensities of calcium and temperature sensor pillars under different pH values. Figure 5.7 (c) shows the fluorescence intensities of temperature sensor pillars under different temperature. It should be noted that the pH sensor pillars also show fluorescence responses to temperature change. It is because FITC is sensitive to both pH and temperature. The temperature change can also lead to fluorescence changes of FITC. In order to eliminate interference from temperature, temperature compensation is needed for pH calibration.

For temperature compensation, fluorescence responses of pH sensor pillars to temperature changes in different pH values are shown in Fig. 5.8 (a). The fluorescence

change of pH sensor pillars induced by temperature change ($\Delta F_{(FITC)}$) is described as equation 5.1. The fluorescence change of pH sensor pillars induced by pH change ($\Delta F_R'$) can be calculated by equation 5.2. Fluorescence responses of different sensor pillars to temperature changes with temperature compensation are shown in Fig. 5.8 (b). Through the calibration results in Fig. 5.7 (a), (b) and Fig.5.8 (b), it is clear that the sensor pillars can respond to calcium, pH, and temperature changes of the surrounding.

$$\Delta F_{R(FITC)} = f(pH) * \Delta T \tag{5.1}$$

$$\Delta F_R' = f(pH) * \Delta T + \Delta F_R \tag{5.2}$$

$\Delta F_{(FITC)}$ is the fluorescence change of pH sensor pillars induced by temperature change, $\Delta F_R'$ is the fluorescence change of pH sensor pillars induced by pH change, ΔF_R is the total fluorescence change of pH sensor pillars induced by surrounding changes.

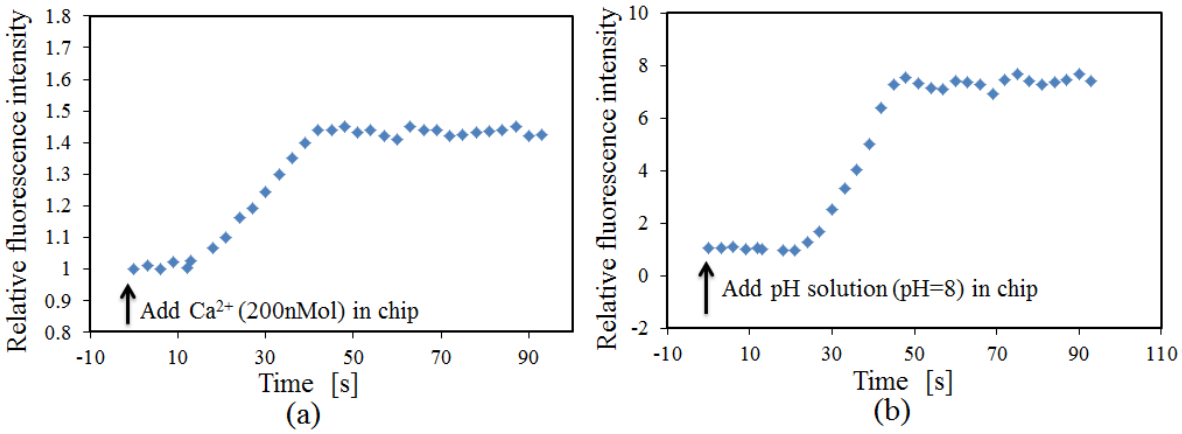

Figure 5.6: The responses of (a) calcium sensor pillar and (b) pH sensor pillar to the changes of calcium and pH respectively.

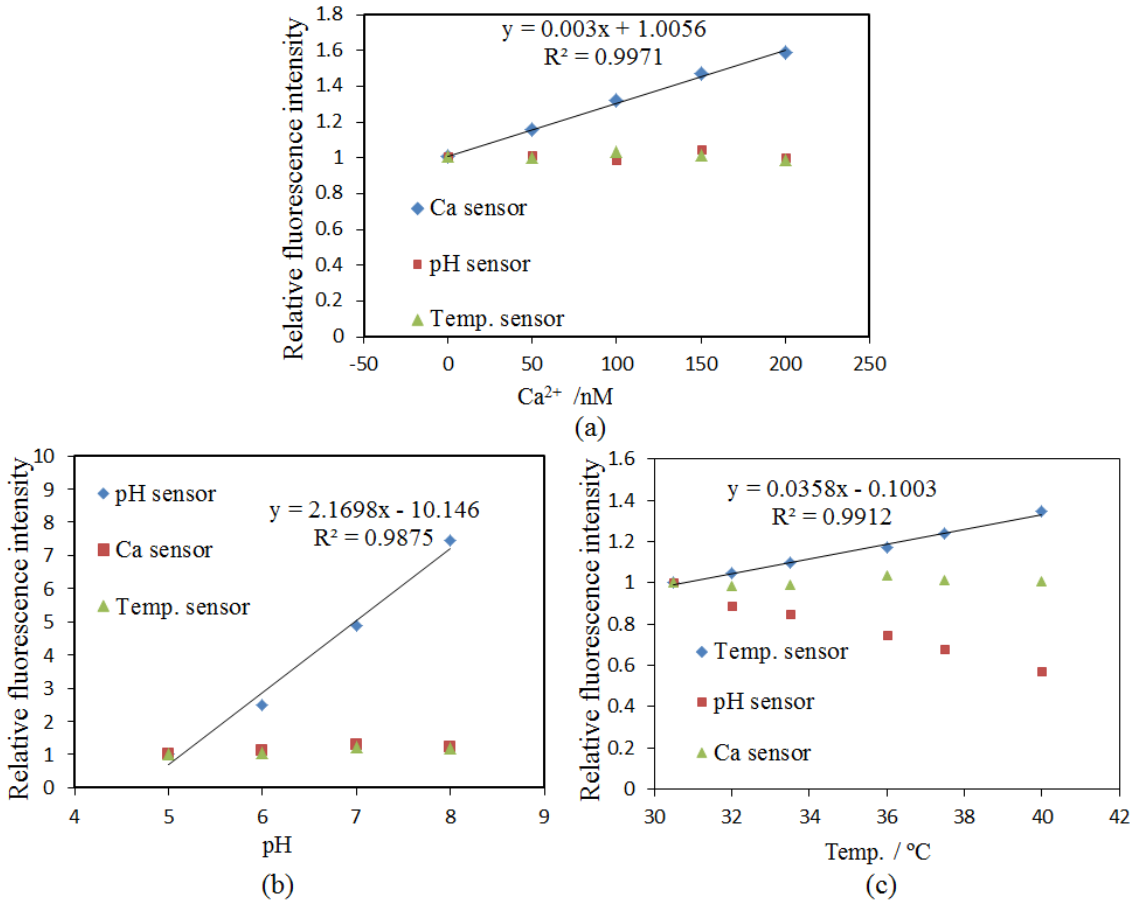

Figure 5.7: Calibration results in OCP chip: (a) calcium sensor pillars (b) pH sensor pillars (c) Temp. sensor pillars

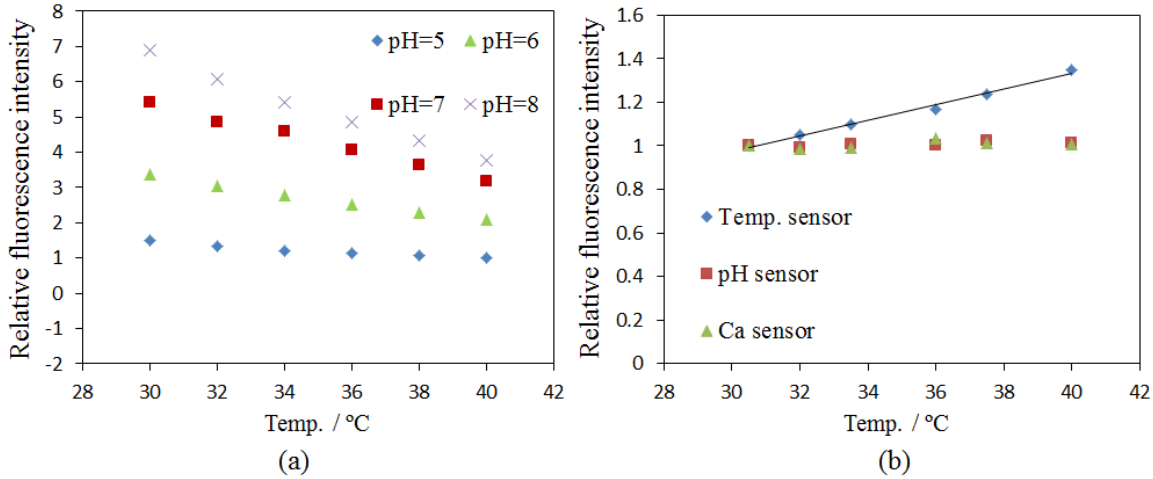

Figure 5.8: (a) Fluorescence responses of pH sensor pillars to temperature changes in different pH values. (b) Fluorescence responses of different sensor pillars to temperature changes after temperature compensation.

5.5.2 Delivery of OCP in chip

After the sensor pillars were fabricated in microchannel, OCP slurry was delivered into OCP microchannel. The OCP slurry was received from Suzuki Laboratory in Touhoku University. The OCP was injected into the chip by micro syringe pump with an injection rate of 3ml/h. As shown in Fig. 5.9, OCP was successfully injected into the upper microchannel, and multi-fluorescent sensor pillars were fabricated in the middle microchannel.

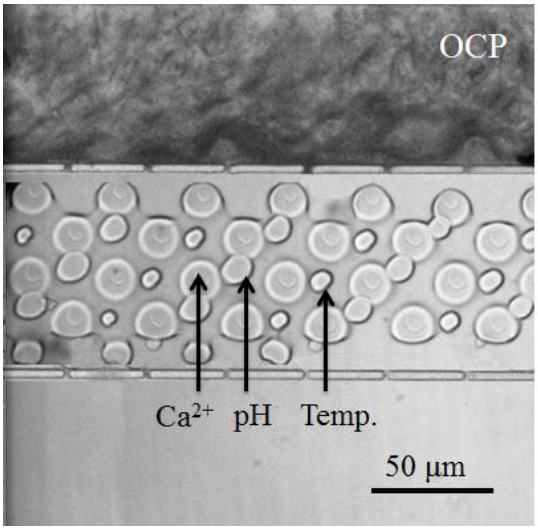

Figure 5.9: The result of delivery of OCP in microfluodic chip

5.5.3 Sensing of Ca, pH and Temp. changes during OCP conversion

After sensor fabrication and OCP delivery in OCP chip, fluoride solution was introduced into the chip. Many researches have proved that fluoride ion can promote the conversion of OCP to HA and FHA. The conversion products are related with the concentration of fluoride ion. The fluoride solution used in our experiment was 100ppm. After the fluoride solution was injected by syringe pump, the relative fluorescent intensity of sensor pillars were detected for more than 1 h by laser confocal microscope. The results are shown in Fig. 5.10. The exposure time for one time is 200ms and the time interval of images is 30s. Then, the calcium changes, pH changes and temperature

changes during OCP conversion at the presence of 100ppm F^- can be calculated from the fluorescence changes in Fig. 5.10 using the sensor sensitivities that is shown in Fig. 5.7. The results are shown in Fig. 5.11. The results show that both of the calcium concentration and pH value of the surroundings in chip decrease with time after fluoride solution was injected in chip. And the values become stable within 1 h. The calcium concentration in OCP chip decreases for 50 nM, while pH value decreases for 0.4 at the presence of 100ppm F^-. No obvious temperature change was found in OCP conversion process. The reasons for the changes during OCP conversion will be discussed.

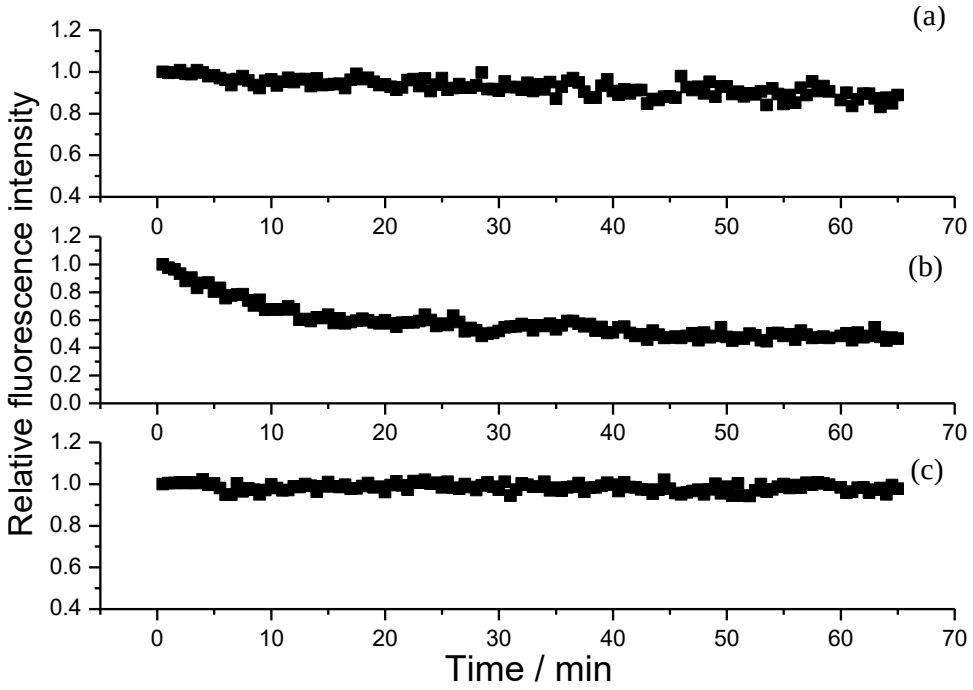

Figure 5.10: Fluorescence intensity changes of (a) calcium sensor pillars, (b) pH sensor pillars, (c) temperature sensor pillars during OCP conversion at the presence of 100ppm F^-.

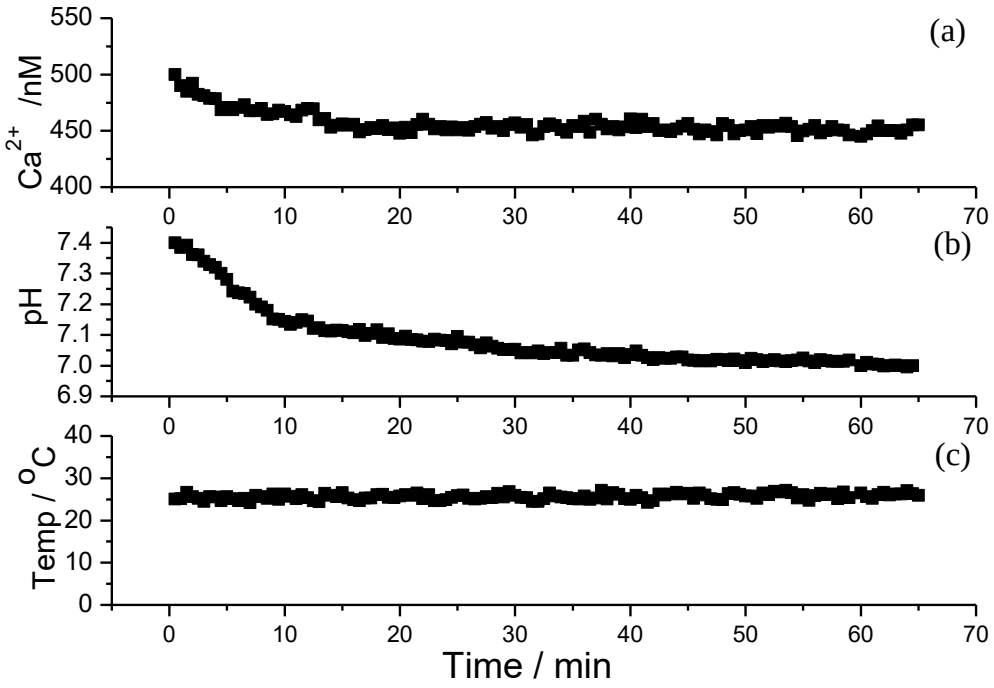

Figure 5.11: Ca^{2+}, pH, Temp. changes during OCP conversion at the presence of 100ppm F^-. (a) The result of cacium change. (b) The result of pH change. (c) The result of temperature change.

5.6 Discussions

OCP is proved to tend to convert to HA during bone regeneration in vivo [114], [131], and OCP is more soluble than HA [132]. This conversion occurs because OCP has a layered structure composed of an apatite layer whose structure is similar to HA and a hydrated layer which contains water and has a triclinic crystal system that can be converted to HA by hydrolysis of the hydrated layers in OCP [117][123]. OCP is converted into HA through (1) a dissolution–reprecipitation mechanism and (2) topotaxial conversion by ion diffusion within the crystal lattice [133][134], which consumes calcium ions from the surrounding milieu and releases phosphate ions from the crystals [133], [135]. As a result, the calcium ions and pH value in the surroundings should decrease during OCP conversion, since the OCP-HA conversion of OCP crystals is accompanied by calcium ion consumption as well as phosphate ion release into the

surrounding solution. Our experimental results are coincident with the theory. The decreases in calcium ion and pH value were detected during OCP-HA conversion in our experiments. In fact, the corresponding changes in ion concentration have also been observed in culture medium incubated with OCP [136], suggesting that the solution-mediated stimulation of osteoblasts occurs not only under in vitro physiological conditions, but also after in vivo implantation.

5.7 Summary

We succeeded in the fabrication of OCP analysis chip and multi fluorescence micro sensor pillars with different sizes for calcium, pH and temperature sensing respectively in microfluidic chip. The different sensor pillars show fluorescence under same laser wavelength and can be recognized by their different sizes. The fluorescent sensor pillars were proved to be responsive to calcium, pH and temperature, respectively. And their sensitivities have been detected. OCP was also delivered into OCP chip successfully. The sensor pillars were used to detect the calcium, pH and temperature changes during OCP conversion at the presence of F^-. The results showed that calcium ion concentration in OCP chip decreased for 50 nM, while pH value decreased for 0.4 during OCP conversion at the presence of 100ppm F^-. No obvious temperature change was found during OCP conversion process.

Chapter 6

Conclusions and future works

6.1 Conclusions

In this thesis, a novel multi-fluorescent micro-sensor based on polymeric microbeads that can simultaneously respond to temperature and pH changes was synthesized. The sensor was proposed to be (1) used in the measurements of temperature and pH changes of virus-infected cell and (2) injected in cytoplasm with short injection time and low damage to cell by applying vibration stimulus on the sensor using optical tweezers. From the experimental results and discussions, the main findings of this work can be summarized as follows:

In chapter 2, we succeeded in the synthesis of a novel multi-fluorescent micro-sensor based on polymeric microbeads that can simultaneously support pH and temperature sensitive FITC dye and temperature sensitive Rhodamine B dye on a single particle. Rhodamine B showed an excellent linear relationship between relative fluorescence intensity and temperature in the range of 32 – 38 ℃, while it was found to be independent on pH. The calibrated sensitivity of Rhodamine B is -3.4%/℃, with a

temperature accuracy of 0.1 ℃. FITC was found to be sensitive to both pH and temperature. We proposed a temperature compensation method for pH calibration. After temperature compensation, the pH accuracy calibrated based on the pH sensitivity of FITC improves from 1.5 to 0.2. This micro-sensor is proved to possess high selectivity for pH and temperature, good stability, and a high tolerance for ionic strength, making it suitable for cellular measurements.

In chapter 3, we successfully used the micro-sensor to measure the temperature and pH of influenza virus-infected and uninfected cells. The fluorescent sensor was attached to virus-bound and virus- unbound cells. The temperatures and pH in virus-bound celland virus-unbound cell were determined using a fluorescence microscope by monitoring the changes in the intensity of fluorescence. We found that influenza virus multiplication increased the temperature of cells by approximately 4–5 ℃ and decreased the pH of cells by approximately 0.5-0.6. The increase in cellular temperature during infection by influenza virus may be due to the massive consumption of ATP over a short period. The decrease in pH should be related with the functions of the virus components in host-cell. Especially, M2 protein on virus surface plays an important role in both during viral entry and egress and is closely related with the pH decrease in cytoplasm.

In chapter 4, a single sensor was successfully manipulated by optical tweezers and adhered selectively to the cell surface via the optical control of the zeta potential of spiropyran. Rapid sensor injection was achieved with an injection time of approximately 30 min by applying cyclic vibration stimulus using optical tweezers. With the vibration method, the injection rate was also increased to 80% compared with that observed in the lipofection method. This study is fundamentally helpful in the delivery of micro-nano particles used in biomedical applications, such as delivery of drugs, genes, or contrast

agents for biomedical imaging and therapy. This technique also makes it possible to measure intracellular pH and temperature, which will be a great contribution to cell biology. We believe that our work will support breakthroughs in the development of new medicine and drug therapy in cancers and viral diseases.

In chapter 5, we succeeded in the fabrication of OCP analysis chip and multi fluorescence micro sensor pillars with different sizes for calcium, pH and temperature sensing respectively in microfluidic chip. The fluorescent sensor pillars were proved to be responsive to calcium, pH and temperature, respectively. And their sensitivities have been detected. OCP was also delivered into OCP chip successfully. The sensor pillars were used to detect the calcium, pH and temperature changes during OCP conversion at the presence of F^-. The results showed that calcium ion concentration in OCP chip decreased for 50 nM, while pH value decreased for 0.4 during OCP conversion at the presence of 100ppm F-. No obvious temperature change was found during OCP conversion process.

As a conclusion, multi-sensing of more than two parameters were realized by introducing several indicators to micro-beads or micro-pillars. Rapid injection of a single particle sensor without damage the cell was also realized by applying vibration stimulus using optical tweezers. For the microbeads which possess high accuracy, it can be manipulated easily by optical tweezers and have a great potential in single cell measurements. For the pillar sensors, they show potentials in the measurements of microenvironments in microfluidic chips. These applications are quite important in future biomedical fields.

6.2 Future works

The future works are consist of three parts.

Sensor manipulation in cytoplasm

We succeeded in the injection of a single particle sensor in cytoplasm. Then the manipulation of the sensor in cytoplasm is expected by using optical tweezers. The optical tweezers can be used to trap and transfer to target locations inside the cell, such as the cell organelles including nucleus, mitochondria and so on. Therefore, the local measurements inside the cell will be possible. For example, the temperature and pH difference between different organelles and also the temperature and pH difference between cell surface, cytoplasm and nucleus can be investigated. It was suggested that the difference of temperature among organs was influenced by fundamental of cell processes. The research will support breakthroughs in the development of new medicine and drug therapy in cancers and viral diseases.

Sensor application on intracellular measurements

We succeeded in the measurements of temperature and pH changes of influenza virus-infected and uninfected cells on the surface. The temperature outside cells did not have equal effects inside the cell, and even the temperature among different organs was reported to be different which was influenced by fundamental of cell processes. Actually, we also succeeded in the injection of a single particle sensor in cytoplasm. The measurements of intracellular pH and temperature changes of cells after virus infection are possible to be the next work which will be a great contribution to cell biology.

Evaluation of cell activities in OCP analysis chip

We succeeded in the fabrication of multi sensor pillars as well as the delivery of OCP in microfluidic chip. The changes of calcium ion, pH value and temperature in the

surroundings have been detected. The injection of osteocyte into the OCP analysis chip is expected in the next work. The cell can be co-cultured together with OCP, and sensor pillars in the middle channel can be used to measure the microenvironmental changes during OCP chip. At the same time, bone cell proliferation and differentiation can be observed by microscope. The relationship between microenvironmental changes and cell activities can be investigated in the future.

Bibliography

[1] N. de Souza, “Supplement on single-cell analysis,” *Nat. Methods*, vol. 8, no. 4, pp. S1–S40, Apr. 2011.

[2] J. V. Sweedler and E. A. Arriaga, “Single cell analysis,” *Anal. Bioanal. Chem.*, vol. 387, no. 1, pp. 1–2, 2006.

[3] A. Saadatpour, S. Lai, G. Guo, and G.-C. Yuan, “Single-Cell Analysis in Cancer Genomics,” *Trends Genet.*, vol. 31, no. 10, pp. 576–586, Oct. 2015.

[4] S. Lindström and H. Andersson-Svahn, Eds., *Single-Cell Analysis - Methods and Protocols | Sara Lindström | Springer*. Humana Press, 2012.

[5] Y. Takei, S. Arai, A. Murata, M. Takabayashi, K. Oyama, S. Ishiwata, S. Takeoka, and M. Suzuki, “A nanoparticle-based ratiometric and self-calibrated fluorescent thermometer for single living cells.,” *ACS Nano*, vol. 8, no. 1, pp. 198–206, Jan. 2014.

[6] D. Di Carlo and L. P. Lee, “Dynamic single-cell analysis for quantitative biology.,” *Anal. Chem.*, vol. 78, no. 23, pp. 7918–7925, 2006.

[7] S. Ishii, K. Tago, and K. Senoo, “Single-cell analysis and isolation for microbiology and biotechnology: methods and applications.,” *Appl. Microbiol. Biotechnol.*, vol. 86, no. 5, pp. 1281–92, May 2010.

[8] T. Ishøy, T. Kvist, P. Westermann, and B. K. Ahring, “An improved method for single cell isolation of prokaryotes from meso-, thermo- and hyperthermophilic environments using micromanipulation.,” *Appl. Microbiol. Biotechnol.*, vol. 69, no. 5, pp. 510–4, Jan. 2006.

[9] K. Kubo, M. Ichikawa, K. Yoshikawa, Y. Koyama, T. Niidome, T. Yamaoka, and S.-I. M. Nomura, “Optically driven transport into a living cell,” *Appl. Phys. Lett.*, vol. 83, no. 12, p. 2468, Sep. 2003.

[10] O. Kutsch, E. N. Benveniste, G. M. Shaw, and D. N. Levy, “Direct and Quantitative Single-Cell Analysis of Human Immunodeficiency Virus Type 1 Reactivation from Latency,” *J. Virol.*, vol. 76, no. 17, pp. 8776–8786, Sep. 2002.

[11] D. Ramsköld, S. Luo, Y.-C. Wang, R. Li, Q. Deng, O. R. Faridani, G. A. Daniels, I. Khrebtukova, J. F. Loring, L. C. Laurent, G. P. Schroth, and R. Sandberg, “Full-length mRNA-Seq from single-cell levels of RNA and individual circulating tumor cells.,” *Nat. Biotechnol.*, vol. 30, no. 8, pp. 777–82, Aug. 2012.

[12] R. N. Zare and S. Kim, “Microfluidic Platforms for Single-Cell Analysis,” *Rev. Biomed. Eng*, vol. 12, pp.187-201. 2010.

[13] H. Yin and D. Marshall, “Microfluidics for single cell analysis.,” *Curr. Opin. Biotechnol.*, vol. 23, no. 1, pp. 110–9, Feb. 2012.

[14] S. Humez, M. Monet, F. van Coppenolle, P. Delcourt, and N. Prevarskaya, “The role of intracellular pH in cell growth arrest induced by ATP.,” *Am. J. Physiol. Cell Physiol.*, vol. 287, no. 6, pp. C1733–46, Dec. 2004.

[15] D. A. Warner and R. Shine, “The adaptive significance of temperature-dependent sex determination in a reptile.,” *Nature*, vol. 451, no. 7178, pp. 566–8, Jan. 2008.

[16] K. Okabe, N. Inada, C. Gota, Y. Harada, T. Funatsu, and S. Uchiyama, “Intracellular temperature mapping with a fluorescent polymeric thermometer and fluorescence lifetime imaging microscopy.,” *Nat. Commun.*, vol. 3, p. 705, Jan. 2012.

[17] R. A. Gottlieb, J. Nordberg, E. Skowronski, and B. M. Babior, “Apoptosis induced in Jurkat cells by several agents is preceded by intracellular acidification.,” *Proc. Natl. Acad. Sci.*, vol. 93, no. 2, pp. 654–658, Jan. 1996.

[18] A. Ishaque and M. Al-Rubeai, “Use of intracellular pH and annexin-V flow cytometric assays to monitor apoptosis and its suppression by bcl-2 over-expression in hybridoma cell culture,” *J. Immunol. Methods*, vol. 221, no. 1–2, pp. 43–57, Dec. 1998.

[19] M. Monti, L. Brandt, J. Ikomi-Kumm, and H. Olsson, “Heat production rate in blood lymphocytes as a prognostic factor in non-Hodgkin’s lymphoma,” *Eur. J. Haematol.*, vol. 45, no. 5, pp. 250–254, Apr. 2009.

[20] F. Ciampor, C. A. Thompson, S. Grambas, and A. J. Hay, “Regulation of pH by the M2 protein of influenza A viruses,” *Virus Res.*, vol. 22, no. 3, pp. 247–258, Mar. 1992.

[21] S. Abdullah, M. Ridzuan, and Z. Awang, “Jurnal Teknologi Intracellular Thermal Sensor for Single Cell Analysis -Short review,” vol. 6, pp. 71–80, 2015.

[22] D. Ellis and R. C. Thomas, “Microelectrode measurement of the intracellular pH of mammalian heart cells,” *Nature*, vol. 262, no. 5565, pp. 224–225, Jul. 1976.

[23] A. Parthasarathy, “Temperature Dependence of the Electrode Kinetics of Oxygen Reduction at the Platinum/Nafion® Interface—A Microelectrode Investigation,” *J. Electrochem. Soc.*, vol. 139, no. 9, p. 2530, Sep. 1992.

[24] R. C. Thomas, “Intracellular sodium activity and the sodium pump in snail neurones,” *J. Physiol.*, vol. 220, no. 1, pp. 55–71, Jan. 1972.

[25] J. Bryzek, “Impact of MEMS technology on society,” *Sensors Actuators A Phys.*, vol. 56, no. 1–2, pp. 1–9, Aug. 1996.

[26] “Method for fabricating a structure for a microelectromechanical systems (MEMS) device.” 21-Sep-2004.

[27] C.-M. Ho and Y.-C. Tai, “MICRO-ELECTRO-MECHANICAL-SYSTEMS (MEMS) AND FLUID FLOWS,” *Annu. Rev. Fluid Mech.*, vol. 30, no. 1, pp. 579–612, Jan. 1998.

[28] V. Zeeb, M. Suzuki, and S. Ishiwata, “A novel method of thermal activation and temperature measurement in the microscopic region around single living cells.,” *J. Neurosci. Methods*, vol. 139, no. 1, pp. 69–77, Oct. 2004.

[29] C. Wang, R. Xu, W. Tian, X. Jiang, Z. Cui, M. Wang, H. Sun, K. Fang, and N. Gu, “Determining intracellular temperature at single-cell level by a novel

thermocouple method.," *Cell Res.*, vol. 21, no. 10, pp. 1517–9, Oct. 2011.

[30] M. Suzuki, V. Tseeb, K. Oyama, and S. Ishiwata, "Microscopic detection of thermogenesis in a single HeLa cell.," *Biophys. J.*, vol. 92, no. 6, pp. L46–8, Mar. 2007.

[31] J. El-Ali, I. R. Perch-Nielsen, C. R. Poulsen, D. D. Bang, P. Telleman, and A. Wolff, "Simulation and experimental validation of a SU-8 based PCR thermocycler chip with integrated heaters and temperature sensor," *Sensors Actuators A Phys.*, vol. 110, no. 1–3, pp. 3–10, 2004.

[32] P. C. Caldwell, "Studies on the internal pH of large muscle and nerve fibres," *J. Physiol.*, vol. 142, no. 1, pp. 22–62, Jun. 1958.

[33] P. C. Caldwell, "An investigation of the intracellular pH of crab muscle fibres by means of micro-glass and micro-tungsten electrodes," *J. Physiol.*, vol. 126, no. 1, pp. 169–180, Oct. 1954.

[34] R. C. Thomas, "Intracellular pH of snail neurones measured with a new pH-sensitive glass micro-electrode," *J. Physiol.*, vol. 238, no. 1, pp. 159–180, Apr. 1974.

[35] X. Wang, O. S. Wolfbeis, and R. J. Meier, "Luminescent probes and sensors for temperature.," *Chem. Soc. Rev.*, vol. 42, no. 19, pp. 7834–69, Oct. 2013.

[36] S. Wang, S. Westcott, and W. Chen, "Nanoparticle Luminescence Thermometry," *J. Phys. Chem. B*, vol. 106, no. 43, pp. 11203–11209, Oct. 2002.

[37] A. S. Susha, A. M. Javier, W. J. Parak, and A. L. Rogach, "Luminescent CdTe nanocrystals as ion probes and pH sensors in aqueous solutions," *Colloids Surfaces A Physicochem. Eng. Asp.*, vol. 281, no. 1–3, pp. 40–43, Jun. 2006.

[38] A. Al Salman, A. Tortschanoff, M. B. Mohamed, D. Tonti, F. van Mourik, and M. Chergui, "Temperature effects on the spectral properties of colloidal CdSe nanodots, nanorods, and tetrapods," *Appl. Phys. Lett.*, vol. 90, no. 9, p. 093104, Feb. 2007.

[39] S. M. Borisov, C. Krause, S. Arain, and O. S. Wolfbeis, “Composite Material for Simultaneous and Contactless Luminescent Sensing and Imaging of Oxygen and Carbon Dioxide,” *Adv. Mater.*, vol. 18, no. 12, pp. 1511–1516, Jun. 2006.

[40] S. Nagl and O. S. Wolfbeis, “Optical multiple chemical sensing: status and current challenges.,” *Analyst*, vol. 132, no. 6, pp. 507–11, Jun. 2007.

[41] H. Maruyama, T. Otake, and F. Arai, “Photoprocessible Hydrogel Microsensor for Local Environment Measurement on a Microfluidic Chip,” *IEEE/ASME Trans. Mechatronics*, vol. 16, no. 5, pp. 845–852, Oct. 2011.

[42] J. Han and K. Burgess, “Fluorescent Indicators for Intracellular pH,” *Chem. Rev.*, vol. 110, no. 5, pp. 2709–2728, May 2010.

[43] K. Oyama, M. Takabayashi, Y. Takei, S. Arai, S. Takeoka, S. Ishiwata, and M. Suzuki, “Walking nanothermometers: spatiotemporal temperature measurement of transported acidic organelles in single living cells.,” *Lab Chip*, vol. 12, no. 9, pp. 1591–3, May 2012.

[44] M. Bradley, L. Alexander, K. Duncan, M. Chennaoui, A. C. Jones, and R. M. Sánchez-Martín, “pH sensing in living cells using fluorescent microspheres.,” *Bioorg. Med. Chem. Lett.*, vol. 18, no. 1, pp. 313–7, Jan. 2008.

[45] A. Burns, H. Ow, and U. Wiesner, “Fluorescent core-shell silica nanoparticles: towards ‘Lab on a Particle’ architectures for nanobiotechnology.,” *Chem. Soc. Rev.*, vol. 35, no. 11, pp. 1028–42, Nov. 2006.

[46] A. Burns, P. Sengupta, T. Zedayko, B. Baird, and U. Wiesner, “Core/Shell fluorescent silica nanoparticles for chemical sensing: towards single-particle laboratories.,” *Small*, vol. 2, no. 6, pp. 723–6, Jun. 2006.

[47] A. Schulz and C. McDonagh, “Intracellular sensing and cell diagnostics using fluorescent silica nanoparticles,” *Soft Matter*, vol. 8, no. 9, p. 2579, Feb. 2012.

[48] H. Maruyama, F. Arai, and T. Fukuda, “On-chip pH measurement using functionalized gel-microbeads positioned by optical tweezers.,” *Lab Chip*, vol. 8,

no. 2, pp. 346–51, Feb. 2008.

[49] H. Maruyama, T. Fukuda, and F. Arai, “Functional gel-microbead manipulated by optical tweezers for local environment measurement in microchip,” *Microfluid. Nanofluidics*, vol. 6, no. 3, pp. 383–390, Jan. 2009.

[50] W. Wu and S. Zhou, “Hybrid micro-/nanogels for optical sensing and intracellular imaging.,” *Nano Rev.*, vol. 1, Jan. 2010.

[51] J. Shen, “Intelligent nano/microgels for cell scaffold and drug delivery system,” Proquest, 2014.

[52] T. S. Troutman, S. J. Leung, and M. Romanowski, “Light-Induced Content Release from Plasmon Resonant Liposomes.,” *Adv. Mater.*, vol. 21, no. 22, pp. 2334–2338, Jun. 2009.

[53] K. P. McNamara, T. Nguyen, G. Dumitrascu, J. Ji, N. Rosenzweig, and Z. Rosenzweig, “Synthesis, Characterization, and Application of Fluorescence Sensing Lipobeads for Intracellular pH Measurements,” *Anal. Chem.*, vol. 73, no. 14, pp. 3240–3246, Jul. 2001.

[54] K. Inoue, T. Tanikawa, and T. Arai, “Micro-manipulation system with a two-fingered micro-hand and its potential application in bioscience.,” *J. Biotechnol.*, vol. 133, no. 2, pp. 219–24, Jan. 2008.

[55] D. Delgado, A. del Pozo-Rodríguez, M. Á. Solinís, and A. Rodríguez-Gascón, “Understanding the mechanism of protamine in solid lipid nanoparticle-based lipofection: the importance of the entry pathway.,” *Eur. J. Pharm. Biopharm.*, vol. 79, no. 3, pp. 495–502, Nov. 2011.

[56] L. Gu and S. K. Mohanty, “Targeted microinjection into cells and retina using optoporation.,” *J. Biomed. Opt.*, vol. 16, no. 12, p. 128003, Dec. 2011.

[57] G. V Orsinger, J. D. Williams, and M. Romanowski, “Focal activation of cells by plasmon resonance assisted optical injection of signaling molecules.,” *ACS Nano*, vol. 8, no. 6, pp. 6151–62, Jun. 2014.

[58] J. Kuncova and P. Kallio, “Challenges in capillary pressure microinjection.,” *Conf. Proc. ... Annu. Int. Conf. IEEE Eng. Med. Biol. Soc. IEEE Eng. Med. Biol. Soc. Annu. Conf.*, vol. 7, pp. 4998–5001, Jan. 2004.

[59] K. K. Tan, S. C. Ng, Y. Xie, and Y. W. YIP, “Optimal intra-cytoplasmic sperm injection with a piezo micromanipulator,” *Control Intell. Syst.*, vol. 32, no. 3, pp. 138–145.

[60] T. Nakayama, “A New Assisted Hatching Technique Using a Piezo-Micromanipulator,” *Fertil. Steril.*, vol. 69, no. 4, pp. 784–788, Apr. 1998.

[61] Y. Tan, D. Sun, W. Huang, and S. H. Cheng, “Mechanical modeling of biological cells in microinjection.,” *IEEE Trans. Nanobioscience*, vol. 7, no. 4, pp. 257–66, Dec. 2008.

[62] Y. Shen, Z. Zhang, and T. Fukuda, “Bending spring rate investigation of nanopipette for cell injection.,” *Nanotechnology*, vol. 26, no. 15, p. 155702, Apr. 2015.

[63] T. Hayakawa, S. Fukada, and F. Arai, “Fabrication of an On-Chip Nanorobot Integrating Functional Nanomaterials for Single-Cell Punctures,” *IEEE Trans. Robot.*, vol. 30, no. 1, pp. 59–67, Feb. 2014.

[64] H. Sun, R. V Benjaminsen, K. Almdal, and T. L. Andresen, “Hyaluronic acid immobilized polyacrylamide nanoparticle sensors for CD44 receptor targeting and pH measurement in cells.,” *Bioconjug. Chem.*, vol. 23, no. 11, pp. 2247–55, Nov. 2012.

[65] T. S. Troutman, J. K. Barton, and M. Romanowski, “Biodegradable Plasmon Resonant Nanoshells.,” *Adv. Mater.*, vol. 20, no. 13, pp. 2604–2608, Jul. 2008.

[66] T. Masuda, H. Maruyama, A. Honda, and F. Arai, “Multi-layered liposome containing nanosensor for transfecting into a cell nucleus,” in *2013 13th IEEE International Conference on Nanotechnology (IEEE-NANO 2013)*, 2013, pp. 162–165.

[67] C. Bao, G. Pähler, B. Geil, and A. Janshoff, “Optical fusion assay based on membrane-coated spheres in a 2D assembly.,” *J. Am. Chem. Soc.*, vol. 135, no. 33, pp. 12176–9, Aug. 2013.

[68] L. Gu and S. K. Mohanty, “Targeted microinjection into cells and retina using optoporation.,” *J. Biomed. Opt.*, vol. 16, no. 12, p. 128003, Dec. 2011.

[69] K. Dhakal, B. Black, and S. Mohanty, “Introduction of impermeable actin-staining molecules to mammalian cells by optoporation.,” *Sci. Rep.*, vol. 4, p. 6553, Jan. 2014.

[70] M. D. Wang, H. Yin, R. Landick, J. Gelles, and S. M. Block, “Stretching DNA with optical tweezers.,” *Biophys. J.*, vol. 72, no. 3, pp. 1335–46, Mar. 1997.

[71] A. Ashkin, J. M. Dziedzic, and T. Yamane, “Optical trapping and manipulation of single cells using infrared laser beams.,” *Nature*, vol. 330, no. 6150, pp. 769–71, Jan. 1987.

[72] M. Li, T. Lohmüller, and J. Feldmann, “Optical injection of gold nanoparticles into living cells.,” *Nano Lett.*, vol. 15, no. 1, pp. 770–5, Jan. 2015.

[73] T. Sugiura, H. Miyoshi, T. Nishio, and A. Honda, “Cell palpation with an optically trapped particle,” *J. Micro-Nano Mechatronics*, vol. 7, no. 4, pp. 131–136, Nov. 2012.

[74] H. Miyoshi, T. Sugiura, and K. Minato, “Cell Palpation System Based on a Force Measurement by Optical Tweezers for Investigation of Local Mechanical Properties of a Cell Membrane,” *Jpn. J. Appl. Phys.*, vol. 48, no. 12, p. 120223, Dec. 2009.

[75] A. Ashkin, J. M. Dziedzic, J. E. Bjorkholm, and S. Chu, “Observation of a single-beam gradient force optical trap for dielectric particles,” *Opt. Lett.*, vol. 11, no. 5, p. 288, May 1986.

[76] A. Ashkin, “Acceleration and Trapping of Particles by Radiation Pressure,” *Phys. Rev. Lett.*, vol. 24, no. 4, pp. 156–159, Jan. 1970.

[77] A. Ashkin and J. Dziedzic, “Optical trapping and manipulation of viruses and bacteria,” *Science (80-.).*, vol. 235, no. 4795, pp. 1517–1520, Mar. 1987.

[78] A. Ashkin and J. Dziedzic, “Optical trapping and manipulation of viruses and bacteria,” *Science (80-.).*, vol. 235, no. 4795, pp. 1517–1520, Mar. 1987.

[79] J. P. Mills, L. Qie, M. Dao, C. T. Lim, and S. Suresh, “Nonlinear elastic and viscoelastic deformation of the human red blood cell with optical tweezers,” *Mech. Chem. Biosyst.*, vol. 1, no. 3, pp. 169–180, 2004.

[80] C. McDougall, D. J. Stevenson, C. T. A. Brown, F. Gunn-Moore, and K. Dholakia, “Targeted optical injection of gold nanoparticles into single mammalian cells.,” *J. Biophotonics*, vol. 2, no. 12, pp. 736–43, Dec. 2009.

[81] B. F. Godley, F. A. Shamsi, F.-Q. Liang, S. G. Jarrett, S. Davies, and M. Boulton, “Blue Light Induces Mitochondrial DNA Damage and Free Radical Production in Epithelial Cells,” *J. Biol. Chem.*, vol. 280, no. 22, pp. 21061–21066, Mar. 2005.

[82] G. V. Orsinger, J. D. Williams, and M. Romanowski, “Focal Activation of Cells by Plasmon Resonance Assisted Optical Injection of Signaling Molecules,” Jun. 2014.

[83] J. L. Tan, J. Tien, D. M. Pirone, D. S. Gray, K. Bhadriraju, and C. S. Chen, “Cells lying on a bed of microneedles: an approach to isolate mechanical force.,” *Proc. Natl. Acad. Sci. U. S. A.*, vol. 100, no. 4, pp. 1484–9, Feb. 2003.

[84] N. Q. Balaban, U. S. Schwarz, D. Riveline, P. Goichberg, G. Tzur, I. Sabanay, D. Mahalu, S. Safran, A. Bershadsky, L. Addadi, and B. Geiger, “Force and focal adhesion assembly: a close relationship studied using elastic micropatterned substrates.,” *Nat. Cell Biol.*, vol. 3, no. 5, pp. 466–72, May 2001.

[85] T. Hayakawa, H. Maruyama, and F. Arai, “High thermal conductive nano pillars for temperature distribution measurement of a single cell,” in *2012 International Symposium on Micro-NanoMechatronics and Human Science (MHS)*, 2012, pp. 488–490.

[86] T. Xu, N. Zhu, M. Y.-C. Xu, L. Wosinski, J. S. Aitchison, and H. E. Ruda, "Pillar-array based optical sensor.," *Opt. Express*, vol. 18, no. 6, pp. 5420–5, Mar. 2010.

[87] M. Melli, G. Scoles, and M. Lazzarino, "Fast detection of biomolecules in diffusion-limited regime using micromechanical pillars.," *ACS Nano*, vol. 5, no. 10, pp. 7928–35, Oct. 2011.

[88] Y. Zhao and X. Zhang, "Cellular mechanics study in cardiac myocytes using PDMS pillars array," *Sensors Actuators A Phys.*, vol. 125, no. 2, pp. 398–404, Jan. 2006.

[89] Y. Wang and L. Liu, "Fabrication of microstructures using the DMD-based modulating projection printing method," in *10th IEEE International Conference on Nano/Micro Engineered and Molecular Systems*, 2015, pp. 625–629.

[90] W. Roos, "Biomimetic cytoskeleton assemblies and living cells on micropillar force sensor arrays." 13-Jan-2004.

[91] H. Maruyama, R. Kariya, S. Nakamura, T. Matsuda, Y. Matsuda, T. Niimi, A. Honda, and F. Arai, "Ultra long-lifetime and high-sensitive fluorescent measurement using difference compensation method for single cell analysis," in *2012 IEEE/RSJ International Conference on Intelligent Robots and Systems*, 2012, pp. 3235–3240.

[92] J. Zhou, C. Fang, T. Chang, X. Liu, and D. Shangguan, "A pH sensitive ratiometric fluorophore and its application for monitoring the intracellular and extracellular pHs simultaneously," *J. Mater. Chem. B*, vol. 1, no. 5, pp. 661–667, Jan. 2013.

[93] L. L. Moore, D. A. Bostick, and R. F. Garry, "Sindbis virus infection decreases intracellular pH: Alkaline medium inhibits processing of sindbis virus polyproteins," *Virology*, vol. 166, no. 1, pp. 1–9, Sep. 1988.

[94] Y. Liu, W. Liu, X.-D. Song, and J. Zuo, "Effect of GRP75/mthsp70/PBP74/mortalin overexpression on intracellular ATP level,

mitochondrial membrane potential and ROS accumulation following glucose deprivation in PC12 cells," *Mol. Cell. Biochem.*, vol. 268, no. 1–2, pp. 45–51, Jan. 2005.

[95] T. Ando, H. Imamura, R. Suzuki, H. Aizaki, T. Watanabe, T. Wakita, and T. Suzuki, "Visualization and Measurement of ATP Levels in Living Cells Replicating Hepatitis C Virus Genome RNA," *PLoS Pathog.*, vol. 8, no. 3, p. e1002561, Mar. 2012.

[96] P. Pushko, T. M. Tumpey, F. Bu, J. Knell, R. Robinson, and G. Smith, "Influenza virus-like particles comprised of the HA, NA, and M1 proteins of H9N2 influenza virus induce protective immune responses in BALB/c mice.," *Vaccine*, vol. 23, no. 50, pp. 5751–9, Dec. 2005.

[97] M. Takeda, A. Pekosz, K. Shuck, L. H. Pinto, and R. A. Lamb, "Influenza A Virus M2 Ion Channel Activity Is Essential for Efficient Replication in Tissue Culture," *J. Virol.*, vol. 76, no. 3, pp. 1391–1399, Feb. 2002.

[98] L. H. Pinto and R. A. Lamb, "The M2 proton channels of influenza A and B viruses.," *J. Biol. Chem.*, vol. 281, no. 14, pp. 8997–9000, Apr. 2006.

[99] T. Betakova, "M2 Protein-A Proton Channel of Influenza A Virus," *Curr. Pharm. Des.*, vol. 13, no. 31, pp. 3231–3235, Nov. 2007.

[100] G. Neumann, T. Noda, and Y. Kawaoka, "Emergence and pandemic potential of swine-origin H1N1 influenza virus.," *Nature*, vol. 459, no. 7249, pp. 931–9, Jun. 2009.

[101] B. S. Lukyanov and M. B. Lukyanova, "Spiropyrans: Synthesis, Properties, and Application. (Review)," *Chem. Heterocycl. Compd.*, vol. 41, no. 3, pp. 281–311, Mar. 2005.

[102] K. C. Neuman and S. M. Block, "Optical trapping.," *Rev. Sci. Instrum.*, vol. 75, no. 9, pp. 2787–809, Sep. 2004.

[103] S. T. Truschel, E. Wang, W. G. Ruiz, S.-M. Leung, R. Rojas, J. Lavelle, M.

Zeidel, D. Stoffer, and G. Apodaca, “Stretch-regulated exocytosis/endocytosis in bladder umbrella cells.,” *Mol. Biol. Cell*, vol. 13, no. 3, pp. 830–46, Mar. 2002.

[104] E. M. Winter and J. T. Groves, “Surface binding affinity measurements from order transitions of lipid membrane-coated colloidal particles.,” *Anal. Chem.*, vol. 78, no. 1, pp. 174–80, Jan. 2006.

[105] R. Blonder, E. Katz, I. Willner, V. Wray, and A. F. Bückmann, “Application of a Nitrospiropyran-FAD-Reconstituted Glucose Oxidase and Charged Electron Mediators as Optobioelectronic Assemblies for the Amperometric Transduction of Recorded Optical Signals: Control of the ‘On’−‘Off’ Direction of the Photoswitch,” *J. Am. Chem. Soc.*, vol. 119, no. 49, pp. 11747–11757, Dec. 1997.

[106] M. Paulmichl, F. Friedrich, E. Wöll, H. Weiss, and F. Lang, “Effects of serotonin on electrical properties of Madin-Darby canine kidney cells,” *Pflűgers Arch. Eur. J. Physiol.*, vol. 411, no. 4, pp. 394–400, Apr. 1988.

[107] V. Helms, “Principles of computational cell biology,” 2008.

[108] K. Onda and F. Arai, “Multi-beam bilateral teleoperation of holographic optical tweezers.,” *Opt. Express*, vol. 20, no. 4, pp. 3633–41, Feb. 2012.

[109] N. Mukohzaka, N. Yoshida, H. Toyoda, Y. Kobayashi, and T. Hara, “Diffraction efficiency analysis of a parallel-aligned nematic-liquid-crystal spatial light modulator.,” *Appl. Opt.*, vol. 33, no. 14, pp. 2804–11, May 1994.

[110] P. G. Coupland, S. J. Briddon, and J. W. Aylott, “Using fluorescent pH-sensitive nanosensors to report their intracellular location after Tat-mediated delivery.,” *Integr. Biol. (Camb).*, vol. 1, no. 4, pp. 318–23, Apr. 2009.

[111] A. S. Urban, T. Pfeiffer, M. Fedoruk, A. A. Lutich, and J. Feldmann, “Single-step injection of gold nanoparticles through phospholipid membranes.,” *ACS Nano*, vol. 5, no. 5, pp. 3585–90, May 2011.

[112] P. L. Felgner, T. R. Gadek, M. Holm, R. Roman, H. W. Chan, M. Wenz, J. P. Northrop, G. M. Ringold, and M. Danielsen, “Lipofection: a highly efficient,

lipid-mediated DNA-transfection procedure.," *Proc. Natl. Acad. Sci.*, vol. 84, no. 21, pp. 7413–7417, Nov. 1987.

[113] J. P. Yang and L. Huang, "Overcoming the inhibitory effect of serum on lipofection by increasing the charge ratio of cationic liposome to DNA.," *Gene Ther.*, vol. 4, no. 9, pp. 950–60, Sep. 1997.

[114] O. Suzuki, M. Nakamura, Y. Miyasaka, M. Kagayama, and M. Sakurai, "Bone Formation on Synthetic Precursors of Hydroxyapatite.," *Tohoku J. Exp. Med.*, vol. 164, no. 1, pp. 37–50, Aug. 1991.

[115] F. Sugihara, Y. Mandai. M. Yoshikawa, "Experimental-study of octacalcium phosphate for bone substitute material", Amer. Assoc. Dental. Reseach, vol. 74, no. 3, p. 973, 1995 .

[116] F. Sugihara, H. Oonishi, K. Minamigawa and Y. Mandai, "Bone tissue reaction of octacalcium phosphate-collagen conjugated sponge," *The 9th Ceramics in medicine: Bioceramics*, Japan(Otsu), vol. 9, pp. 399–401, 1996

[117] W. E. Brown, J. P. Smith, J. R. Lehr, and A. W. Frazier, "Octacalcium Phosphate and Hydroxyapatite: Crystallographic and Chemical Relations between Octacalcium Phosphate and Hydroxyapatite," *Nature*, vol. 196, no. 4859, pp. 1050–1055, Dec. 1962.

[118] J. Wergedal and D. Baylink, "Fluoride directly stimulates proliferation and alkaline phosphatase activity of bone-forming cells," *Science (80-.).*, vol. 222, no. 4621, pp. 330–332, Oct. 1983.

[119] E. C. Moreno, M. Kresak, and R. T. Zahradnik, "Fluoridated Hydroxyapatite Solubility and Caries Formation," *Nature*, vol. 247, no. 5435, pp. 64–65, Jan. 1974.

[120] M. Iijima, H. Kamemizu, N. Wakamatsu, T. Goto, Y. Doi, and Y. Moriwaki, "Transition of octacalcium phosphate to hydroxyapatite in solution at pH 7.4 and 37 ℃," *J. Cryst. Growth*, vol. 181, no. 1–2, pp. 70–78, Oct. 1997.

[121] Y. Shiwaku, Y. Honda, T. Anada, S. Morimoto, T. Masuda, K. Sasaki, and O. Suzuki, “Analysis of physicochemical properties of octacalcium phosphate prepared by hydrolysis and co-precipitation with fluoride ions,” *J. Ceram. Soc. Japan*, vol. 118, no. 1378, pp. 402–405, Jun. 2010.

[122] D. G. A. Nelson and J. D. McLean, “High-resolution electron microscopy of octacalcium phosphate and its hydrolysis products,” *Calcif. Tissue Int.*, vol. 36, no. 1, pp. 219–232, Dec. 1984.

[123] M. Kamitakahara, N. ITO, S. MURAKAMI, N. WATANABE, and K. IOKU, “Hydrothermal synthesis of hydroxyapatite from octacalcium phosphate: effect of hydrothermal temperature,” *J. Ceram. Soc. Japan*, vol. 117, no. 1363, pp. 385–387, Mar. 2009.

[124] F. Barrère, C. A. van Blitterswijk, and K. de Groot, “Bone regeneration: molecular and cellular interactions with calcium phosphate ceramics.,” *Int. J. Nanomedicine*, vol. 1, no. 3, pp. 317–32, Jan. 2006.

[125] W. Zhan, G. H. Seong, and R. M. Crooks, “Hydrogel-Based Microreactors as a Functional Component of Microfluidic Systems,” *Anal. Chem.*, vol. 74, no. 18, pp. 4647–4652, Sep. 2002.

[126] A. Revzin, R. J. Russell, V. K. Yadavalli, W.-G. Koh, C. Deister, D. D. Hile, M. B. Mellott, and M. V. Pishko, “Fabrication of Poly(ethylene glycol) Hydrogel Microstructures Using Photolithography,” *Langmuir*, vol. 17, no. 18, pp. 5440–5447, Sep. 2001.

[127] G. H. Seong, W. Zhan, and R. M. Crooks, “Fabrication of Microchambers Defined by Photopolymerized Hydrogels and Weirs within Microfluidic Systems: Application to DNA Hybridization,” *Anal. Chem.*, vol. 74, no. 14, pp. 3372–3377, Jul. 2002.

[128] N. Y. Lee, Y. K. Jung, and H. G. Park, “On-chip colorimetric biosensor based on polydiacetylene (PDA) embedded in photopolymerized poly(ethylene glycol) diacrylate (PEG-DA) hydrogel,” *Biochem. Eng. J.*, vol. 29, no. 1–2, pp. 103–108,

Apr. 2006.

[129] J. Yu, Z. Liu, Q. Liu, K. T. Yuen, A. F. T. Mak, M. Yang, and P. Leung, “A polyethylene glycol (PEG) microfluidic chip with nanostructures for bacteria rapid patterning and detection,” *Sensors Actuators A Phys.*, vol. 154, no. 2, pp. 288–294, Sep. 2009.

[130] G. H. Seong, W. Zhan, and R. M. Crooks, “Fabrication of Microchambers Defined by Photopolymerized Hydrogels and Weirs within Microfluidic Systems: Application to DNA Hybridization,” *Anal. Chem.*, vol. 74, no. 14, pp. 3372–3377, Jul. 2002.

[131] O. Suzuki, S. Kamakura, T. Katagiri, M. Nakamura, B. Zhao, Y. Honda, and R. Kamijo, “Bone formation enhanced by implanted octacalcium phosphate involving conversion into Ca-deficient hydroxyapatite.,” *Biomaterials*, vol. 27, no. 13, pp. 2671–81, May 2006.

[132] L. C. Chow, *Octacalcium Phosphate*, vol. 18. Basel: KARGER, 2001.

[133] W. E. Brown, M. Mathew, and M. S. Tung, “Crystal chemistry of octacalcium phosphate,” *Prog. Cryst. Growth Charact.*, vol. 4, no. 1–2, pp. 59–87, Jan. 1981.

[134] T. Kawai, T. Anada, T. Masuda, Y. Honda, Y. Sakai, Y. Kato, S. Kamakura, S. Echigo, and O. Suzuki, “The effect of synthetic octacalcium phosphate in a collagen scaffold on the osteogenicity of mesenchymal stem cells.,” *Eur. Cell. Mater.*, vol. 22, pp. 124–36, 2011.

[135] O. Suzuki, S. Kamakura, and T. Katagiri, “Surface chemistry and biological responses to synthetic octacalcium phosphate.,” *J. Biomed. Mater. Res. B. Appl. Biomater.*, vol. 77, no. 1, pp. 201–12, Apr. 2006.

[136] M. Takami, A. Mochizuki, A. Yamada, K. Tachi, B. Zhao, Y. Miyamoto, T. Anada, Y. Honda, T. Inoue, M. Nakamura, O. Suzuki, and R. Kamijo, “Osteoclast differentiation induced by synthetic octacalcium phosphate through receptor activator of NF-kappaB ligand expression in osteoblasts.,” *Tissue Eng. Part A*, vol. 15, no. 12, pp. 3991–4000, Dec. 2009.

Accomplishments

I. Journal Articles

1. **Hengjun Liu**, Hisataka Maruyama, Taisuke Masuda, Ayae Honda, Fumihito Arai, “Multi-fluorescent micro-sensor for accurate measurement of pH and temperature variations in micro-environments”, *Sensors and Actuators B: Chemical*, Vol.203, pp. 54–62, (2014)
2. **Hengjun Liu**, Hisataka Maruyama, Taisuke Masuda, Fumihito Arai, “Vibration-assisted optical injection of a single fluorescent sensor into a target cell”, *Sensors and Actuators B: Chemical*, Vol.220, pp.40–49, (2015)
3. Jing Zhong, **Hengjun Liu**, Hisataka Maruyama and Fumihito Arai, “Optical heating of metallic nanoparticles for fast injection of nanoscale sensor into living cells”, *Sensors and Actuators B: Chemical*, 2015, submitted

II. International conferences

1. **Hengjun Liu**, Hisataka Maruyama, Taisuke Masuda, Fumihito Arai, “Sensitivity compensation of multi-fluorescence sensor toward on-chip cell measurement”, 24th 2013 International Symposium on Micro- NanoMechatronics and Human Science (MHS2013), Nov. 10-13, Nagoya (Japan), 2013
2. **Hengjun Liu**, Hisataka Maruyama, Taisuke Masuda, Ayae Honda, Fumihito Arai, “Rapid Injection of Fluorescence Sensor into a Target Cell by Local Mechanical Stimulus of Optical Tweezers”, The 14th International Conference on Nanotechnology (IEEE Nano),

Aug.18-21, Canada (Toronto), 2014

3. **Hengjun Liu**, Hisataka Maruyama, Taisuke Masuda, Osamu Suzuki, Fumihito Arai, “Multi-fluorescence sensor pillars for simultaneous calcium and pH and temperature sensing in chip”, The 19th International Conference on Miniaturized Systems for Chemistry and Life Sciences (MicroTAS 2015), Korea (Gyeongju), Oct. 25-29, 2015